INSIDE TRACK with **MINI-CIRCUITS' HARVEY KAYLIE** p32

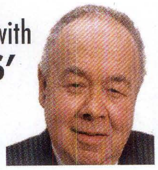

TARGETING ADVANCES IN RADAR SYSTEMS p39

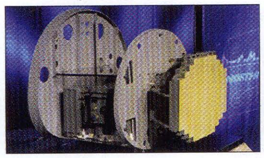

TUNE TO NEW ANTENNA DEVELOPMENTS p104

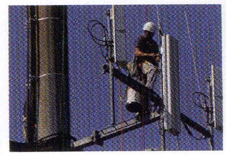

MicroWaves&RF

JUNE 2012 TRUSTED ENGINEERING RESOURCE FOR 50 YEARS www.MWRF.com

AVIONICS & RADAR

GENERATORS Fashion Clean Signals to 6 GHz

A PENTON PUBLICATION Periodicals Postage Paid • USPS 100 Approved Poly

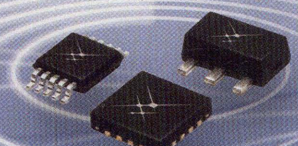

JUNE | 2012

Volume 51, Issue 6

MicroWaves&RF

CONTENTS

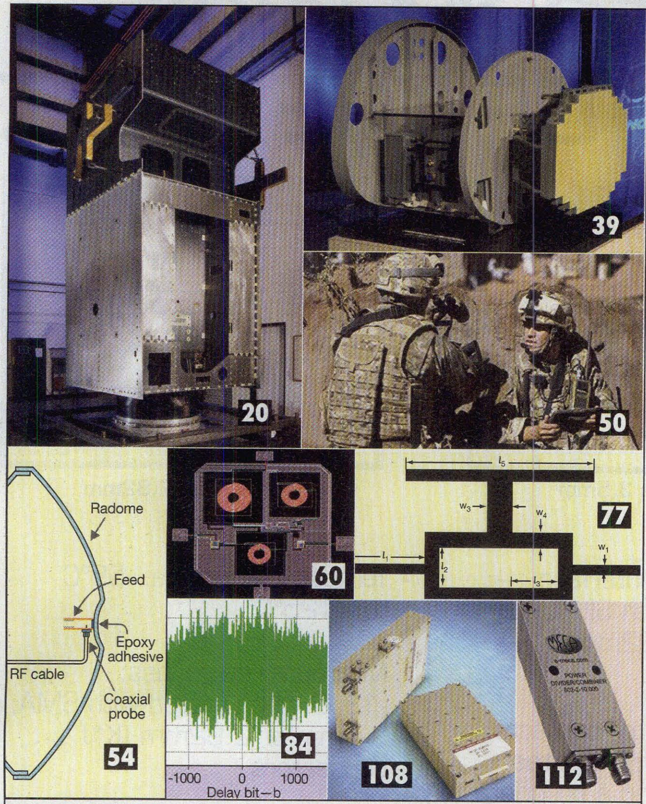

Penton
Design Engineering & Sourcing Group


ITT EXELIS
THE POWER OF INGENUITY
Pushing the boundaries of RF and Digital integration.
Photo property of the U.S. Air Force.

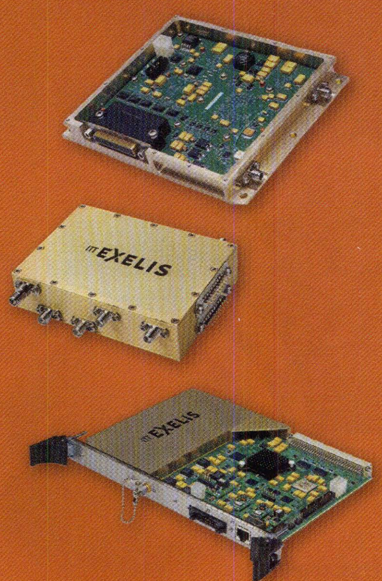

RF Amplifiers and Sub-Assemblies for Every Application

Delivery from Stock to 2 Weeks ARO from the catalog or built to your specifications!

- Competitive Pricing & Fast Delivery
- Military Reliability & Qualification
- Various Options: Temperature Compensation, Input Limiter Protection, Detectors/TTL & More
- Unconditionally Stable (100% tested)

ISO 9001:2000 and AS9100B CERTIFIED

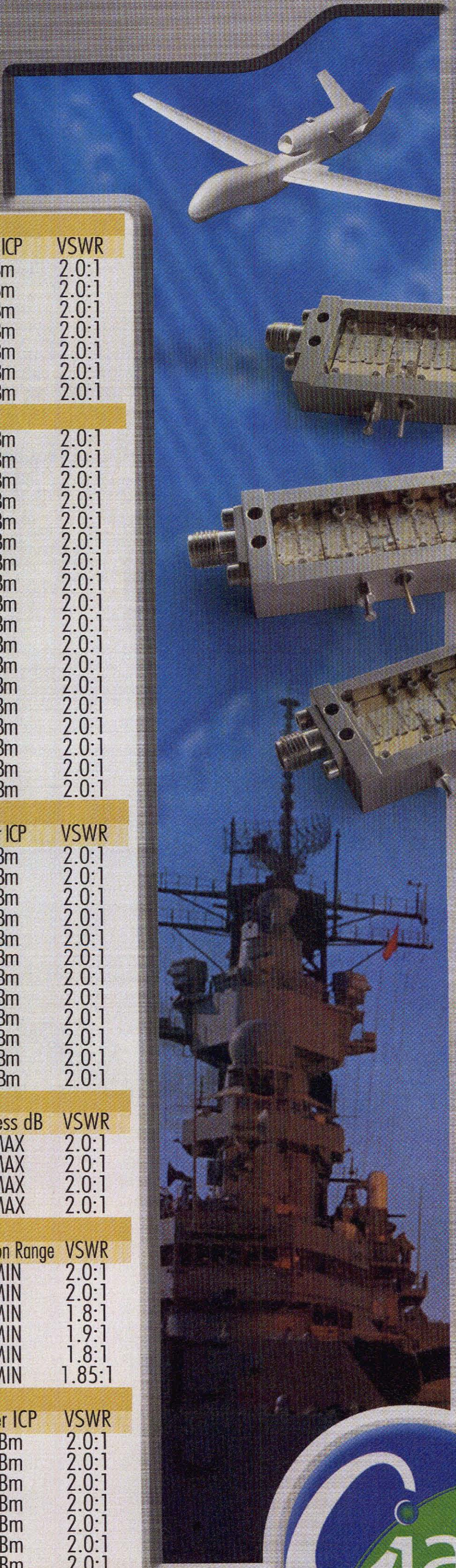

OCTAVE BAND LOW NOISE AMPLIFIERS

Model No.	Freq (GHz)	Gain (dB) MIN	Noise Figure (dB)	Power-out @ P1-dB	3rd Order ICP	VSWR
CA01-2110	0.5-1.0	28	1.0 MAX, 0.7 TYP	+10 MIN	+20 dBm	2.0:1
CA12-2110	1.0-2.0	30	1.0 MAX, 0.7 TYP	+10 MIN	+20 dBm	2.0:1
CA24-2111	2.0-4.0	29	1.1 MAX, 0.95 TYP	+10 MIN	+20 dBm	2.0:1
CA48-2111	4.0-8.0	29	1.3 MAX, 1.0 TYP	+10 MIN	+20 dBm	2.0:1
CA812-3111	8.0-12.0	27	1.6 MAX, 1.4 TYP	+10 MIN	+20 dBm	2.0:1
CA1218-4111	12.0-18.0	25	1.9 MAX, 1.7 TYP	+10 MIN	+20 dBm	2.0:1
CA1826-2110	18.0-26.5	32	3.0 MAX, 2.5 TYP	+10 MIN	+20 dBm	2.0:1

NARROW BAND LOW NOISE AND MEDIUM POWER AMPLIFIERS

Model No.	Freq (GHz)	Gain (dB) MIN	Noise Figure (dB)	Power-out @ P1-dB	3rd Order ICP	VSWR
CA01-2111	0.4 - 0.5	28	0.6 MAX, 0.4 TYP	+10 MIN	+20 dBm	2.0:1
CA01-2113	0.8 - 1.0	28	0.6 MAX, 0.4 TYP	+10 MIN	+20 dBm	2.0:1
CA12-3117	1.2 - 1.6	25	0.6 MAX, 0.4 TYP	+10 MIN	+20 dBm	2.0:1
CA23-3111	2.2 - 2.4	30	0.6 MAX, 0.45 TYP	+10 MIN	+20 dBm	2.0:1
CA23-3116	2.7 - 2.9	29	0.7 MAX, 0.5 TYP	+10 MIN	+20 dBm	2.0:1
CA34-2110	3.7 - 4.2	28	1.0 MAX, 0.5 TYP	+10 MIN	+20 dBm	2.0:1
CA56-3110	5.4 - 5.9	40	1.0 MAX, 0.5 TYP	+10 MIN	+20 dBm	2.0:1
CA78-4110	7.25 - 7.75	32	1.2 MAX, 1.0 TYP	+10 MIN	+20 dBm	2.0:1
CA910-3110	9.0 - 10.6	25	1.4 MAX, 1.2 TYP	+10 MIN	+20 dBm	2.0:1
CA1315-3110	13.75 - 15.4	25	1.6 MAX, 1.4 TYP	+10 MIN	+20 dBm	2.0:1
CA12-3114	1.35 - 1.85	30	4.0 MAX, 3.0 TYP	+33 MIN	+41 dBm	2.0:1
CA34-6116	3.1 - 3.5	40	4.5 MAX, 3.5 TYP	+35 MIN	+43 dBm	2.0:1
CA56-5114	5.9 - 6.4	30	5.0 MAX, 4.0 TYP	+30 MIN	+40 dBm	2.0:1
CA812-6115	8.0 - 12.0	30	4.5 MAX, 3.5 TYP	+30 MIN	+40 dBm	2.0:1
CA812-6116	8.0 - 12.0	30	5.0 MAX, 4.0 TYP	+33 MIN	+41 dBm	2.0:1
CA1213-7110	12.2 - 13.25	28	6.0 MAX, 5.5 TYP	+33 MIN	+42 dBm	2.0:1
CA1415-7110	14.0 - 15.0	30	5.0 MAX, 4.0 TYP	+30 MIN	+40 dBm	2.0:1
CA1722-4110	17.0 - 22.0	25	3.5 MAX, 2.8 TYP	+21 MIN	+31 dBm	2.0:1

ULTRA-BROADBAND & MULTI-OCTAVE BAND AMPLIFIERS

Model No.	Freq (GHz)	Gain (dB) MIN	Noise Figure (dB)	Power-out @ P1-dB	3rd Order ICP	VSWR
CA0102-3111	0.1-2.0	28	1.6 Max, 1.2 TYP	+10 MIN	+20 dBm	2.0:1
CA0106-3111	0.1-6.0	28	1.9 Max, 1.5 TYP	+10 MIN	+20 dBm	2.0:1
CA0108-3110	0.1-8.0	26	2.2 Max, 1.8 TYP	+10 MIN	+20 dBm	2.0:1
CA0108-4112	0.1-8.0	32	3.0 MAX, 1.8 TYP	+22 MIN	+32 dBm	2.0:1
CA02-3112	0.5-2.0	36	4.5 MAX, 2.5 TYP	+30 MIN	+40 dBm	2.0:1
CA26-3110	2.0-6.0	26	2.0 MAX, 1.5 TYP	+10 MIN	+20 dBm	2.0:1
CA26-4114	2.0-6.0	22	5.0 MAX, 3.5 TYP	+30 MIN	+40 dBm	2.0:1
CA618-4112	6.0-18.0	25	5.0 MAX, 3.5 TYP	+23 MIN	+33 dBm	2.0:1
CA618-6114	6.0-18.0	35	5.0 MAX, 3.5 TYP	+30 MIN	+40 dBm	2.0:1
CA218-4116	2.0-18.0	30	3.5 MAX, 2.8 TYP	+10 MIN	+20 dBm	2.0:1
CA218-4110	2.0-18.0	30	5.0 MAX, 3.5 TYP	+20 MIN	+30 dBm	2.0:1
CA218-4112	2.0-18.0	29	5.0 MAX, 3.5 TYP	+24 MIN	+34 dBm	2.0:1

LIMITING AMPLIFIERS

Model No.	Freq (GHz)	Input Dynamic Range	Output Power Range Psat	Power Flatness dB	VSWR
CLA24-4001	2.0 - 4.0	-28 to +10 dBm	+7 to +11 dBm	+/- 1.5 MAX	2.0:1
CLA26-8001	2.0 - 6.0	-50 to +20 dBm	+14 to +18 dBm	+/- 1.5 MAX	2.0:1
CLA712-5001	7.0 - 12.4	-21 to +10 dBm	+14 to +19 dBm	+/- 1.5 MAX	2.0:1
CLA618-1201	6.0 - 18.0	-50 to +20 dBm	+14 to +19 dBm	+/- 1.5 MAX	2.0:1

AMPLIFIERS WITH INTEGRATED GAIN ATTENUATION

Model No.	Freq (GHz)	Gain (dB) MIN	Noise Figure (dB)	Power-out @ P1-dB	Gain Attenuation Range	VSWR
CA001-2511A	0.025-0.150	21	5.0 MAX, 3.5 TYP	+12 MIN	30 dB MIN	2.0:1
CA05-3110A	0.5-5.5	23	2.5 MAX, 1.5 TYP	+18 MIN	20 dB MIN	2.0:1
CA56-3110A	5.85-6.425	28	2.5 MAX, 1.5 TYP	+16 MIN	22 dB MIN	1.8:1
CA612-4110A	6.0-12.0	24	2.5 MAX, 1.5 TYP	+12 MIN	15 dB MIN	1.9:1
CA1315-4110A	13.75-15.4	25	2.2 MAX, 1.6 TYP	+16 MIN	20 dB MIN	1.8:1
CA1518-4110A	15.0-18.0	30	3.0 MAX, 2.0 TYP	+18 MIN	20 dB MIN	1.85:1

LOW FREQUENCY AMPLIFIERS

Model No.	Freq (GHz)	Gain (dB) MIN	Noise Figure dB	Power-out @ P1-dB	3rd Order ICP	VSWR
CA001-2110	0.01-0.10	18	4.0 MAX, 2.2 TYP	+10 MIN	+20 dBm	2.0:1
CA001-2211	0.04-0.15	24	3.5 MAX, 2.2 TYP	+13 MIN	+23 dBm	2.0:1
CA001-2215	0.04-0.15	23	4.0 MAX, 2.2 TYP	+23 MIN	+33 dBm	2.0:1
CA001-3113	0.01-1.0	28	4.0 MAX, 2.8 TYP	+17 MIN	+27 dBm	2.0:1
CA002-3114	0.01-2.0	27	4.0 MAX, 2.8 TYP	+20 MIN	+30 dBm	2.0:1
CA003-3116	0.01-3.0	18	4.0 MAX, 2.8 TYP	+25 MIN	+35 dBm	2.0:1
CA004-3112	0.01-4.0	32	4.0 MAX, 2.8 TYP	+15 MIN	+25 dBm	2.0:1

CIAO Wireless can easily modify any of its standard models to meet your "exact" requirements at the Catalog Pricing.

Visit our web site at www.ciaowireless.com for our complete product offering.

Ciao wireless

Ciao Wireless, Inc. 4000 Via Pescador, Camarillo, CA 93012

Tel (805) 389-3224 Fax (805) 389-3629 sales@ciaowireless.com

Techniques for Making Measurements of Noise-Like Signals with a SPECTRUM ANALYZER

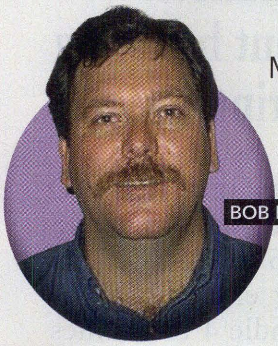

BOB NELSON

MANY OF TODAY'S COMMUNICATION FORMATS, such as W-CDMA, cdma2000®, and WLAN, produce signals that are noise-like in nature. Accurately measuring these types of signals requires tools and setups that are different than traditionally used for continuous-wave (CW) signals. In this web-exclusive article, Agilent Technologies' Bob Nelson examines the best approach for doing so.

To read the article in its entirety, *visit www.mwrf.com.*

VIDEO FOCUS: IMS2011

Held in Baltimore June 5 to 10, IMS2011 lived up to its billing as the must-attend microwave event of the year. But if you weren't able to make the trip to Charm City this time around, never fear: *Microwaves & RF's* correspondents were pounding the pavement, interviewing industry luminaries and getting the scoop on the hottest new product offerings. Visit www.engineeringtv.com to check out dozens of exclusive videos from the show floor.

engineering tv

Microwaves for the World
IMS2011 Baltimore

NEWS UPDATES Sent To Your Desktop

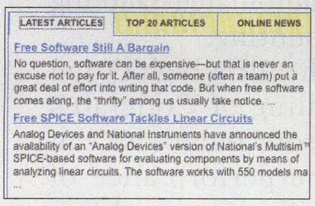

LATEST ARTICLES | TOP 20 ARTICLES | ONLINE NEWS

Free Software Still A Bargain

No question, software can be expensive—but that is never an excuse not to pay for it. After all, someone (often a team) put a great deal of effort into writing that code. But when free software comes along, the "thrifty" among us usually take notice. ...

Free SPICE Software Tackles Linear Circuits

Analog Devices and National Instruments have announced the availability of an "Analog Devices" version of National's Multisim™ SPICE-based software for evaluating components by means of analyzing linear circuits. The software works with 550 models ma ...

Don't believe everything you read, unless it's in the latest issue of *Microwaves & RF UPDATE.* The industry's longest-running weekly e-mail newsletter, it combines insightful commentary with the latest product and industry business news. It is sent directly to your computer desktop each week, and often contains the little things that engineers love, such as links to free white papers and even design software. If you're not already reading it, subscriptions are free, and available from the *Microwaves & RF* website at www.mwrf.com.

MWRF.com has archives of print and online articles dating back to October 2002. Visit MWRF.com today and click the "Back Issues" link. And while you're taking a look around the site, click on "Product Directory" to gain access to our complete directory of products and suppliers.

SHARE YOUR THOUGHTS with QUICK POLLS

Quick polls allow you to regularly share your opinion on a wide range of topics.

LATEST POLL RESULT:

Should the annual IEEE IMS Conference and Exhibition always be held within the United States' borders?

46% YES

36% NO

18% Doesn't Matter

NEW POLL QUESTION:

Will traditional radio architectures eventually be replaced by software-defined radios (SDRs) and cognitive radios?

YES NO

DON'T KNOW

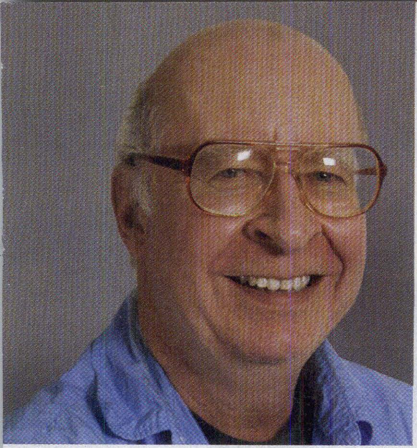

From the
Editor

Making More With Less

OWING ALMOST $16 trillion dollars can make even the most free-spending of governments more fiscally responsible. The Pentagon has been the beneficiary of 10 continuous years of military budget increases. But with planning for the Fiscal Year (FY) 2013 federal budgets coming during an election year, there is no doubt that the US Department of Defense (DoD) will have less operating capital next year. And less DoD dollars will directly translate into less RF and microwave dollars.

The DoD's budget accounts for about 20% of total annual federal spending, the impact of which can be readily seen in many of the catalogs and websites for companies throughout the RF/microwave industry. Affected products range from electronic components and modules for electronic-warfare (EW) and radar applications to devices for terrestrial and satellite-communications (satcom) systems.

Some of the reductions in defense spending will come from diminishing overseas operations (e.g., the wars in Iraq and Afghanistan). Overall, the Pentagon is planning for a year-over-year decrease in its FY2013 budget and, hopefully, the start of a trend that will result in about $487 billion in cuts over the next decade. The DoD goal is for a smaller, more-agile fighting force, with less fighter aircraft, ships, and fighting forces.

Politicians will argue that a defense force with so many fewer troops will be "toothless" when needed. But military professionals should take some comfort from the concept of more agile fighting forces, backed by judicious use of technology.

Scaled-back military budgets should not put an end to technology advancements at major contractors, but merely a rethinking of their approaches. Far-reaching and over-ambitious efforts should be replaced with more practical attempts to equip soldiers in the field with reliable and secure communications, EW, radar, and countermeasures systems. History has shown that almost any electronic product can be improved over time and made smaller and lighter and for less. The move towards using commercial-off-the-shelf (COTS) electronic components was a step in the right direction.

In addition, many of the technologies that military funding has helped to develop—such as software-defined radios (SDRs) and cognitive radios (CRs)—lend themselves to cost reductions over time by "borrowing" technology from leading computer chip manufacturers, without sacrificing the encryption security and in-the-field reliability that those radio technologies provide. Quite often, the DoD's Defense Advanced Research Projects Agency (DARPA) is viewed as a form of "cash channel" to different industries, including the RF/microwave industry, for technologies that may serve little purpose. But it should also be pointed out that DARPA's funding of this industry has enabled such technologies as GaAs MMICs, and GaN and SiC power transistors.

Cutbacks in the defense budget will no doubt impact some companies in this industry. But those same cutbacks will also mean opportunities for others, provided they are willing to work with defense contractors on finding the means to advance technology while also achieving cost reductions. MWRF

Jack Browne

Contributing Editor

MicroWaves&RF

THE FINAL ROUND

After I presented my position based on facts and experiments ("Feedback," March 2012), Mr.Monzello attacks again, without any facts to support his erroneous position. GPS and satellite systems all utilize superheterodyne receivers with noise figures significantly lower than 3 dB, which as Mr. Monzello repeats is "not possible." His own experiment results confirmed my position. How he knows what "is not disputed by the engineering community" I do not know, but his conclusion is plainly wrong.

JIRI POLIVKA

In a final response to Mr. Polivka, I would first like to clear up some fallacies that he continues to espouse. First, I do not, and have never been, in the business of selling analysis software. Like many, I have always enjoyed writing my own code to aid in my hardware design efforts. Second, I have never stated nor implied that you cannot achieve receiver noise figures less than 3 dB. By eliminating the image noise, or employing the proper circuit architecture, receiver noise figures of less than 1 dB are achievable. This can be accomplished by employing architectures such as DSB receivers, zero-IF receivers, and image reject filters and mixers.

Third, the Friis equation for cascaded two ports cannot be directly applied to receiver chains that do not eliminate the image band noise. The Friis equation may still be used if the proper effective noise figure is used to account for the noise contribution from the image band (see "Practical RF System Design," page 65, by William F. Egan). And lastly, the lab measurements I supplied to Mr. Polivka are clearly in agreement with the established theory as put forth in the article, and have been incorrectly interpreted by Mr. Polivka.

The theory of receiver noise figure degradation, due to image noise folding over into the IF band, is well established and thoroughly discussed in the literature. A list of some of the technical publications available that support this view are available upon request.

ROY MONZELLO

EDITOR'S NOTE

While all of us at *Microwaves & RF* appreciate the passion Mssrs. Polivka and Monzello have brought to this debate, we must eventually free our "Feedback" section for other contributors. Hence, we invited both authors to contribute their final comments on the subject, which are printed above. We would like to thank both Mr. Polivka and Mr. Monzello for their input during this exchange.

JACK BROWNE
TECHNICAL CONTRIBUTOR

SBIRS Stays The Course

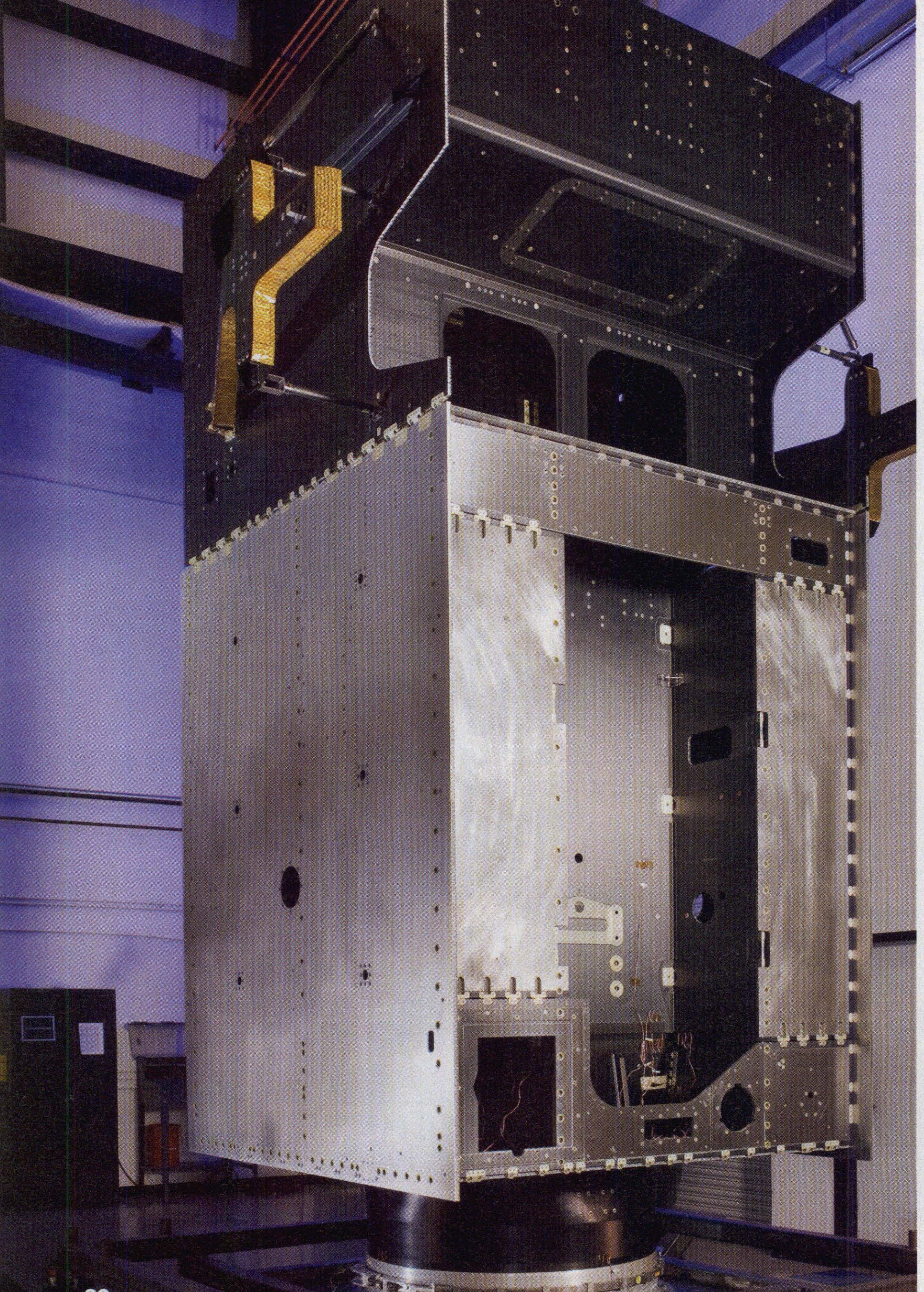

One of the United States' highest-priority space programs—the Space Based Infrared System (SBIRS)—recently hit another milestone toward completion.

THE CORE STRUCTURE OF THE US Navy's fourth SBIRS geosynchronous satellite (GEO-4) has been delivered to Lockheed Martin (www.lockheedmartin.com). A team of engineers and technicians at the company's Mississippi Space & Technology Center (Stennis, MS) will now integrate the spacecraft's propulsion subsystem.

Featuring a mix of GEO satellites **(see photo)**, four highly elliptical orbiting (HEO) payloads, and associated ground hardware and software, SBIRS is intended to bolster the nation's missile-warning capabilities. In addition, it will contribute to missile defense, technical intelligence, and battlespace awareness. The GEO-4 structure, which is identical to its three predecessor spacecraft, is made from lightweight, high-strength composite materials. It is designed to withstand the accelerations and vibrations generated during launch and support the spacecraft throughout on-orbit operations.

Once the Lockheed Martin team

Pictured is a core structure for a SBIRS geosynchronous (GEO) satellite, which is made from lightweight, high-strength composite materials. (Photo courtesy of Lockheed Martin)

has finished integrating the propulsion subsystem with the core structure, the module will be shipped to the company's facility in Sunnyvale, CA for final assembly, integration, and test. (That core is essential for maneuvering the satellite during transfer orbit to its final location, as well as for conducting on-orbit repositioning maneuvers throughout its mission life.) SBIRS GEO-4 is scheduled to be available for launch in 2015.

Lockheed Martin's SBIRS contracts include four HEO payloads; four GEO satellites; and ground assets to receive, process, and disseminate the infrared mission data. It is anticipated that funding for long-lead parts procurement for the fifth and sixth GEO satellites will be received by the end of the year. Under the Air Force's Overhead Persistent Infrared (OPIR) Space Modernization Initiative (SMI), Lockheed Martin also will develop technologies to improve capability and affordability for future SBIRS spacecraft.

The SBIRS team is led by the Infrared Space Systems Directorate at the US Air Force Space and Missile Systems Center (Los Angeles Air Force Base, CA). Lockheed Martin is the SBIRS prime contractor, while Northrop Grumman (www.northropgrumman.com) is the payload integrator. Air Force Space Command (Peterson Air Force Base, CO) operates the SBIRS system.

Radar System Tracks Test-Missile Stages

IN A RECENT DEMONSTRATION, the XSTAR instrumentation radar system successfully tracked both the launch and flight of a multi-stage test missile **(see photo)**. This system, which is the brainchild of General Dynamics (www.generaldynamics.com) and STAR Dynamics (www.stardynamics.com), promises to track and collect test data on one or more flying objects. Such objects require time, space, and position measurements used for system test and evaluation.

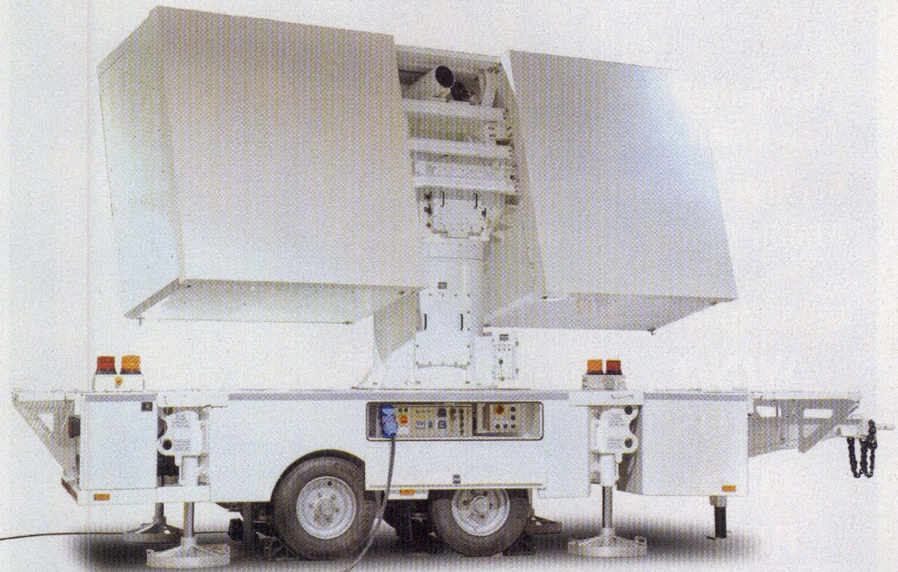

The XSTAR instrumentation radar system has demonstrated great potential for tracking high-speed flying objects. (Photo courtesy of STAR Dynamics)

For this particular demonstration, the XSTAR radar successfully tracked a test missile traveling more than 5000 mph through all three stages of deployment. The radar tracked and recorded the various stages of the missile's launch: the separation of the first- and second-stage boosters, the deployment of the payload, and the separation of debris from the missile.

The XSTAR radar system's design and software-based architecture incorporates commercial-off-the-shelf (COTS) equipment. As a result, individual systems can be customized based on a user's needs. They also can be cost effectively updated to accommodate evolving signal-processing technologies. For more information about the XSTAR radar system, visit www.gdc4s.com/Advanced-Radar-Systems.

MARKETWATCH

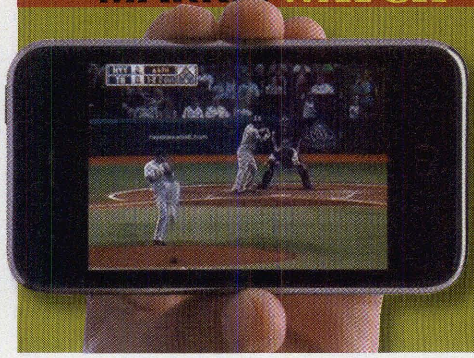

The number of streamed mobile TV users on smartphones will jump to 240 million by 2014

This increase will be driven by increased smartphone penetration as well as growth in the usage of Internet TV and Internet Protocol television (IPTV) services, according to a newly released report from Juniper Research (www.juniperresearch.com).

Teseq Announces IFI Acquisition

IN A MOVE INTENDED to broaden its product line in the RF-amplifier market, Teseq (www.teseq.com) has unveiled plans to acquire Ronkonkoma, NY-based Instruments for Industry (IFI; www.ifi.com). Established in 1953, IFI designs and manufactures RF and microwave, solid-state, and traveling-wave-tube amplifiers (TWTAs). Such offerings include tetrode tube, millimeter, pulsed, continuous-wave (CW), and combination amplifiers.

As a result of this deal, IFI's New York location will be integrated into the Teseq Group as its fourth competency center. The other competency centers are located in Luterbach, Switzerland; Berlin, Germany; and Ryde, Isle of Wight, United Kingdom. IFI will work in close cooperation with another recent Teseq acquisition, MILMEGA, at the Isle of Wight location. Moving forward, the new business unit will focus primarily on TWTs, class AB technology, and customer-specific models for the general amplifier and military markets.

All current IFI sales and distribution channels will have continued access to the IFI product range until the end of this year. Possible changes will be worked out by September. Teseq, Inc. will remain the sales, distribution, and service channel for both Teseq and MILMEGA products in North America.

Latest Wi-Fi Certification Rolls Out

WITH MORE THAN 1 BILLION Wi-Fi devices shipped in 2011 alone, it's indisputable that wires are ceding ground to this technology in the so-called "digital home." Indeed, ABI Research (www.abiresearch.com) predicts annual growth rate for Wi-Fi consumer devices over the next four years will exceed 30%.

The Wi-Fi Alliance (www.wi-fi.org), a non-profit industry association facilitating Wi-Fi adoption, certified almost 1500 digital home and mobile devices last year. Now, the organization is finalizing its certification program for Wi-Fi devices to support display applications. A new certification mark has been defined to designate these products: Wi-Fi CERTIFIED Miracast.

Devices bearing this designation make use of a Wi-Fi connection to deliver audio and video content from one device to another, without cables or a connection to an existing Wi-Fi network. These devices connect directly, enabling such tasks as watching videos from a smartphone on a big-screen television. Televisions, set-top boxes, handsets, and tablets are among the device types which will be certified. Wi-Fi CERTIFIED Miracast products will have implemented the Wi-Fi Alliance Wi-Fi Display Specification, and will have proven interoperability through laboratory testing.

Test Titan Announces Acquisition

ADDING TO ITS ALREADY diversified portfolio of technology holdings—among them, instrumentation, digital imaging products, and defense electronics—Teledyne Technologies (www.teledyne.com) has entered into a definitive agreement to acquire test and measurement house LeCroy Corp. (www.lecroy.com).

Per the agreement, Teledyne will acquire all of the outstanding common shares of LeCroy for $14.30 per share, payable in cash. The aggregate value for the transaction is approximately $291 million (taking into account LeCroy's stock options, stock appreciation rights, and net debt as of March 31, 2012).

The transaction was unanimously approved by the boards of directors of both companies. In addition, LeCroy directors and executive officers (including Founder Walter LeCroy) have agreed to vote their shares in favor of the transaction.

Founded in 1964 and headquartered in Chestnut Ridge, NY, LeCroy has approximately 500 employees worldwide. For its fiscal year ended July 2, 2011, the company posted sales of approximately $178.1 million. Consistent with Teledyne's acquisition history, LeCroy is expected to continue operating under its current leadership team as a relatively autonomous entity.

World IPv6 Launch Day Gets Backup

ON JUNE 6, numerous Internet service providers (ISPs), home-networking-equipment manufacturers, and Web companies all participated in World IPv6 Launch Day, transitioning their products and services over to the new IPv6 Internet protocol. Playing a key supporting role in this changeover was the Broadband Forum (www.broadband-forum.org), a non-profit industry organization that promotes improved broadband connectivity.

Last year, the Forum issued its BroadbandSuite 4.0 release (also known as the IPv6 Toolkit), a group of related specifications that enable the integration of the IPv6 addressing protocol into network and remote management platforms. Since BroadbandSuite 4.0's release, the group has focused on developing transition options for network operations, intended to aid their shift from the older IPv4 standard to IPv6. One document currently in development, "IPv6 Transition Mechanisms for Broadband Networks," will outline specific transition strategies. The text is expected to completed later this year, and will then be made publicly available.

PEOPLE

LOCKHEED MARTIN—Chairman and Chief Executive Officer Bob Stevens has announced his retirement as CEO effective January 1, 2013. Subject to election by shareholders and approval by the board of directors, Stevens will remain Chairman through January 2014. A 25-year veteran of the company, he was appointed to his present role in 2004. The board has chosen President and Chief Operating Officer Chris Kubasik to succeed Stevens as CEO. Kubasik has served with Stevens in the executive office of the Chairman since 2011. The board has also elected Marillyn A. Hewson, Executive Vice President of the Electronic Systems business area, to succeed Kubasik as President and COO.


HEWSON

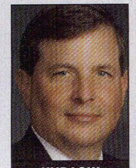
KUBASIK

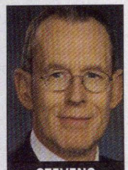
STEVENS

MICREL—Has promoted Robert Wahl to Managing Director of Worldwide Supply Chain Management and Backend Operations. In addition to the new position, Wahl will continue fulfilling the duties of his previous role as Director of the Global Supply Chain.

ROGERS CORP.—Has appointed Jeffrey Grudzien as Vice President of its Advanced Circuit Materials Division. Grudzien, who joined Rogers in 2000, most recently served as Vice President of Global Sales and Marketing.

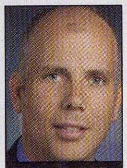
ARMSTRONG

SYMMETRICOM—Has appointed Dr. James Armstrong to the new role of Chief Technology Officer. Armstrong previously served as Executive Vice President and General Manager of the company's communications business segment.

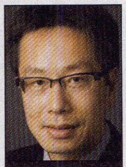
HSIEH

LITEPOINT—Richard Hsieh has joined the company as Vice President and General Manager of its Taipei-based Taiwan operations. Hsieh spent 12 years with LitePoint's parent company, Teradyne, in various roles—most recently as Taiwan Sales Director.

NATIONAL INSTRUMENTS—Has promoted Jin Bains to Vice President of Research and Development of RF products. Bains previously served as the company's Director of Research and Development.

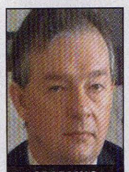
SPARLING

LINWAVE TECHNOLOGY—Has appointed Neil Sparling to the role of Technical Director. Sparling has extensive experience in both component and system design.


THOMPSON

MEMSSTAR—Has named Mike Thompson Chief Executive Officer. Thompson replaces interim CEO Peter Connock, who remains with the company as Chairman of the Board. Thompson previously served as Chief Technical Officer and Chief Operating Officer at Replisaurus Technologies.

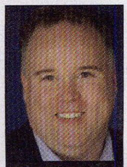
DOYLE

XMA CORP.—Has appointed James Doyle as the company's new President and Chief Executive Officer. Most recently, Doyle worked as the Congressional Affairs Liaison for Emerson Embedded Computing in Washington, DC.

KUDOS

INDIUM CORP.—Has been recognized for its support of SMTA China. The company was named 2012 Member Sponsor of the Year at SMTA China's Annual Recognition Ceremony, which took place during NEPCON China in Shanghai.

IEEE COMMUNICATIONS SOCIETY (COMSOC)—Is commemorating its 60th anniversary year. ComSoc has grown to more than 50,000 members. It now encompasses more than 200 international chapters and maintains working relationships with an additional 30 international societies.

LOCKHEED MARTIN—Marillyn A. Hewson, Executive Vice President of the Electronic Systems business area, has been awarded the United Service Organizations' (USO's) 2012 Woman of the Year Award for non-military leaders.

INTERPLEX ELECTRONIC (HANGZHOU)—Has received First-Class Enterprise certification for export industries—a designation awarded by the Entry-Exit Inspection and Quarantine Bureau of Zhejiang province, China.

IEEE—Jack H. Winters and Andreas F. Molisch have been awarded the 2012 IEEE Eric E. Sumner Award. Sponsored by Alcatel-Lucent Bell Labs, the award recognizes both engineers for contributions to the theory and application of multiple-antenna systems in wireless communications.

AT4 WIRELESS—Noemi Perez, one of the company's Bluetooth Qualification Experts, has been recognized by the Bluetooth Special Interest Group (SIG) as the Outstanding Qualification Expert for 2011.

ARMMS—At the April meeting of the organization's RF & Microwave Society, Robert Smith of Cardiff University and Stephen Russell of Glasgow University received the newly introduced Young Engineer prize. Smith was recognized for his work on the push-pull configuration at microwave frequencies, with Russell's focused on transistors fabricated from diamond. In addition, Charles Suckling of TriQuint was the receipient of the Steve Evans-Pughe memorial prize for best paper. Suckling's work addressed thermal modelling of gallium-nitride (GaN) devices.

CARLISLE INTERCONNECT TECHNOLOGIES—The company's interconnect division, located in El Segundo, CA, has been named a recipient of the 2011 Boeing Performance Excellence Award. This is the third consecutive year that Carlisle has won the award.

DIGI-KEY—Has been named one of Emerson Connectivity's 2011 Top Distributors. The award was presented May 8 during the Electronic Distribution Show in Las Vegas, NV.

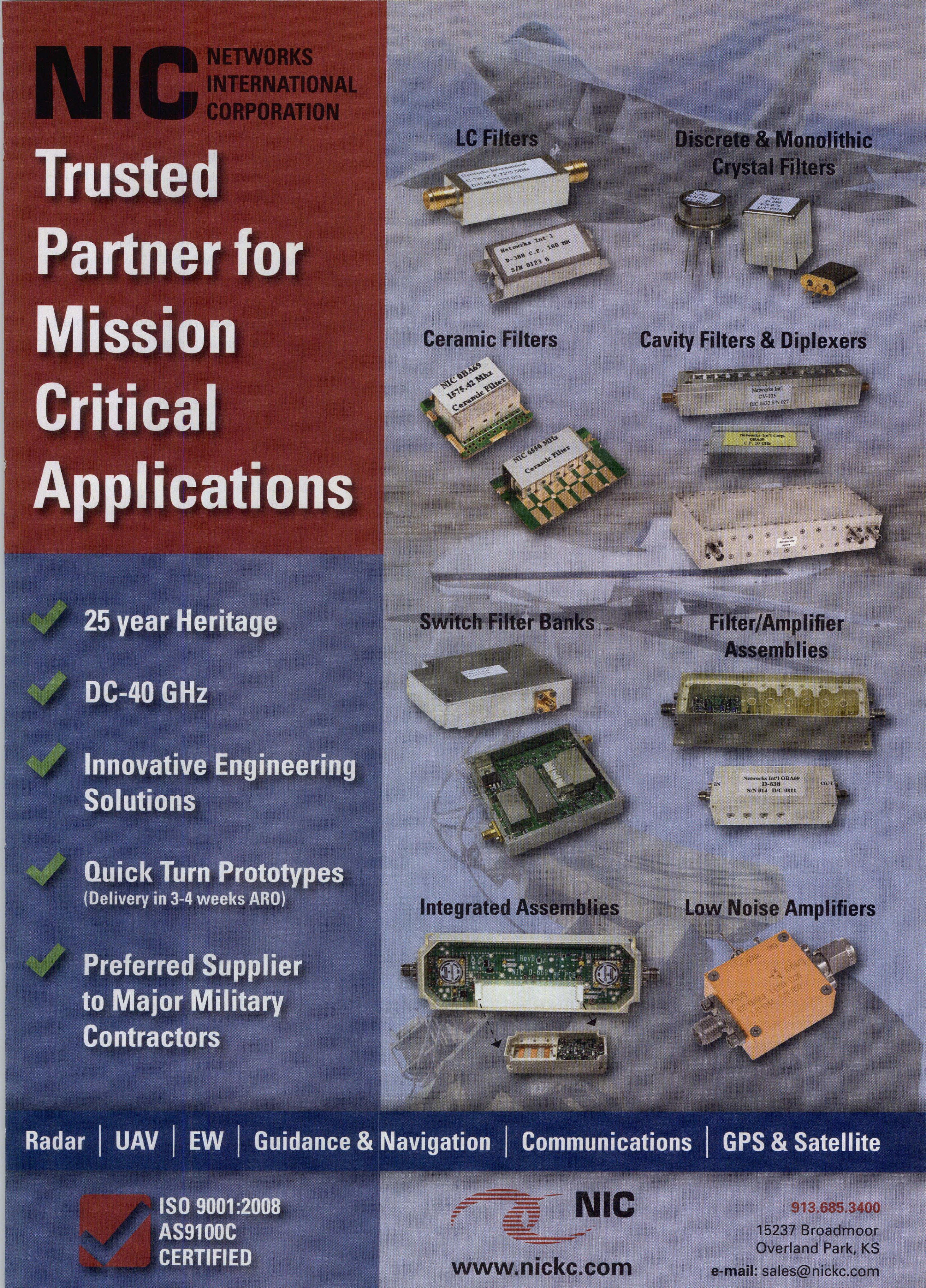
NIC NETWORKS INTERNATIONAL CORPORATION
Trusted Partner for Mission Critical Applications
25 year Heritage
DC-40 GHz
Innovative Engineering Solutions
Quick Turn Prototypes
(Delivery in 3-4 weeks ARO)
Preferred Supplier to Major Military Contractors
LC Filters
Discrete & Monolithic Crystal Filters
Ceramic Filters
Cavity Filters & Diplexers
Switch Filter Banks
Filter/Amplifier Assemblies
Integrated Assemblies
Low Noise Amplifiers
Radar | UAV | EW | Guidance & Navigation | Communications | GPS & Satellite
ISO 9001:2008
AS9100C
CERTIFIED
NIC
www.nickc.com
913.685.3400
15237 Broadmoor
Overland Park, KS
e-mail: sales@nickc.com

FRESH STARTS

AVX Corp.—GAM Technology, the first tantalum smelter to achieve EICC/GeSI Conflict-Free Smelter validation, has joined the company's Solutions for Hope Project. GAM Technology will process the fourth shipment of validated conflict-free tantalite ore mined in the Democratic Republic of the Congo (DRC).

W.L. Gore & Associates—Has developed new testing protocols for the acoustic vents (used for water and particulate protection) found in portable electronic devices. These new protocols were developed to more effectively match real-life environmental conditions. In addition, the company has created a new business unit, GORE Portable Electronic Vents (PEV). This unit will develop solutions to protect devices from water, dust, and dirt ingress.

Digi-Key—Has launched www.digikey.co.il, a website servicing the Israeli market. The site can be viewed in both Hebrew and English. It provides local customer and engineering support.

National Technical Systems (NTS)—Is now offering a comprehensive certification program for Smart Energy devices. The program is comprised of three parts: iSmart (focusing on interoperability testing), rSmart (focusing on RF performance), and sSmart (focusing on security).

General Dynamics—Has announced plans to acquire IPWireless, Inc. The transaction is expected to be completed in the third quarter of this year.

On Track Innovations (OTI)—Has received an order for 30,000 near-field-communication (NFC) and contactless payment readers to be deployed across the US.

CST and Delcross—Per a distribution agreement, CST will become an authorized reseller of Delcross' Electromagnetic Interference Toolkit (EMIT) in North America.

Wireless Power Consortium—Würth Elektronik has joined the organization. The firm is currently developing transformers and storage chokes that will be used on both the primary and secondary side of wireless-charging systems.

Northrop Grumman—To take advantage of pending ground-based radar opportunities in Indonesia, the firm is collaborating with PT Industri Telekomunikasi Indonesia and the Research Centre For Electronics And Telecommunications of the Indonesian Institute Of Sciences.

Lockheed Martin—Has delivered its 100th and 101st commercial geostationary communications satellites—a precursor to the first dual launch of satellites built by the company aboard an Ariane rocket. The JCSAT-13 was built for SKY Perfect JSAT Corp. while the VINASAT-2 was manufactured for Vietnam Posts and Telecommunications Group (VNPT).

China GrenTech—Has completed its previously announced merger with Talenthome Management and its Xing Sheng Corp. subsidiary. As a result, Talenthome Management has become a wholly owned subsidiary of China GrenTech.

TowerJazz—Has transferred its CMOS-image-sensor (CIS) technology from its Migdal Haemek, Israel facility to its Newport Beach, CA fab. Intended for digital-imaging applications, the CIS process enables the customization of pixels.

Nujira—Has filed its 150th patent related to envelope-tracking (ET) technology. This milestone comes 12 months after Nujira reached the 100 patent mark in April 2011.

Spacek Labs—Has appointed The Thorson Co., based out of Signal Hill, CA, as its sales representative in Southern California.

CONTRACTS

RAYTHEON Wins Contract Modification

LOCKHEED MARTIN Scores Dual Armed Forces Deal

Megaphase—Planetary Resources, which plans to mine near-Earth asteroids for raw materials, will utilize the company's GrooveTube cable assemblies. Megaphase's cables were previously used by the Japanese Hayabusa space probe. That probe was tasked with capturing asteroid particles.

Agilent—The company's Advanced Design System (ADS) software has been selected by ADATA Technology Co., a Taipei, Taiwan-based developer of memory modules.

Texas Instruments (TI) and PureWave Networks—Have collaborated on the PureWave Constellation, a family of Long-Term-Evolution (LTE) small-cell base stations. TI contributed KeyStone-based wireless-infrastructure systems-on-a-chip (SoCs) to the effort.

Altair Semiconductor—The company's Hornet TD-LTE chipset has been selected by Olive Telecom, an India-based developer of Long-Term-Evolution (LTE) -enabled products. The chipset was only recently introduced to the Indian market.

Raytheon Co.—Has been awarded a $106.4-million contract modification by the US Navy. The previously awarded contract was for the production of Aegis-related equipment, including the AN/SPY-1(D)V radar transmitter and MK99 Mod 14 Fire Control System.

Lockheed Martin—Has been awarded a $1.05-billion, five-year contract by the US Navy. Lockheed Martin will provide more than 200 digital cockpits and integrated mission systems and sensors for the MH-60R "Romeo" and MH-60S "Sierra" helicopters. In addition, the company has been awarded $391 million in production orders by the US Army for a new radar system. This system is intended to provide soldiers with enhanced 360-deg. protection from rocket, mortar, and artillery fire.

Murata—Has selected Black Sand Technologies to provide silicon power-amplifier (PA) technology, which will be utilized for integrated RF front-end products. These products will be used to increase the integration of Third-Generation (3G) smartphones, tablets, and datacards.

ANADIGICS—Is shipping production volumes of its AWT6621 HELP4 PA to NEC Casio Mobile Communications. The PAs are intended for the MEDIAS IS11N smartphone.

ASC Signal—Will be providing a significant number of Ka-band antennas to a European satellite operator. With uniquely designed sub-reflector-tracking (SRT) technology, the antennas claim to provide a heightened level of tracking accuracy and gain stability compared to other antennas in this category.

Magal Security Systems—Has secured two contracts to supply and install multi-layer Perimeter Intrusion Detection Systems (PIDS) in two new prisons in Latin America. The contracts total $2.5 million.

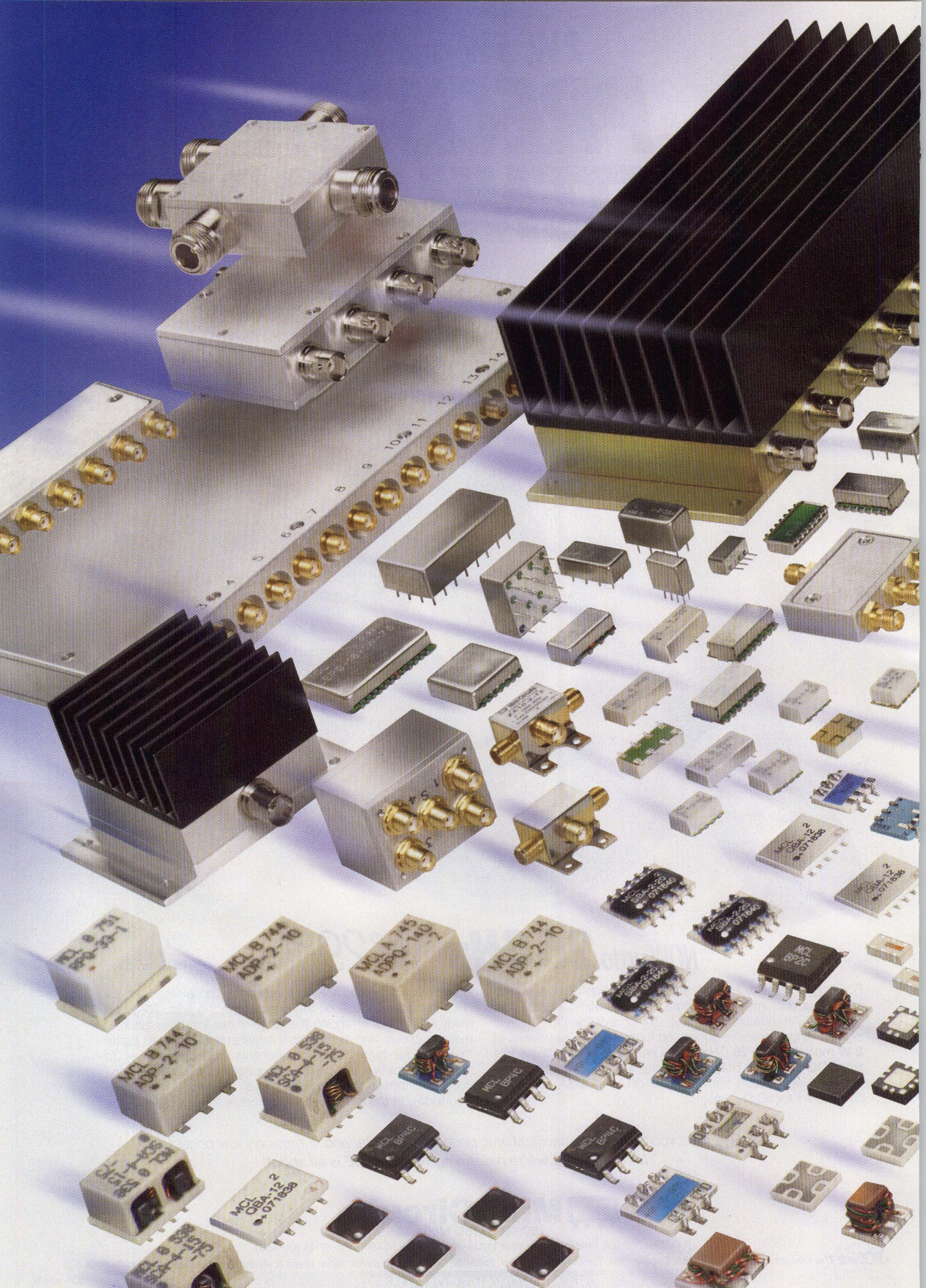
MCL B 744
ADP-2-10
MCL
QBA-12
071838

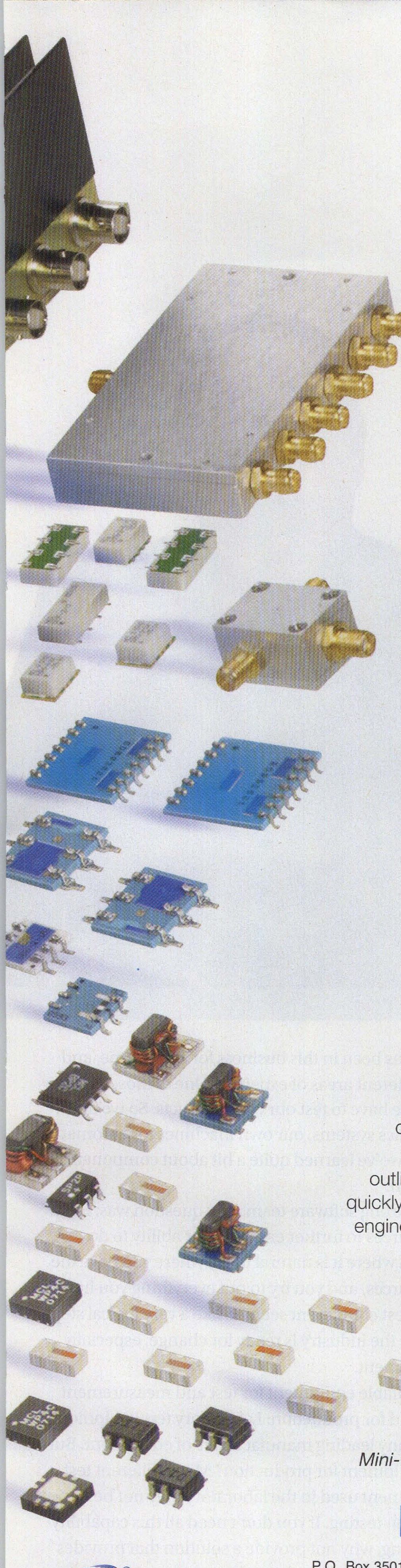

Inside Track with Harvey Kaylie, PRESIDENT, MINI-CIRCUITS

Interview by JACK BROWNE

JB: This past January, we ran a Cover Feature on the MAC series mixers, a line of hermetically sealed mixers based on low-temperature-cofired-ceramic (LTCC) technology. How have they done so far commercially?

HK: The MAC mixers are intended for military applications and anywhere high reliability is important, such as in test equipment. In fact, one of our customers who manufactures test equipment had equipment failures. It turned out the equipment was used in a high-humidity industrial environment. We switched over to a hermetic ceramic package and the failures went away. That is just one example of where hermeticity made a difference in reliability.

Whenever you introduce a new product, the customers go through an evaluation phase. Customers will buy a small quantity for evaluating performance. We have been fortunate to see a good response from many of our customers. They are recognizing that the reliability, performance, and very attractive price of the MAC series provide real value to them. The other big deal about these new mixers is the operating temperature range and size. These are tiny rugged mixers only 0.06 inches high. We have operated them without failures at temperatures up to +125°C for 1000 hours.

JB: So, it is normal with a new product to take some time to gain traction in the industry?

HK: It has to take time—this is our experience. But these low-cost hermetic mixers are going to be around for a long time. In my opinion, this is a "right on" product that meets both existing and emerging needs.

JB: Some people have an impression of Mini-Circuits as simply a "components company." But obviously, the company is changing over time. The power sensors, the moves into test products...what got you started in these different directions?

HK: Mini-Circuits has been in this business for a long time, and we have built up different areas of expertise. One of those areas is in testing, since we have to test our own products. So we developed our own robotics systems, our own machines for automated testing, etc. And we've learned quite a bit about components and how to test them.

We also have a strong software team. The question was: How do we use our resources to further enhance our ability to do business? So you go where it is natural to go, where you have the talent and the resources, and you try to put everything you have together. Portable test equipment seemed like a very logical step for us. And I believe the industry is ready for change, especially in test and measurement.

We looked at available equipment for test and measurement in the laboratory and for production. Laboratory test equipment is well served by many leading manufacturers of equipment. But what about test equipment for production? Many different test functions for equipment used in the laboratory may not be necessary for production testing. If you don't need all this capability for production testing, why not provide a solution that provides value to the customer? We know the business because we are testing our own components. So we understand where there is and isn't value in equipment functions used for production testing.

For example, we developed a power sensor that when used with a personal computer (PC) turns into a smart power meter. Why do we call it a "smart" power meter? If you look at a traditional power meter, it is simply a power meter and you use it to measure power. I consider that the "dumb" part. But a smart power meter should be able to do a lot more.

Sometimes you are in a noisy environment, where the value of a measurement can change from one instant to the next. So we take many measurements and average them, and we get pretty good results. You can take as many as 100 measurements and get an average. So now the accuracy will improve. Secondly, we use power meters for burn-in and life testing. Wouldn't it be great if you could continuously monitor measurements over the entire test period and review the data every 15 minutes automatically to look for variations? Our smart power meter software can easily produce a plot showing variations in power over time.

The third is to allow users to remotely monitor a circuit or system and, if a problem is detected, it can send a warning signal over the Internet. These are new features that make the power meter smart. Sometimes when you are measuring the gain of an amplifier, and you have attenuators in the transmission path, you would like to have the attenuation contribution subtracted from the measurements. The power meter provides an offset function that allows the user to zero out the attenuation and measure gain directly.

JB: Mini-Circuits has always offered tremendous quality for the price, and this is apparently part of the set of guiding principles for this company. Can you describe briefly those guiding principles?

HK: Our guiding principles come from seeing things as our customers see them. When I buy something, I expect it to work for its intended use and for as long as I need it. Some people might say that kind of thinking is like Pollyanna, but I don't believe that. You have to be smart when you take this approach. Every manufacturer will tell you that they have products that have good quality, but what are you really doing to make it happen?

So one of the things we learned very early, starting with the Motorola Six Sigma quality program, is that variation is a key factor. So in everything we do, we design it to reduce variation. For example, we previously used toroidal cores to manufacture transformers. But, because the shape is circular, there is no reference point for placement of the wire windings. We switched over to rectangular or square transformer cores, so we were able to define the wire positions during winding. It is a question of designing to reduce variation.

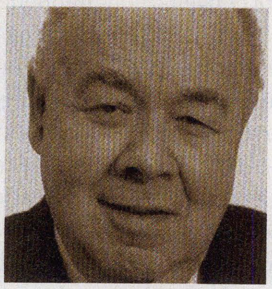

"We try to look at reliability from the perspective that we are not to give a customer a headache."

We talk about Skinny Sigma and Fat Sigma. We want Skinny Sigma. So all of our testing—everything we do—we compare to previous production runs, we look at variation, and we use this as a monitor to see that the present run is within well-controlled limits. But we make a big effort to reduce variation in all our processes. We went to component attachment by means of welding rather than soldering because it results in greater precision, reducing variation from different solder heights. Some may say that striving for this greater precision must be more expensive. The truth is, it is less expensive.

We also pay great attention to materials and components at incoming inspection, with the goal of minimizing variation. Even with our marking methods, we strive for consistency. We used to use engraving or ink stamping. Now we use laser marking because it is very legible, it's fast, and you can't rub it off. We continue to invest in order to reduce variation and to establish process monitors in order to be able to measure our quality. And I have to tell you, it pays off big-time.

If you think of the number of units that pass through our manufacturing, we are talking between 50 and 100 million pieces every year. What kind of rejects can you expect to get? If we have 1% rejects, we are out of business. Even one-tenth of a percent—we couldn't handle it. We work with defects measured in parts per million. Whenever there is a variation issue, we put engineering, quality assurance, and the whole team to find the cause and solution, because we don't want rejects at all.

Consider semiconductor manufacturing and qualification. Everybody accepts 1000 hours for life testing. We perform 5000 hours for life testing on semiconductors. Why? Because we saw that sometimes after 1500 hours or 2000 hours, you can get rejects. So, do you ask the customer, "Would you be happy if the part lasts 1000 hours and then we don't know what's going to happen?" The customer doesn't want to have a problem at all. We try to look at reliability from the perspective that we are not to give a customer a headache. And the only way to make it happen is to do a tremendous amount of testing, provide quality control of our processes, and continuously make improvements to our processes and material control to reduce Sigma by getting smarter and tighter.

Even if there isn't a problem, if we see a way to tighten up a process, we will tighten it up. My philosophy is that if we test 100 units and they all pass, but one is marginal, I would rather throw away that one and sell the 99. Because the question that will always come up is, "Why was it a little bit different than the rest?" And most of the time, you don't know. And if you don't know, there is an uncertainty. And if you eliminate uncertainty, then you get better quality. MWRF

Editor's Note: To read MWRF's interview with Harvey Kaylie in its entirety, be sure to check out the online version of this article at www.mwrf.com.

CMOS RF FRONT END Improves Universal-Tuner Performance

DUE TO THE wideband nature of broadcast signals, local-oscillator (LO) mixing problems arise with odd harmonic frequencies. Such issues are not considered in the design of conventional narrowband receivers. Yet this odd harmonic mixing poses a serious problem, as the undesired channels are aliasing into the desired channel. As a result, the receiver's signal-to-noise ratio (SNR) is degraded. For universal tuners, a wideband, highly linear, low-noise CMOS RF front end has been proposed by Donggu Im and Kwyro Lee from the Korea Advanced Institute of Science and Technology together with Hongteuk Kim from Seoul's LG Electronics Institute of Technology.

Their front end comprises an inductorless, wideband low-noise amplifier (LNA), integrated passive tunable filter, harmonic rejection mixer (HRM), and loop-through amplifier. This LNA shows a gain control range beyond 55 dB with a gain step of 0.5 dB or better while achieving higher linearity and a lower noise figure. For its part, the tunable filter covers the very-high-frequency (VHF) bands entirely without dividing the frequency range by multiple filters. Because the tunable filter and HRM work together, an overall harmonic rejection ratio (HRR) above –65 dBc is reached.

The researchers proposed an active-feedback loop-through amplifier (LTA) through a complementary source follower (CSF). The proposed RF front end achieves voltage gain to 42 dB with a minimum noise figure of 4.7 dB. It achieves a high second-order and third-order input intercept point with low power consumption. See "A Broadband CMOS RF Front-End for Universal Tuners Supporting Multi-Standard Terrestrial and Cable Broadcasts," *IEEE Journal Of Solid-State Circuits*, Feb. 2012, p. 392.

VCO FREQUENCY-CALIBRATION APPROACH Delivers Speed And Accuracy

IN MULTIBAND, multimode RF transceivers, engineers often opt to use a single, wideband phase-locked-loop (PLL) synthesizer. Before the PLL's closed-loop locking process begins, voltage-controlled-oscillator (VCO) frequency calibration is used to find the closest sub-band turning curve to a target frequency. A method that is suitable for $\Delta\Sigma$ fractional-N synthesizers is now being reported by Jaewook Shin from the University of California in Los Angeles and Hyunchol Shin from Seoul's Kwangwoon University.

Typically, a PLL synthesizer's wide tuning range is realized by employing an LC-tuned VCO with a switched capacitor bank. This approach suffers drawbacks, however—particularly when the required tuning range grows wider. Many therefore opt for the fast and accurate auto-calibration of the VCO frequency and loop bandwidth. The approach presented in this project is mainly based on a high-speed frequency-to-digital converter (FDC), which detects the VCO frequency on chip. That information is then used to calibrate the VCO frequency and loop bandwidth.

Essentially, the loop-bandwidth calibration circuit measures the VCO gain. It then uses it to control the charge-pump current. For the VCO frequency calibration, a minimum error-code finding block improves the calibration accuracy by finding the code that is closest to the target frequency.

The researchers implemented a 1.9-to-3.8-GHz $\Delta\Sigma$ fractional-N synthesizer in 0.13-μm CMOS. In doing so, they were able to demonstrate that the loop-bandwidth calibration is completed in 1.1 to 6.0 μs with ±2% accuracy. See "A 1.9-3.8 GHz $\Delta\Sigma$ Fractional-N PLL Frequency Synthesizer with Fast Auto-Calibration of Loop Bandwidth and VCO Frequency," *IEEE Journal Of Solid-State Circuits*, March 2012, p. 665.

Differential DCXO Boasts Sine-Wave Outputs

TO ALLEVIATE issues like spurious noise and crystal resonator harmonics, a differential digitally controlled crystal oscillator (DCXO) with sine-wave outputs may present a suitable option for cellular applications. A signal-shaping technique was recently used to produce a 26-MHz differential DCXO. This oscillator, which is the brainchild of a team of engineers from Broadcom Corp., inhabits a total silicon area of 0.15 mm^2. It offers a fine-tuning range of ±44 ppm while providing about 14 b of resolution and an average step size of 0.005 ppm. The DCXO frequency-tuning function is provided by two banks of identical capacitor arrays.

All of the device's signals that connect externally to input/output (I/O) pins are sine waves. Because the DCXO core generates a pair of true differential sine waves, neighboring I/O pins experience the coupled crystal-signal amplitudes with opposite polarity.

Fabricated in 65-nm CMOS, the 26-MHz DCXO provides phase noise of –149.1 dBc/Hz at 10-kHz offset. The team has measured typical frequency pulling of 0.01 ppm, which arises from turning the sine-wave buffer on and off. The DCXO dissipates 1.2 mA of current. See "A Differentially Digitally Controlled Crystal Oscillator with a 14-bit Tuning Resolution and Sine-Wave Outputs for Cellular Applications," *IEEE Journal Of Solid-State Circuits*, Feb. 2012, p. 421.


A
1 COM 2
D
B
C
Mini-Circuits
USB-4SPDT-A18
DC-18 GHz

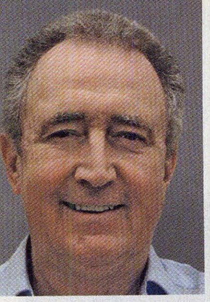

Microwaves in Europe

PAUL WHYTOCK, *European Editor*

Test And Chip Breakthroughs Create Smaller, Faster, More Dependable Consumer Products

WIRELESS CONSUMER-ELECTRONIC products increasingly include data-intensive applications. Meanwhile, applications below 10 GHz—such as wireless local-area networking (WLAN)—face spectrum scarcity. Consequently, wireless-system designers have to explore higher frequency bands, such as the unlicensed band around 60 GHz. This band is available globally and enables multi-gigabit/second wireless communication over short distances. To make 60-GHz radio solutions a realistic proposition, however, cost, size and power consumption need to be reduced. Belgian research center Imec (www.imec.be) and Japanese conglomerate Panasonic (www.panasonic.com) believe that their ultra-low-power CMOS-based solution is a step toward solving these problems.

The transceiver chip is capable of data rates to 7 Gb/s over short distances. It achieves its performance capability via the four channels specified by the IEEE 802.11ad standard. For example, the transceiver front-end prototype achieves an error vector magnitude (EVM) beyond –7 dB for 16-state quadrature amplitude modulation (16QAM) in the four channels specified by that standard. The transmitter signal path [consisting of a power amplifier (PA) and mixer] consumes 90 mW with +10.2 dBm output power at 1-dB compression. The receiver signal path, which comprises a low-noise amplifier (LNA) and mixer, consumes 35 mW with a noise figure of 5.5 dB and 30 dB gain. The chip survives electrostatic discharge (ESD) of more than 4 kV based on the human body model (HBM).

The integrated circuit (IC) is fabricated in 40-nm, low-power digital CMOS. With a core area of 0.7 mm^2, this transceiver front-end solution is suitable for use in phased antenna arrays. Chip area is kept low with the use of lumped components—even at 60 GHz—in conjunction with compact, millimeter-wave, CMOS layout techniques.

SET-TOP BOXES, tablet personal computers (PCs), and smartphones boast digital video interfaces, such as the high-definition multimedia interface (HDMI) and mobile high-definition link (MHL). These interfaces need to be tested for functionality and compliance, which is the goal of the newly developed video test center (VTC) from Rohde & Schwarz (www.rohde-schwarz.com). This entirely modular platform provides real-time protocol and media-content analysis **(see photo)**. It can be modified to meet the requirements of specific test environments. The platform also can be upgraded to comply with new standards.

The test center accommodates up to eight test modules. Separate options are available for the HDMI and MHL interfaces. In combination with the HDMI options, the VTC performs real-time analyses of video and audio parameters as well as information frames. To test sources and sinks, it can perform system protocol tests in line with the latest HDMI-compliance test, specification 1.4c.

This newly developed video test center can test both the functionality and compliance of digital video interfaces, which are found in products ranging from set-top boxes to tablet PCs and smartphones.

Also targeting MHL and HDMI signals are options for the automatic analysis of media content. The R&S VT-K2100 video-analysis option measures the timing and level of each video signal component in real time. In doing so, it makes it possible to verify whether color transmission is correct. The R&S VT-K2110 AV inspection and R&S VT-K2111 AV distortion-analysis options assist users in performing picture-difference analyses. In addition to the graphical result display, objective measured values like PSNR, SSIM, and MOS are displayed in real time. Bit errors in video content, for example, also can be identified. One option even includes a conclusive audio-analysis function. The R&S VTC identifies key parameters, such as audio level and frequency response.

The VTC has an 11-in. touchscreen. It also can be operated remotely via LAN using a PC or tablet. The VXI-11 interface allows the device to be integrated into automated test setups. The VTC and the VT-B2360/2361 HDMI RX options—as well as all software options—will be available this August. Currently, Rohde & Schwarz is developing an analog audio/video interface module and a modulator module for broadcasting standards.

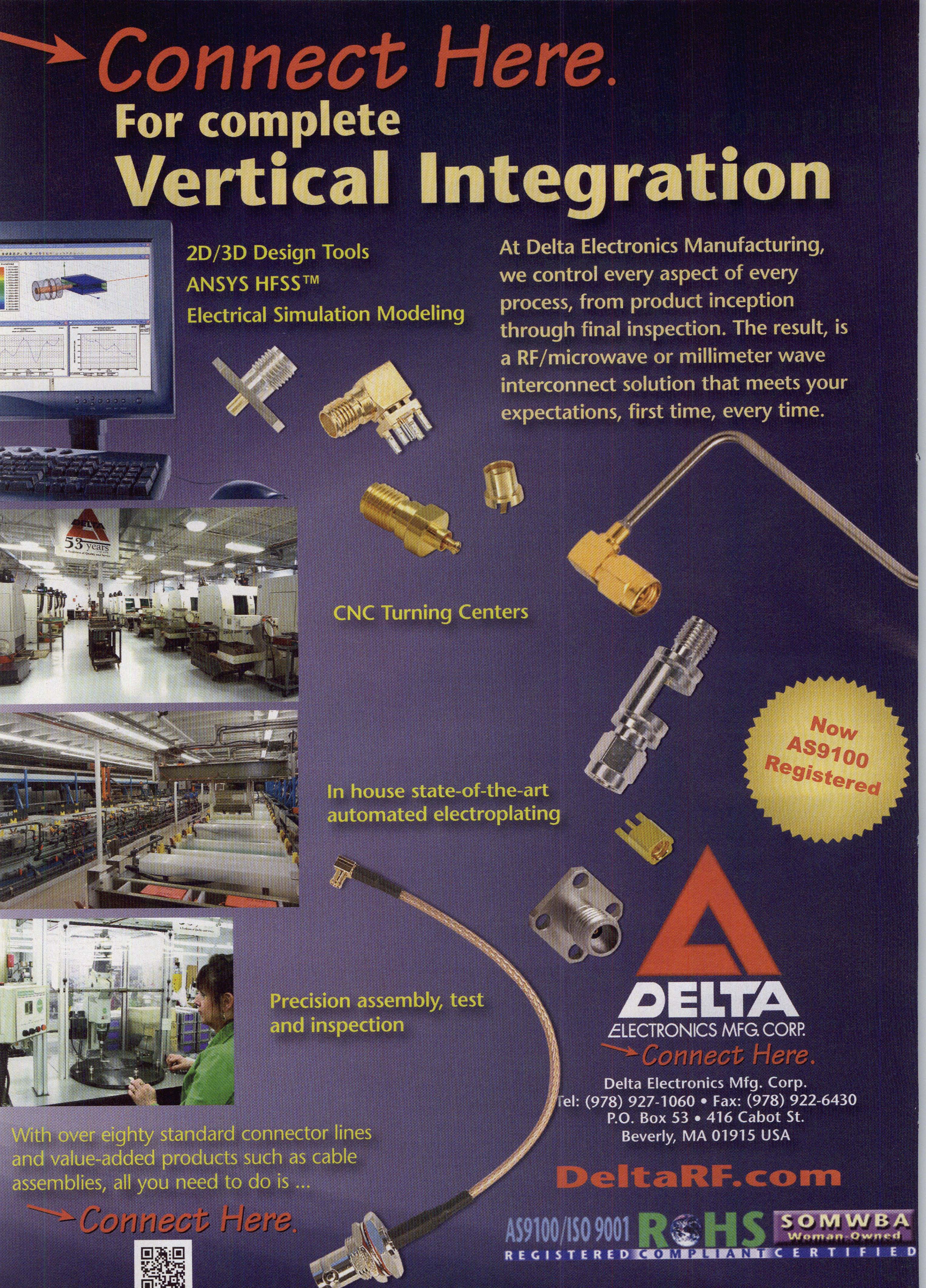
Connect Here.
For complete
Vertical Integration
2D/3D Design Tools
ANSYS HFSS™
Electrical Simulation Modeling
At Delta Electronics Manufacturing, we control every aspect of every process, from product inception through final inspection. The result, is a RF/microwave or millimeter wave interconnect solution that meets your expectations, first time, every time.
53 years
CNC Turning Centers
Now AS9100 Registered
In house state-of-the-art automated electroplating
Precision assembly, test and inspection
DELTA
ELECTRONICS MFG. CORP.
Connect Here.
Delta Electronics Mfg. Corp.
Tel: (978) 927-1060 • Fax: (978) 922-6430
P.O. Box 53 • 416 Cabot St.
Beverly, MA 01915 USA
With over eighty standard connector lines and value-added products such as cable assemblies, all you need to do is ...
Connect Here.
DeltaRF.com
AS9100/ISO 9001 REGISTERED
RoHS COMPLIANT
SOMWBA Woman-Owned CERTIFIED

JACK BROWNE | Technical Contributor

Radar Systems

Ride Device Advances

EFFORTS TO MAKE A WIDE ARRAY OF MILITARY AND COMMERCIAL RADAR SYSTEMS SMALLER, LIGHTER, AND LESS EXPENSIVE DEPEND LARGELY ON INCREASED DIGITAL PROCESSING AND HIGHER LEVELS OF ANALOG INTEGRATION.

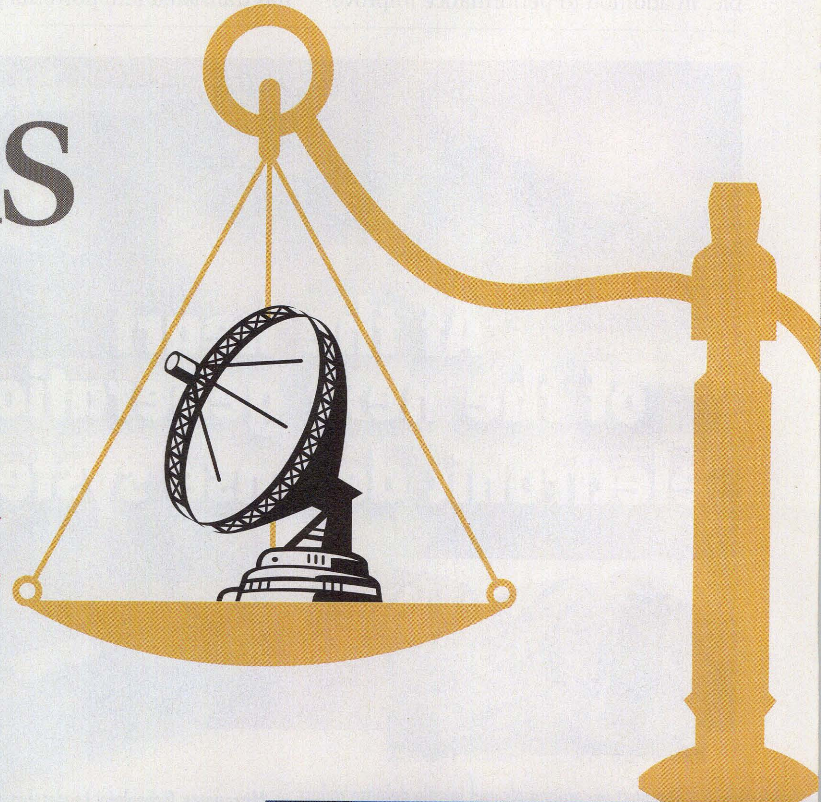

RADAR SYSTEMS HAVE REPRESENTED A VITAL CORE MARKET AREA for the RF/microwave industry since before there even was an industry—beginning around 1939 with the invention of the cavity magnetron. Once suitable signal power levels were available from that and succeeding device technologies, the simple idea of transmitting a high-frequency signal and measuring reflected return signals gave birth to what would become present-day radar technologies. Today, these are used for everything from automotive collision-avoidance systems to weather and weapons detection. And as practical uses for radar technologies continue to expand, the effects are felt throughout the industry.

For example, avionics and satellite-communications (satcom) systems typically demand lighter-weight components than those used for terrestrial applications, but without sacrifices in performance. Packaging must be hermetic to withstand harsh environments. In fact, in recent years, most designers of radar and avionics systems and their components and assemblies will agree that they have been asked to make everything smaller, lighter, and at lower cost. These three customer demands drive the technologies for radar and avionics applications from the systems level to the device, component, and even substrate materials levels. And as a kind of "design glue" that helps efficiently brings all the parts together, computer-aided-engineering (CAE) simulation software continues to meet the needs of system designers.

Modern radar benefits from a number microwave-based advances, including improvements in active antenna arrays and the use of agile beam steering. Also of note is progress in digital devices, including digital signal processors (DSPs) and

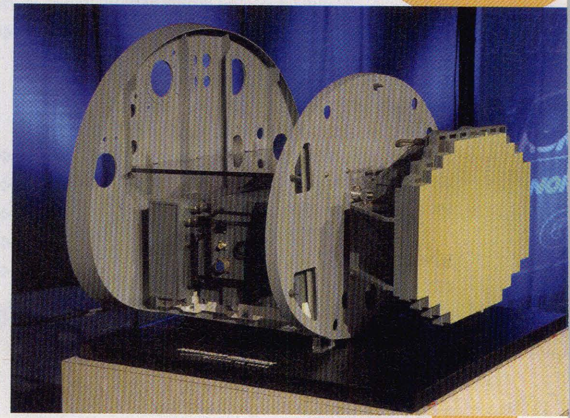

1. The SABR system used on the F-16 fighter is one example of a radar system using active electronically scanned array (AESA) antenna technology. [Photo courtesy of Northrop Grumman Corp. (www.northropgrumman.com).]

field-programmable gate arrays (FPGAs). Larger portions of newer radar systems are devoted to digital processing and circuitry, with the goals of the antennas and front-end circuitry to render received signals into the digital realm as quickly as possible. In addition to performance improvements, these enhancements in electronic components, such as active antenna arrays, can lead to increased reliability due to less reliance on moving parts.

The used of phased-array antennas and electronic beam-steering techniques has translated into powerful performance improvements for some major tactical radar systems. Raytheon Co. (www.raytheon.com), for example, has built its next-generation radar systems around active electronically scanned array (AESA) technology. The firm's APG-82(V)1 radar system for the US Air Force's F-15E fighters (and also employed on the F-15C, F/A-18E/F and EA-18G aircraft) is an extended-range platform with multiple-target tracking capabilities. More than 300 AESA-based radar systems are now in use.

2. The SeaVue XMC radar system with expanded mission capability is being used by US Customs and Border Protection aboard a drone surveillance plane. [Photo courtesy of Raytheon Co. (www.raytheon.com).]

That AESA technology is a staple of Northrop Grumman's (www.northrop-grumman.com) newest radar systems, along with the beam-steering technology and multifunction sensors used on the Scalable Agile Beam Radar (SABR) developed for the F-16 fighter. The SABR is an airborne AESA-based fire-control radar system that is designed to operate in dense electronic threat signal environments. The AESA technology is also employed in the firm's Highly Adaptable Multimission Radar (HAMMR) system. A lightweight ground radar system with AESA antenna technology, it provides 360-deg. coverage while mounted on a vehicle (Fig. 1).

The HAMMR's AESA system consists of more than 1000 programmable transmit/receive (T/R) modules that combine for a wide range of antenna patterns under software programmable control. Because system performance can be quickly redefined, the HAMMR system can readily adapt to new threats without additional hardware. Also, groups of modules can

Hand Flex Cables conform to any shape required.

from 8^{69} IN STOCK ea. (qty.1-9) DC to 18 GHz

Get the performance of semi-rigid cable, and the versatility of a flexible assembly. Mini-Circuits Hand Flex cables offer the mechanical and electrical stability of semi-rigid cables, but they're easily shaped by hand to quickly form any configuration needed for your assembly, system, or test rack. Wherever they're used, the savings in time and materials really add up!

Excellent return loss, low insertion loss, DC-18 GHz. Across their entire bandwidth, Hand Flex cables deliver excellent return loss (>26 dB typ for up to 50" runs) and low insertion loss (0.2 dB typ at 9 GHz for a 3-inch cable). So why waste time measuring and bending semi-rigid cables, when you can easily install a Hand Flex interconnect?

Two popular diameters to fit your needs. Hand Flex cables are available in 0.086" or 0.141" diameters, with a turn radius of 6 or 8 mm, respectively. Straight SMA connectors are standard, and now we've added right-angle connectors to our Hand Flex lineup, for applications with tightly-packed components.

Standard lengths in stock, custom models available. Standard lengths from 3 to 50" are in stock for same-day shipping. You can even get a Designer's Kit, so you always have a few on hand. Custom lengths, or two-right-angle models, are also available by preorder. Check out our website for details, and simplify your high-frequency connections with Hand Flex! *RoHS compliant*

Mini-Circuits...we're redefining what VALUE is all about!

Mini-Circuits®

ISO 9001 ISO 14001 AS9100

P.O. Box 350166, Brooklyn, New York 11235-0003 (718) 934-4500 Fax (718) 332-4661

YONI2® U.S. Patents 7739260, 7761442 ***The Design Engineers Search Engine*** *finds the model you need, Instantly* • For detailed performance specs & shopping online see **minicircuits.com**

IF/RF MICROWAVE COMPONENTS

482 Rev. E

be dedicated to different targets, allowing them to be tracked simultaneously.

The Active Phased Array multifunction Radar (APAR) system developed by Thales (www.thalesgroup.com) also employs phased-array antenna technology and T/R modules in its design. The APAR antenna features four arrays, each with more than 3000 T/R elements. The four arrays together enable full 360-deg. coverage. Having control over so many T/R modules provides for excellent antenna beam control. Conversely, the large number of modules can drive the cost of these phased-array-based radar systems, and requires carefully manufacturing control.

3. The EQ-36 counterfire target acquisition radar can scan a full 90 deg. in search of sources of enemy fire. [Photo courtesy of Lockheed Martin (www.lockheedmartin.com).]

Reliability improvements are critical, as radar systems are being used for a growing number of applications and on non-traditional platforms. Last year, Raytheon announced that it delivered the first of three SeaVue airborne surveillance radar systems with expanded mission capability (SeaVue XMC)—not to the Navy for installation on a fighter, but to the US Customs and Border Protection to fly on the organization's second Guardian unmanned aerial vehicle (UAV). The Guardian **(Fig. 2)** is a maritime version of the Predator B UAV used for surveillance in Iraq and Afghanistan. Raytheon will deliver an additional pair of the SeaVue radar systems for installation on traditional P-3 anti-submarine/surveillance aircraft.

Lockheed Martin (www.lockheedmartin.com) has also participated in the evolution of radar technology, notably through its 360-deg. scanning technology on the EQ-36 radar. The enhanced AN/TPQ-36 (EQ-36) counterfire target acquisition radar **(Fig. 3)** is now in production as the AN/TPQ-53 (Q-53) Counterfire Target Acquisition radar system. It can operate in 90- and 360-deg. modes, detecting, identifying, tracking, and locating the source of indirect enemy fire.

The design and development team for the EQ-36 radar system included SRC, Inc. (www.src.com), which last year received a contract from the US Army's Intelligence and Information Warfare Directorate to develop an omnidirectional weapon location (OWL) radar system, with a technolo-

Aethercomm®

We make hardware that saves lives.™

HIGH POWER RF SWITCHES

Aethercomm has been designing and manufacturing solid state high power RF switches for over 12 years for our own high power systems. We are now offering them to the industry as stand alone modules.

Custom Modules Available:

- Different Frequency Ranges
- Smaller Volumes
- Higher Isolation
- Higher Power Levels
- Faster Switching Speeds
- Lower Insertion Loss

Standard Product Offerings Available:

Model Number	Frequency Range	CW Power Rates	Peak Power Handling	Insertion Loss	Isolation	VSWR	Switching Speed	Size
SSHPS 0.96-1.22-3000	960-1220 MHz	250 Watts	3000 Watts	0.8 dB	60 dB	2.0:1	4 µsec	4.5 x 3.5 x 1.0 inches
SSHPS 1.2-1.4-4000	1200-1400 MHz	200 Watts	4000 Watts	0.7 dB	60 dB	1.6:1	4 µsec	4.5 x 3.5 x 1.0 inches
SSHPS 2.7-2.9-1000	2.7-2.9 GHz	100 Watts	1000 Watts	0.8 dB	40 dB	1.7:1	4 µsec	3.5 x 3.5 x 1.0 inches
SSHPS 2.9-3.1-1000	2.9-3.1 GHz	100 Watts	1000 Watts	0.8 dB	40 dB	1.8:1	4 µsec	3.5 x 3.5 x 1.0 inches
SSHPS 2.7-3.5-1000	2.7-3.5 Ghz	50 Watts	1000 Watts	0.9 dB	40 dB	2.0:1	4 µsec	3.5 x 3.5 x 1.0 inches
SSHPS 0.020-1.000-200	20-1000 MHz	200 Watts	1500 Watts	0.7 dB	25 dB	2.0:1	5 µsec	3.0 x 3.0 x 1.0 inches
SSHPS 0.225-0.450-400	225-450 MHz	400 Watts	2000 Watts	0.7 dB	40 dB	2.0:1	5 µsec	3.0 x 3.0 x 1.0 inches
SSHPS 1.0-2.5-200	1000-2500 MHz	200 Watts	1000 Watts	0.9 dB	25 dB	1.5:1	4 µsec	4.0 x 6.0 x 1.3 inches

SSHPS 1.03-1.09-5000 Typical Data

- Operation from 1030-1090 MHz
- Peak Power Handling of 5000 Watts
- Insertion Loss = 0.4 dB nominal
- Isolation = 58 dB typical
- Operation into an Infinite VSWR
- -40C to +70C Operation
- Internal BIT
- < 5µSec Switching Speed
- Return Loss, All Ports = -14 dB nominal
- 4.5" wide x 3.5" long x 1.0" high
- All switches High Power Tested & ESS Screened

SSHPS 1.03-1.09-5000

Tel 760.208.6002
sales@aethercomm.com

BSI REGISTERED
ISO 9001:2008
FM 89386

BSI
AS 9100
FM 551035

12 YEARS IN BUSINESS
1999-2011

www.aethercomm.com

gy demonstrator prototype for evaluation in 2013. The OWL system, which provides surveillance over a hemispherical coverage area, will be able to track and locate weapons sources over a wide range of threat trajectories.

Of course, the OWL and other electronically steered radar systems count on the availability of such components as T/R modules, beam-steering networks, and even high-performance circuit materials to form reliable circuits at radar frequencies and power levels. Traditionally, solid-state radar T/R modules have been fabricated by means of gallium arsenide (GaAs) monolithic-microwave-integrated-circuit (MMIC) technology. But with the emergence of alternative semiconductor materials, such as silicon carbide (SiC) and gallium nitride (GaN), opportunities exist for creating T/R radar modules with higher transmit levels.

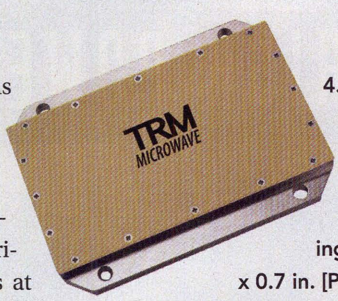

4. This compact beamformer integrates multiple passive power dividers, combiners, and delay lines in a housing measuring just 2.0 x 3.5 x 0.7 in. [Photo courtesy of TRM Microwave (www.trmmicrowave.com).]

Last year, for example, Fujitsu Laboratories Ltd. (www.fujitsu.com) unveiled details on a T/R module based on high-electron-mobility-transistor (HEMT) GaN technology. The module combined a power amplifier capable of 10 W transmit power from 6 to 18 GHz with a low-noise amplifier (LNA), and could support applications in phased-array radars, as well as in communications systems. The LNA chip, which measures just 2.7 x 1.2 mm, provides 16-dB gain from 3 to 20 GHz with noise figure of 2.7 dB or less.

Teledyne Microwave (www.teledyne-microwave.com) is another supplier of T/R modules for radar applications, applying GaAs, GaN, and even indium-phosphide (InP) device technologies where appropriate (including for use in millimeter-wave commercial automotive radar systems). The firm's British Teledyne Defence Ltd. has developed a complete radar-warning receiver (RWR) in a component-type housing measuring just 114.5 x 62.85 x 14.05 mm and weighing only 200 g. The model RR009 RWR contains two amplitude measurement channels to allow direction finding (DF) by amplitude comparison between adjacent antennas. It covers 8 to 18 GHz with 6-b frequency measurement resolution (156 MHz) and detects signals at levels from –63 to 0 dBm and minimum pulse widths of 100 ns. The small size and light weight make it ideal for use on UAVs.

In support of a variety of phased-array systems, model BFN 44122 from TRM Microwave (www.trmmicrowave.com) is a beamforming network **(Fig. 4)** that has been used on Raytheon's ALR-67(V)3 digital radar warning receiver (RWR). This receiver is integrated on such vehicles as the F/A-18 A/B/C/D Hornets and the F/A-18E/F Super Hornets. The RWR features a channelized digital receiver architecture with dual processors. In a housing measuring just 2.0 x 3.5 x 0.7 in., the passive assembly integrates ferrite, coaxial, and microstrip technologies, with eight 0-deg. power dividers, four 0-deg. power combiners, four 180-deg. power combiners, and 50-Ω coaxial delay lines.

The greatest number of RF/microwave hardware suppliers for military and commercial radar systems are still at the component level, so that system-level contractors such as Raytheon often buy the functions they need at the component level and perform in-house module design and fabrication. A large number of RF/microwave companies currently provide component-level functions suitable for use in radar T/R modules.

Several years ago, TriQuint Semiconductor (www.triquint.com) supported several EASA-based systems with GaAs-based amplifiers and bulk-acoustic-wave (BAW) filters for use in T/R modules for phased-array radars. In recent years, the firm appears more focused on higher frequencies, developing transceiver ICs for 77-GHz automotive distance-sensing and collision-avoidance radar systems.

M/A-COM Technology Solutions (www.macomtech.com) recently introduced its model MASW-011021 monolithic SPDT switch for high-power X-band radar circuits from 6 to 14 GHz. The surface-mount chip-scale device measures about 2.7 x 4.9 mm but can handle 10 W CW power. It exhibits typical insertion loss of 0.70 dB at 8 GHz and 0.65 dB at 12 GHz, with typical input-to-output isolation of 30 dB at all frequencies. It has typical switching speed of 130 ns.

Finally, Mini-Circuits (www.minicircuits.com) also supplies the miniature, rugged components needed for reliable radar T/R modules. Among these are the wideband model ZX60-183+ amplifier, with 24-dB typical gain from 6 to 18 GHz, accompanied by typical gain flatness of ±1 dB. The two-stage amplifier, which runs on a single +5-VDC supply, is housed in a package measuring 0.75 x 0.74 in. MWRF

Editor's Note: For a more in-depth review of current-generation radar systems, don't miss the the October/November issue of Defense Electronics, a supplement to Microwaves & RF.

JACK BROWNE | Technical Contributor

Converting Frequencies With Microwave Mixers

Frequency translation is necessary within many high-frequency systems, and RF/microwave mixers are the key components providing this vital function.

DOWNCONVERSION AND UPCONVERSION are performed in most high-frequency receivers and transmitters by means of an often-overlooked component: the RF/microwave mixer. Over the last 20-plus years, mixers have changed a great deal in appearance and are now available in a wide variety of package styles. Still, their main functionality has not changed: to translate the frequency of a signal (usually carrying some form of information via modulation) to a second frequency (either higher or lower than the original frequency).

An RF/microwave mixer is essentially a three-port component, which can be fabricated as a passive component based on diodes or an active component based on biased field-effect transistors (FETs). A mixer's three ports are commonly known as the radio-frequency (RF), local-oscillator (LO), and intermediate-frequency (IF) ports, with two serving as input ports and one as the output port. The LO port is always an input port, so that the RF and IF ports are the ones that switch functions, depending upon whether a mixer is used for frequency downconversion or frequency upconversion.

In downconversion, a high-frequency RF input signal is mixed with a high-frequency LO signal—usually over a similar frequency range as the LO signal—to produce a lower-frequency IF output signal. In upconversion, lower-frequency IF signals serve as inputs, and are mixed with higher-frequency LO signals to produce RF output signals. The latter have been translated higher in frequency than the

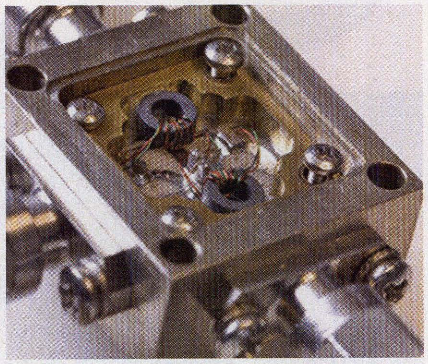

1. Traditional mixer packaging includes coaxial connectors and rugged metal housings. [Photo courtesy of Spectrum Microwave (www.spectrummicrowave.com).]

IF input signals while maintaining the modulation information of the IF signals. Downconversion is normally part of a receiver; upconversion is typically used in a transmitter. The translation of frequencies follows a simple mathematical mixing function:

$$n(f_{RF} \pm f_{LO}) = f_{IF}$$

where:

f_{LO} = the LO signal frequency;
f_{RF} = the RF signal frequency;
f_{IF} = the IF signal frequency; and
n = the harmonic number.

Here is a simple example of downconversion, using an RF at 2100 MHz and an LO at 2000 MHz: Fundamental-frequency mixing would yield IF sum and difference signals, with one IF signal at 2100 − 2000 = 100 MHz and one at 2100 + 2000 = 4100 MHz. If the lower-frequency signal product is desired, the higher-frequency product can be removed—for instance, through the addition of a lowpass filter at the mixer's IF output. It should be noted that it is the difference between the mixing signals that is important, and the difference of LO − RF can also be used.

Many different types of RF/microwave mixers have been developed over the years in support of a diversity of different types of communications systems. These include single-balanced mixers (which can be designed with a single diode), double-balanced mixers, triple-balanced mixers, image-reject mixers, in-phase/quadrature (I/Q) mixers, single-sideband mixers, double-sideband mixers, harmonic mixers, and subharmonic mixers.

Traditional double-balanced mixers, for example, are typically based on four Schottky diodes in a quad ring configuration, which provides acceptable performance for many applications. When certain levels of enhanced performance are needed, a pair of these diode quads are incorporated in the mixer circuitry to form a triple-balanced mixer. Mixers that can process signals with I and Q components are ideal for use in systems employing digital modulation, while harmonic mixers—which can extract higher harmonics from the mixing process—are typically used in generating and processing millimeter-wave signals.

Ideally, when a downconverting mixer processes LO and RF input signals to produce a lower-frequency IF signal in a receiver, the received signals are mixed

with the injected LO signal. But any signals appearing at a mixer's RF port that are at that target frequency range but not the desired signals—usually referred to as "image" signals—will produce IF output signals. Receivers often employ preselector filters to remove any unwanted image signals that fall into the bandwidth of the mixer's RF port. The alternative is to use an image-reject mixer which has been designed to attenuate these unwanted image signals.

Mixers are characterized by a number of performance parameters—some of which (such as conversion loss) only apply to mixers and not to other high-frequency components. Other important mixer parameters include port-to-port isolation, VSWR, noise figure, 1-dB compression, and third-order intercept point. For example, isolation describes the separation between ports, or how much power will feed through from one port to another. High isolation indicates a mixer with minimal signal leakage between ports.

A mixer's dynamic range is the difference between the maximum amplitude of signals it can handle (as determined by the 1-dB compression point) and the lowest-level signals it can process (determined by its noise figure). Of course, choosing any mixer is a matter of matching the mixer's overall performance to a required system frequency plan. This includes whether the need is for upconversion or downconversion, how the IF will be handled, the available LO power, and even the type of mixer package desired for printed-circuit-board (PCB) mounting.

If a mixer is employed for frequency downconversion, as typically used in an RF/microwave receiver, a great deal of its performance will be dependent on the available LO signals. For example, noise in the LO signals will contribute to noise at a downconverting mixer's IF port. But a minimal LO amplitude will also limit the available dynamic range of the mixer. Mixers are typically optimized for different LO signal levels, such as +7, +10, and +14 dBm; this is the power that energizes a mixer's nonlinear switching elements, whether they are diodes or transistors. At levels above the optimal LO amplitude, a mixer will start to experience compression, where an increase in LO input power no longer results in an increase in IF output power. Early signs of compression are indicated by a mixer's 1-dB compression point.

A companion parameter for determining a mixer's linearity is the third-order intercept point (IP3), which refers to a level of intermodulation distortion caused by two tones at a mixer's RF port. For mixers used in digital communication systems, for example, excellent linearity is important in maintaining the accuracy of I and Q signal components processed by the mixer, with higher third-order-intercept-point values representing enhanced linearity performance.

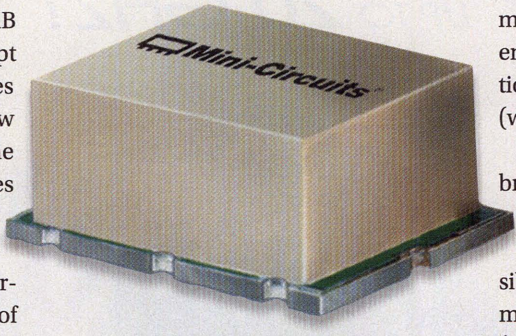

2. This compact plastic surface-mount package measures just 0.38 x 0.50 x 0.23 in. (9.65 x 12.70 x 5.84 mm) but supports mixer circuits well into the microwave frequency range. [Photo courtesy of Mini-Circuits (www.minicircuits.com).]

Passive mixers are characterized by their conversion loss, which is caused by losses due to impedance mismatches in the mixer circuit, to diode junctions, and to other circuit-connection points in a mixer design. In a mixer used for downconversion, the conversion loss is the difference in signal level between the RF input amplitude and the IF output amplitude, while in a mixer used for upconversion the difference in amplitude is between the IF input amplitude and the RF output amplitude. Conversion-loss values of 6 to 8 dB are not unusual in standard double-balanced RF/microwave mixers. Of course, it is also possible to achieve conversion gain in an active mixer, through the use of an amplification stage and active circuit devices in the mixer. But this gain will also require the addition of bias power for the mixer's active circuitry, as if biasing an amplifier.

RF/microwave mixers were once fairly large components, featuring metal housings with three coaxial connectors for the ports. For some applications—such as rack-mount receivers, transmitters, and test equipment—such mixer packaging is still a good match **(Fig. 1)**. But as more high-frequency designers are asked to miniaturize circuits and systems, mixer packaging has followed with increasingly smaller surface-mountable and PCB-mountable packages **(Fig. 2)**, which allow engineers to achieve frequency translation in extremely small areas of a circuit (when including the LO source).

Newer mixers can be specified for broadband or narrowband use, depending on the specific application. In terms of the performance levels possible in small packages, mixers such as the model SYM-63LH+ from Mini-Circuits (www.minicircuits.com) is a double-balanced mixer based on a diode quad that can handle RF/LO signals from 1 to 6000 MHz. The same firm's MAC Series of mixers is based on low-temperature-cofired-ceramic (LTCC) circuit substrates for RF/LO coverage from 0.3 to 12.0 GHz in a surface-mount package that is only 0.06 in. high. And the SGS-5-17 double-balanced mixer from Synergy Microwave (www.synergymwave.com) uses the company's SYNSTRIP multilayer circuit technology to achieve RF/LO coverage from 3 to 19 GHz in a package measuring only 0.275 x 0.200 x 0.050 in.

In addition, a growing number of integrated-circuit (IC) manufacturers are fabricating mixer functions as part of entire front-end assemblies. These also include preselector filters, amplification, matching transformers, and IF filters to greatly simplify the task of RF/microwave receiver and transmitter designers looking for a compact, frequency-translation solution. MWRF

JACK BROWNE | Technical Contributor

SDR Technology Marches Forward

Software-programmable radio technology is steadily replacing fixed-performance conventional radios in a wide range of military and commercial applications.

PROGRESS IN THE development of software-defined radios (SDRs) depends upon improvements in many components and software. Nevertheless, the electronics industry has wholeheartedly embraced the challenges in enhancing SDR technology. The name accurately summarizes the mode of operation for these radios: being able to modify the performance of the hardware components via software code. But accomplishing this still requires high-performance analog and digital components—such as low-noise amplifiers (LNAs) and data converters, respectively—and system-level configurations that lend themselves to interoperability between SDRs from different manufacturers. These radios typically operate in the range from 2 MHz to 2 GHz.

SDR technology is now very much a part of commercial markets, such as cellular communications networks. But the technology owes much of its growth to the on-again, off-again US military Joint Tactical Radio System (JTRS) program. This program's goal has been to replace existing analog tactical radios with some form of a universal, software-programmable radio; the challenge has been to provide communications security in addition to interoperability among different military networks.

The JTRS has been fueled by some of the largest military contractors, including Boeing's (www.boeing.com) efforts on a Ground Mobile Radio (GMR) version of the JTRS network and Lockheed-Martin's (www.lockheed-martin.com) work on an air-and-sea version of the JTRS radio system, known as the airborne/maritime fixed (AMF) JTRS radio. JTRS radios are based on the Software Communications Architecture (SCA), which is an open-architecture framework that defines how the hardware and software work together.

Unfortunately, delays and cost overruns by Boeing led to a cancellation of their part of the JTRS program late last year (although the contract was scheduled to end in March of 2012). Boeing was working with Northrop-Grumman (www.northropgrumman.com), Rockwell Collins (www.rockwellcollins.com), BAE Systems (www.baesystems.com), and Harris RF Communications (www.rf.harris.com) on the development of these high-performance GMR JTRS radios. Of course, cutbacks in the Army's part of the JTRS program can be traced back to the related Future Combat Systems (FCS) program, an ambitious and expensive effort at creating technology for the soldier of the future. The FCS program was cancelled in 2009.

The Falcon III® AN/PRC-152A wideband handheld tactical radio uses SDR technology for adapting to different waveform applications. [Photo courtesy of Harris RF Communications (www.rf.harris.com).]

Some of the problems that the Department of Defense (DoD) saw with Boeing's JTRS radios were linked to trying to support a wide range of sophisticated waveforms within relatively hardware-limited radios. The US Army, for example, has developed two waveforms for these programmable radios—the Soldier Radio Waveform (SRW) and the Wideband Networking Waveform—for reliable and secure communications.

The SRW-based radios are designed to work with 1.2-MHz bandwidth allotments, while WNW radios operate optimally with 3- or 5-MHz bandwidth allotments. But these are memory/compute-intensive waveforms; Boeing has discovered that it is difficult to cost-effectively deliver an SDR-based radio that supports all of these waveforms and networks simultaneously.

Harris RF Communications has enjoyed a great deal of success owing to its involvement in the JTRS, but also for developing its own SDR-based radios. For example, the company just received a $39 million order from the US Special Operations Command (USSOCOM) for its Falcon III® AN/PRC-152A wideband handheld tactical radios **(see figure)**. This is the initial delivery order from a $400 million indefinite-delivery, indefinite-quantity (IDIQ) contract intended to help modernize SOCOM's tactical radio inventory. The contract also covers the Falcon III AN/PRC-117G multiband manpack radios.

The flexible AN/PRC-152A radio system supports both wideband and narrowband waveforms. Harris' wideband capabilities will be provided by the firm's Networking Wideband Waveform, which has been certified by the National Security Agency (NSA) for Type-1 High Assurance Internet Protocol Encryption (HAIPE). Harris expects to receive NSA Type-1 certification for the AN/PRC-152A to also work with the JTRS SRW later this year.

In addition, Data Link Solutions (DLS; www.datalink-systems.com), a joint venture between Rockwell Collins and BAE Systems, was recently awarded a $25.8 million contract by the Space and Naval Warfare Systems Command (SPAWAR). This order is for the First Full Production & Fielding (FP&F) of Multifunctional Information Distribution System JTRS terminals, intended for the US Navy F/A-18 E/F (Super Hornet), Navy Lab, and NAVSUP (Navy Supply). They will also be provided to the US Air Force E-8 (JSTARS), RC-135 (Rivet Joint), EC-130E (Senior Scout), EC-130H (Compass Call), Air Force Participating Test Unit, and Warner Robins Air Force Base.

Now a part of commercial markets, SDR technology owes much of its growth to the US military JTRS program.

The MIDS JTRS is a four-channel terminal that includes Link-16 capability with the ability to incorporate additional networking waveforms as they become available. The MIDS JTRS project is a cooperative, competitive development effort between Data Link Solutions and ViaSat (www.viasat.com).

Meanwhile, the DoD has instructed Lockheed-Martin to restructure its efforts on JTRS with an eye towards enhanced affordability. The Lockheed-Martin AMF JTRS team—which includes BAE Systems, General Dynamics (www.gd.com), Northrop Grumman, and Raytheon (www.raytheon.com)—is working as part of an initial System Development and Demonstration (SDD) contract valued at $766 million. The AMF JTRS radios are being designed for use by fixed stations, submarines, surface ships, and aircraft.

The DoD's vision of how SDRs fit into the battlefield has changed a great deal since early concepts of SDRs in the 1990s. Recently, the Army's Joint Program Executive Office for JTRS has promoted its interest in JTRS radios developing into full-fledged cognitive radio systems (see www.army.mil/articles), which would also include software-defined antennas (SDAs).

A cognitive radio can be thought of as one step beyond an SDR, using a technique called dynamic spectrum access (DSA). This allows an SDR to detect and use available bandwidth in an operating area, changing its own transmission and reception characteristics to adapt to the available spectrum. In theory, an SDR with DSA can more efficiently and effectively make use of limited spectrum than a standard radio or even a JTRS radio. JTRS cognitive radios will also need to use a technique known as spectrum fragmentation, in which large-bandwidth waveforms can be spread across available portions of bandwidth.

For Lockheed-Martin, tests of the AMF JTRS radios aboard the Army's Apache attack helicopters flying in New Mexico late last year proved encouraging for the SDR technology. A combination of voice, data, and images were communicated from a test bed AH-64 Block III Apache helicopter to ground forces using the SRW. A pre-engineering developmental airborne radio aboard the helicopter linked directly with six ground forces equipped with JTRS Handheld Manpack Small Form Fit (HMS) Rifleman Radios. The Apache provided an aerial network extension, serving as a relay for the ground-based troops. The Apache was able to break all connections in the network and then rejoin all units in the JTRS network, without major delay or information loss.

As noted earlier, not all SDR technology is military, and commercial communications providers are quickly discovering the benefits of having software-definable wireless networks. The industry group known as the Wireless Innovation Forum (www.winnforum.org), is devoted to the development of next-generation radio technologies, including SDR. Also, SDR-BR (www.appr.org) is a group of amateur radio researchers and experimenters interested in SDR.

The uses for SDR technology on the commercial side are many, with new products spanning from component to system levels. Communications equipment and service provider Alcatel-Lucent (www.alcatel-lucent.com) has developed its multicarrier remote radio head (MC-RRH) based on SDR and multicarrier power amplifier (MCPA) technologies. It has become a building block of the firm's converged radio access network. The MC-RRH module enables carriers to handle two different technologies simultaneously, supporting Long Term Evolution (LTE) and multiple-input, multiple-output (MIMO) technologies with a single module.

Components suppliers supporting SDR technology are many. Altera (www.altera.com) boasts lines of field-programmable gate arrays (FPGAs) for SDR applications. Texas Instruments (www.ti.com) offers analog-front-end (AFE) integrated circuits (ICs) for femtocell base stations and portable SDR applications. For example, the latter's low-power, 12-b model AFE7225 AFE integrates a dual 125-Msamples/s analog-to-digital converter (ADC) and dual 250-Msamples/s digital-to-analog converters (DACs).

For the broadcast market, Carlson Wireless (www.carlsonwireless.com) recently announced RuralConnect IP, an SDR that uses "white space" bandwidth left in the VHF and UHF spectra by broadcasters to provide wireless broadband service to underserved and rural areas. Carlson Wireless, which hopes to receive US Federal Communications Commission (FCC) certification for the device, worked with database provider Spectrum Bridge (www.spectrumbridge.com) and KTS Wireless (www.ktswireless.com) to develop the radio. MWRF

JAE-HOON BANG
Research Professor

TSEND SHIRIRBAATAR
Graduate Student

BIERNG-CHEARL AHN
Professor

EUN-JONG CHA
Professor

Chungbuk National University, San 48 Gaesin-dong, Heungdeok-gu, Cheongju-si, Chungcheongbuk-do, 361-763, South Korea, +82 (43) 261-2114, FAX: +82 (43) 263-0612; e-mail: bician@cbu.ac.kr, www.cbu.ac.kr

Reflector Connects

THIS ANTENNA DESIGN FEATURES A SIMPLE, LOW-COST CONSTRUCTION, BUT YIELDS HIGH GAIN AND RELIABLE OPERATION FOR MICROWAVE BACKHAUL POINT-TO-POINT COMMUNICATIONS LINKS.

ANTENNAS CAN TAKE MANY forms for many different applications. One of the less "visible" parts of a wireless network is the backhaul connection, such as between a central routing station and a cellular base station. To serve such needs a low-cost, high-gain reflector was developed for 18.7-GHz links. It employs a compact circular waveguide feed energized by a coaxial cable and bonded to the radome wall. Its relatively simple geometry is inexpensive to produce, yet provides high-gain performance.

The backhaul portion of a wireless communications system typically connects a backbone, such as a central routing system, and an edge node, such as a cellular telephone base station.[1] Backhaul communications have also found applications in the public safety network which enables the real-time transmission of vital data, voice, and video information for public agencies and public-service personnel.[2]

Backhaul communications can take the form of unlicensed wireless point-to-multipoint bridges operating within frequency bands at 900 MHz, 2.4 GHz, 5.3 GHz, 5.8 GHz, and 60 GHz, Alternately, they can manifest in licensed microwave links (also known as point-to-point microwave radios) and operate in bands at 6 GHz, 11 GHz, 18 GHz, 23 GHz, and 80 GHz. Data throughputs in a backhaul system range from 100 Mb/s to 1 Gb/s full duplex.[3]

Point-to-point backhaul applications require antennas that have high gain and a tight sidelobe envelope. To achieve high gain, antennas in the form of a solid or wire-mesh reflector of the prime-focus type are often used. In a prime-focus reflector antenna, the feed is usually supported by a tripod or by a bent waveguide energizing the feed itself, commonly called a gooseneck.[4,5] Back-fire feeds connected at the end of a straight hollow wave-

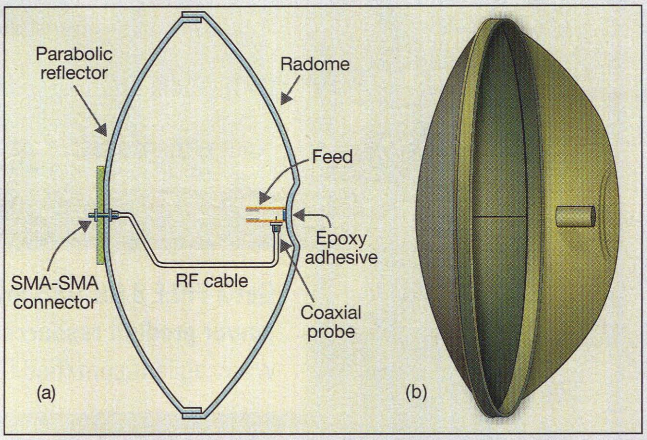

1. This basic antenna structure (a), which was developed for backhaul communications applications, is shown alongside (b) a computer-aided-engineering (CAE) model created for simulation purposes.

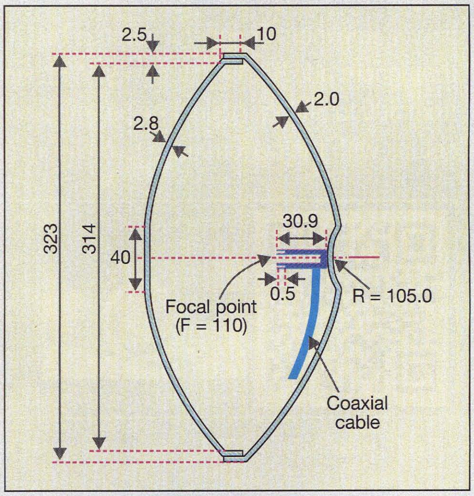

2. This diagram shows the dimensions (in mm) of the prototype backhaul reflector antenna.

18.7-GHz Backhauls

guide or a coaxial cable are also widely used.[7-9] While offering the simplest feed-supporting method, back-fire feeds have two drawbacks. They require sophisticated design skill to implement effectively, and often lead to a large aperture blockage and a high level of the first few sidelobes. In this article, the authors present a simple reflector configuration that is easy to design and can be realized at low cost for backhaul applications.

Figure 1 shows the antenna structure along with a computer-aided-design (CAD) model for the purpose of performing computer simulations of performance. The notable feature of the design is that a small feed is held at the reflector's focus by bonding it to the inside wall of the radome. The feed's energy is routed to the back of the reflector via a short length of a low-loss coaxial cable. With this arrangement, the precise placement of the feed by either a tripod or a gooseneck waveguide is not required. This greatly simplifies the antenna geometry, which in turn significantly reduces the production cost at expense of a small reduction in antenna gain due to the cable loss (around 0.5 dB at 18.7 GHz, when low-loss cable is used).

A prime-focus reflector based on the above concept was designed for operation from 17.7 to 19.7 GHz. For design verification, the researchers used a ready-made set of a parabolic reflector and a radome purchased from a commercial vendor.[9] The parabolic reflector has a diameter of 314 mm (D/λ = 19.6 at 18.7

Plotting gain for the fabricated antenna

Frequency (GHz)	17.7	18.2	18.7	19.2	19.7
Gain (dBi)	32.8	33.1	33.4	33.7	34.1

4. A CAE model of the feed (a) is shown alongside the actual fabricated feed (b).

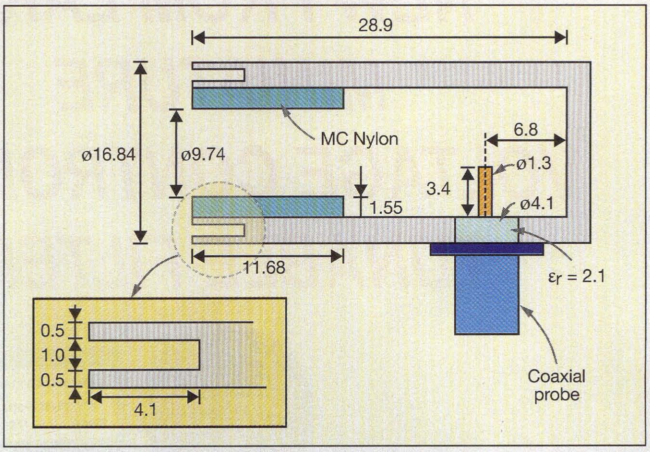

3. This diagram shows the dimensions (in mm) of a circular waveguide that feeds the reflector antenna.

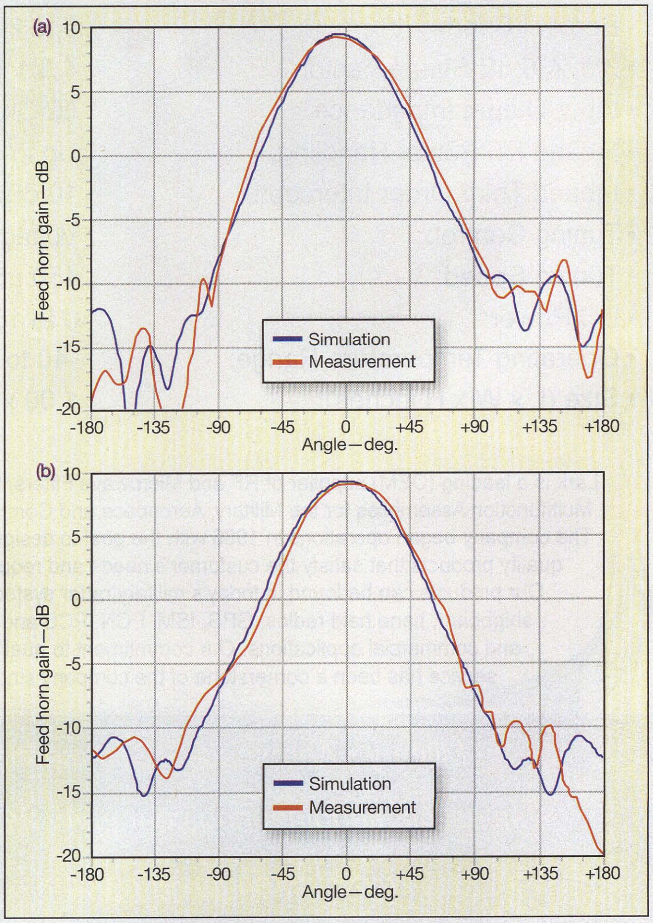

5. These gain patterns show the reflector's (a) E-plane and (b) H-plane behavior at 18.7 GHz.

GHz) and a focal length of 110 mm (F/D = 0.35, feed's half-subtended angle = 71 deg.). The radome is composed of 2-mm-thick acrylonitrile butadiene styrene (ABS) thermoplastic material with a relative dielectric constant (ε_r) of 2.79 and dielectric loss tangent of 0.008 at 10 GHz. The radome's center portion of diameter 40 mm is transformed from a concave shape into a convex form to reduce the reflection from the radome toward the reflector surface and then into the feed. **Figure 2** shows dimensions of the designed reflector antenna.

A critical part of developing any reflector antenna is the design of a high-performance feed structure. The properties sought for the feed of a prime-focus reflector antenna include:

1) a small diameter to minimize aperture blockage;

2) an axisymmetric radiation pattern with specified beamwidth at a level of –13 to –10 dB;

3) low level of back-radiation; and

4) good impedance matching to the system impedance.

Among the many types of feed structure suitable for a prime-focus antenna,[10] one of the simplest and most compact is the dielectric ring-loaded circular waveguide radiator proposed by Raghavan and associates.[11] The dielectric loading generates hybrid modes which make the circular waveguide's radiation pattern symmetric around its axis.

For the design of the backhaul reflector, the feed consisted of a circular waveguide loaded with MC nylon material, which features a relative dielectric constant of 3.0 and loss tangent of 0.01 at 10 GHz. To reduce the feed's back-radiation, a quarter-wave (at 18.7 GHz) choke was formed around the aperture of the feed. The diameter of the circular waveguide was adjusted so that the feed provides a –12-dB taper at the reflector edge for a sidelobe level of –23 dB.

Figure 3 shows the dimensions of the designed feed. It was designed with the aid of the Microwave Studio™ electromagnetic (EM) simulation software from Computer Simulation Technology (www.cst.com).

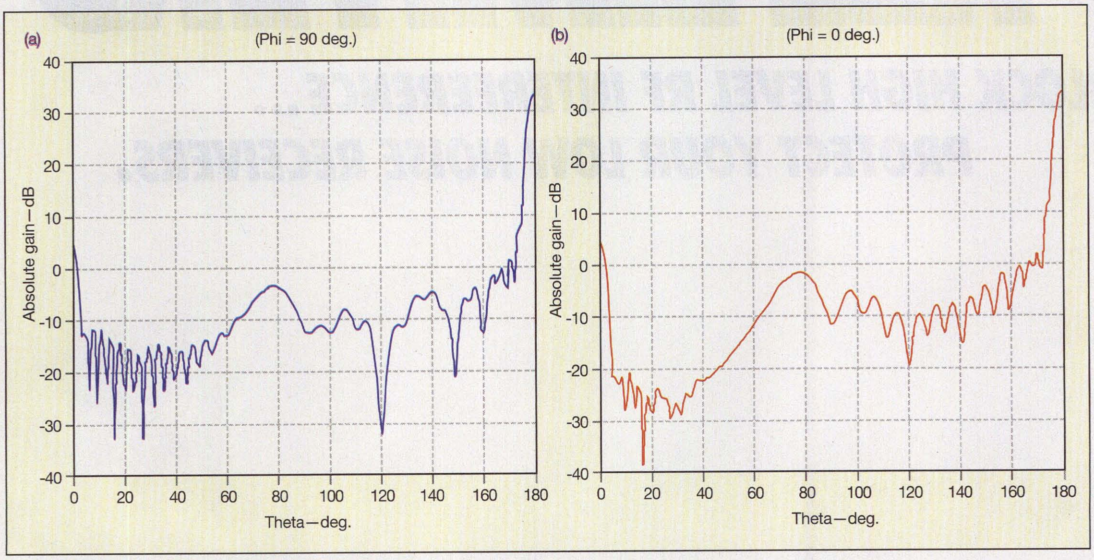

6. These simulators predict the reflector's (a) E-plane and (b) H-plane behavior at 18.7 GHz.

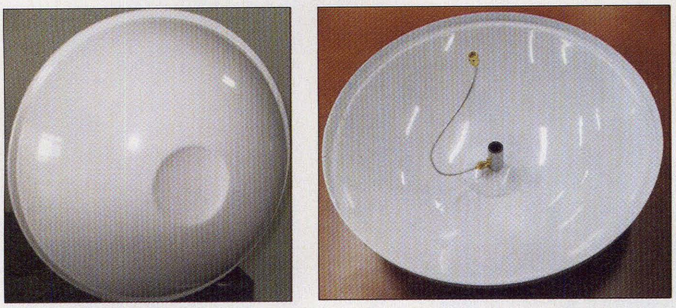

7. The prototype reflector antenna is shown here (a) covered with a radome and (b) with the feed bonded to the inside wall of the radome.

Figure 4(a) shows a CAD model of the feed, while **Fig. 4(b)** shows the fabricated feed. The optimized waveguide diameter is 12.84 mm and the total diameter of the feed including the choke is 16.84 mm (1.05λ at 18.7 GHz). The height and distance from the back short of the coaxial probe in the feed are adjusted for low reflection over the range of 17 to 20 GHz. The length and thickness of the nylon dielectric are adjusted for axisymmetric radiation pattern. The feed length is adjusted so that the feed's phase center will be accurately located at the reflector's focal point when the feed is bonded to the radome wall.

Figure 5 shows the measured E- and H-plane field patterns for the feed at 18.7 GHz. The feed has 9.0 dB gain and a front-to-back ratio of approximately 20 dB. The E- and H-plane taper levels at 71 deg. are –13 and –12 dB, respectively. Combined with the 1/r space taper of -0.85 dB at the reflector edge, the total edge tapers are –13.85 and –12.85 dB, respectively, on the E and H planes. This will yield a first sidelobe level at –23 dB below the main beam peak, assuming a parabolic-on-a-pedestal type distribution for the reflector's aperture field. The feed's phase center is 0.5 mm away from the waveguide aperture plane in the probe direction. The feed's far-field phase patterns are flat over its reflector-edge subtended angle of 142 deg.

Prior to constructing a prototype, Microwave Studio simulation software was used to verify the operation of the antenna design according to the CAD model shown in **Fig. 1(b)**. The simulation was simplified by taking advantage of a four-fold symmetry in the structure, with the circular waveguide feed excited with its TE_{11} mode rather than a coaxial probe. **Figure 6** shows the simulated E- and H-plane gain patterns. From experience, it is known that large reflectors are not amenable to accurate simulation by Microwave Studio software using standard computer resources due to the large number of meshes required in the simulation. As a result, the simulation results must be interpreted with the knowledge that they are not fully converged EM solutions. While they may not represent simulations with the highest accuracy, they provide a fair indication of the proper operation of the reflector antenna. The simulation shows that the antenna delivers 33.0-dBi gain at 18.7 GHz, with E- and H-plane beamwidths of 4 deg., and shoulder-type sidelobes of –21 dB (in the E plane) and –28 dB (in the H plane). The antenna's increased sidelobe levels of –1.5 dBi gain in the E plane and –3.5 dBi gain in the H plane at far-out angles near 90 deg. from boresight (theta = 180 deg. in **Fig. 6**) are caused by diffraction at the reflector rim.

Figure 7 shows the prototype antenna that was constructed for evaluation. The feed is bonded on the inside wall of the radome using an epoxy adhesive. The feed is energized by low-loss cable (about 0.5 dB at 18.7 GHz) of 25-cm length, which is then routed to the rear of the reflector in a shape of minimum obstruction to the antenna's wave. The cable is connected to an SMA-SMA adapter attached on the fixture plate at the rear of the antenna.

Figure 8 shows the measured reflec-

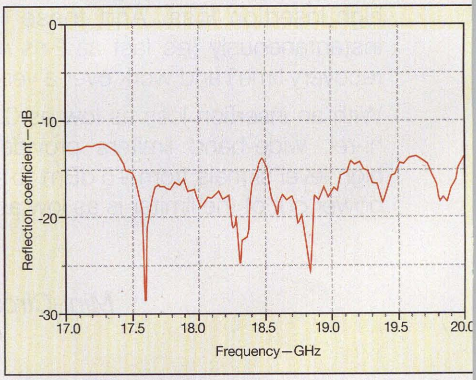

8. These measured results show the reflection coefficient for the reflector antenna.

tion coefficient of the prototype antenna. The antenna's VSWR is less than 1.50:1 over the frequency range from 17.7 to 19.7 GHz. The antenna's gain and radiation pattern were measured using a planar near-field facility. The **table** shows the antenna's gain from 17.7 to 19.7 GHz. At 18.7 GHz, a gain of 33.4 dBi translates into aperture efficiency of 57.8%. When the sum of the cable loss (0.5 dB) and radome loss (0.5 dB, estimated) are taken into account, the antenna's efficiency is 72.7%.

Figure 9 shows the antenna's measured gain patterns at 18.7 GHz, along with radiation pattern envelopes for Class 1 and Class 2 antennas per the European Telecommunications Standards Institute (ETSI; www.etsi.org).[12] The antenna has sidelobes of –22.3 and –20.0 dB, respectively, in the E and H planes, with E- and H-plane beamwidths of 3.74 and 3.62 deg., respectively. The antenna meets the radiation pattern envelope of the ETSI Class 1

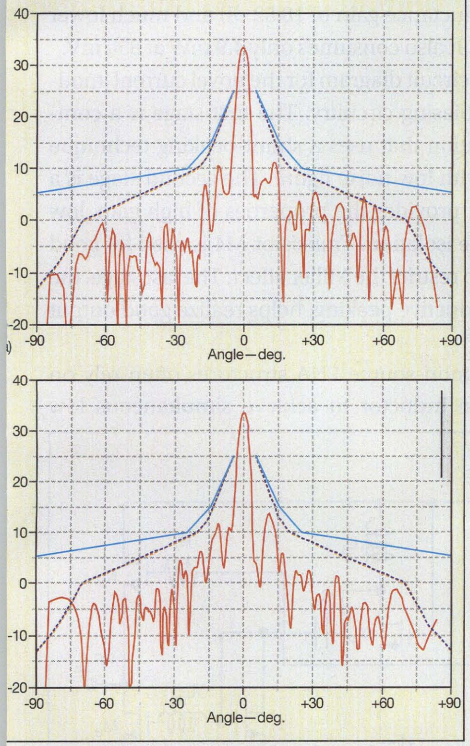

9. The red traces show the measured gain at 18.7 GHz for the reflector's antenna's (a) E-plane patterns and (b) H-plane patterns, while the blue traces show ETSI Class 1 (solid) and Class 2 (dashed) antenna RPE.

antenna (for use in low-interference environments) and nearly satisfies that of the ETSI Class 2 antenna (for high-interference situations). For further improvements in the sidelobe performance, one can apply the shield and absorber lining techniques that have been described in an excellent article by Wojtkowiak[13] in the May 2004 issue of *Microwaves & RF*.

In conclusion, this prime-focus reflector antenna uses a compact feed bonded to the radome wall to effectively serve wireless backhaul applications. Its simple design can be constructed inexpensively as a viable low-cost alternative to existing prime-focus reflector configurations. MWRF

ACKNOWLEDGMENTS

The authors would like to express their appreciation to the financial support by Basic Science Research Program through the National Research Foundation of Korea (NRF) funded by the Ministry of Education, Science and Technology (2011-0001045), and by the Korea Healthcare Technology R&D Project, Ministry of Health & Welfare, Republic of Korea (A100054).

REFERENCES

1. O. Tipmongkolsilp, S. Zaghloul, and A. Jukan, "The evolution of cellular backhaul technologies: current issues and future trends," IEEE Communications Surveys & Tutorials, Vol. 13, No. 1, 2011.
2. California Technology Agency, California Public Safety Microwave Network Strategic Plan, March, 2001.
3. Alpha Omega Wireless, Inc., www.aowireless.com.
4. S. Silver, Microwave Antenna Theory and Design, MIT Radiation Laboratory Series 12, Cambridge, MA, 1949.
5. M.S. Narashimhan, K. Raghavan, and P. Ramanujam, "GTD analysis of the radiation patterns of a prime focus paraboloid with shroud," IEEE Transactions on Antennas & Propagation, Vol. 31, No. 5, 1983, pp. 792-794.
6. P.-S. Kildal, "The hat feed: a dual-mode rear-radiating waveguide antenna with having low cross polarization," IEEE Transactions on Antennas & Propagation, Vol. 30, No. 4, 1982, pp. 529-534.
7. P.R. Foster, C.R. Yeoman, and S.M. Tun, "Performance of a small reflector with a splash plate feed," Proceedings of the IEE Colloquium on Reflector Antennas for the 90's, 1992, pp. 7/1-7/4.
8. A.A. Kishk and L. Shafai, "Small reflector antenna with low sidelobes," IEEE Transactions on Antennas & Propagation, Vol. 52, No. 10, 2003, pp. 2907-2912.
9. Comotech Corp., www.comotech.com.
10. A.D. Olver, P.J.B. Clarricoats, A.A. Kishk, and L. Shafai, Microwave Horns and Feeds, IEEE Press, New York, 1994.
11. K. Raghavan, A.D. Olver, and P.J.B. Clarricoats, "Compact dielectric feeds for prime focus reflector antennas," IEEE Antennas Propagation Society International Symposium Digest, 1988, pp. 350-353.
12. European Telecommunication Standards Institute, "Fixed Radio Systems; Point to Point Antennas; Antennas for point-to-point fixed radio systems operating in the frequency band 3 GHz to 60 GHz," ETS 300 833, June 1999.
13. D. Wojtkowiak, "Consider antenna options for minimal interference," Microwaves & RF, May 2004.

CHUNHUA WANG
Professor
e-mail: wch1227164@sina.com

YUXIANG TU
Graduate Student
e-mail: tuyuxiang2009@126.com

School of Information Science and Engineering, Hunan University, Changsha, 410082, Hunan, People's Republic of China

Novel LNA Cuts Noise, Not Gain

This two-stage amplifier design employs an LC network to eliminate the customary source-degrading inductor, achieving low noise figure with high gain at 5.8 GHz.

LOW-NOISE AMPLIFIERS (LNAs) are vital to the receivers in most wireless applications, although a common design challenge is to achieve high small-signal gain while also attaining low noise figure. LNAs can be constructed in a number of ways, including as voltage-mode amplifiers or as current-mode amplifiers. To demonstrate the effectiveness of the latter approach, a high-gain current-mode LNA with low noise figure was designed for use in IEEE 802.11a wireless local area network (WLAN) applications at 5.8 GHz. The two-stage amplifier employs an inductive-capacitive (LC) network to eliminate the need for a source inductor; it also features an NMOS current mirror using an inductive series peaking technique to achieve optimized current output and high gain. Simulated results reveal 18.52 dB transconductance gain at 5.8 GHz, with noise figure of 0.93 dB and power consumption of only 4.9 mW.

Conventional voltage-mode LNAs can suffer many drawbacks, including limited bandwidth, the need for a high voltage supply, and the requirement for a current-to-voltage transconductance stage due to the presence of high-impedance nodes. In contrast, current-mode LNAs offer many advantages over voltage-mode LNAs, including wide bandwidth, low supply voltage requirements, tunable input impedances, and less susceptibility to power and ground fluctuations.[1] Although some articles about IEEE 802.11a LNAs have been written in recent years,[1-7] few have covered current-mode designs. The IEEE 802.11a standard, based on orthogonal-frequency-division-multiplexing (OFDM) modulation, provides nearly 5 times the data rate and as much as 10 times the system capacity as IEEE 802.11b and 802.11g systems.

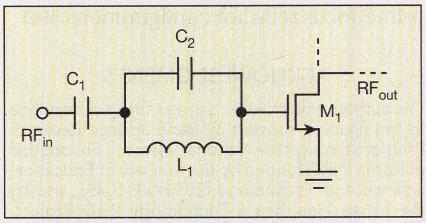

1. This circuit diagram shows the proposed current-mode LNA with its biasing circuit.

In support of the IEEE 802.11a standard, a novel current-mode LNA sans source-degrading inductor was developed. The two-stage design employs a NMOS current mirror for high gain with low noise figure and good impedance matching. Compared with previous LNAs designed for the same frequency[3,6] and nearby frequencies,[4,5,7] the proposed LNA offers higher transconductance gain of 18.52 dB and much lower noise figure of 0.93 dB. It also consumes only 4.9 mW at 850 mV.

Figure 1 shows the circuit diagram for the novel current-mode LNA, including its biasing circuitry. The first stage is a common-source configuration that uses a shunt-peaking technique to achieve high gain with low noise figure. The second stage is a cascode structure that provides the properties of high gain, low noise, and high reverse isolation. Transistor M4 is used for good reverse isolation and to restrict the Miller effect. The last stage, the current mirror with inductive peaking, helps realize good output impedance matching.[8]

Conventional common-source LNA structures often rely on a source degeneration inductor to achieve simultaneous low

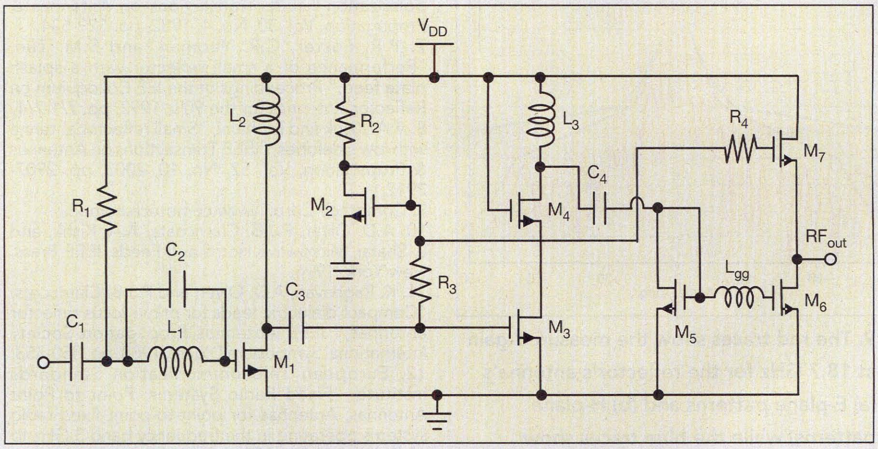

2. This schematic diagram shows the first (input) stage of the proposed current-mode LNA.

noise figure and power matching, but typically sacrifice gain and noise-figure performance levels in the process.[9] The structure presented in this circuit does not include the degeneration inductor. Rather, it uses a LC network at the gate terminal of the common-source stage to eliminate the source degeneration inductor. In doing so, it achieves improved gain with reduced noise, also reducing chip area and dropping the cost when fabricated in a semiconductor process. Circuit elements L1, C1, and C2 are used to implement the LC network.[10] The circuits composed of L2 adopting shunt-peaking technique are used to resonate with the gate-source capacitor, C_{gs}, of M1 to achieve high gain at 5.8 GHz. Capacitors C3 and C4 are added for DC signal choking.

A current mirror formed of circuit elements M2, R2, and R3 is used as a biasing circuit for transistor M3, while circuit elements M2, R2, and R4 form the current mirror used as a biasing circuit for M4. The width of device M2 is reduced to minimize power consumption. Resistors R2, R3, and R4 are added for signal choking; they are selected for large values so that their noise contributions can be neglected.[6,11]

Figure 2 shows the input stage of the proposed LNA. Transistor M1 is operated in its saturation region. Impedance, $Z_{in}(s)$ of the input stage of the proposed LNA, can be expressed as Eq. 1:

$$Z_{in}(s)=\frac{1}{SC_{gs1}}+\left(SL_1//\frac{1}{SC_2}\right) \quad (1)$$

where:

C_{gs1} = the gate-source capacitance of transistor M1.

Figure 3 shows a small-signal model of the input stage of the proposed LNA. The gain of the input stage can be found through analysis, as shown in Eq. 2:

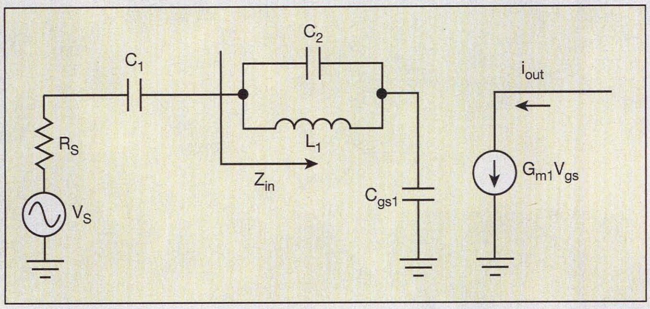

3. This small-signal model was used to simulate the behavior of the LNA's input stage.

$$\frac{V_{in}-V_{gs3}}{R_S}=V_{gs3}\times s\left(C_{gs3}+C_a\right)\rightarrow V_{gs3}=\left[\frac{V_{in}}{1+sR_s\left(C_{gs3}+Ca\right)}\right] \quad (6)$$

$$\frac{V_{out}}{V_{in}}=\frac{-g_{m3}Z_L}{\left[1+\frac{s}{1/R_s(C_{gs3}+C_a)}\right]\left[1+\frac{s}{1/\left[(1/g_{m4})(C_{gs4}+C_b)\right]}\right]} \quad (9)$$

$$\frac{V_{out}}{V_{in}}=\frac{-g_{m3}Z_{L3}}{\left[1+\frac{s}{1/R_s(C_{gs3}+2C_{gd3})}\right]\left[1+\frac{s}{1/\left[(1/g_{m4})(C_{gs4}+C_{gd4}/2)\right]}\right]} \quad (10)$$

$$A=\frac{I_O(s)}{I_{in}(s)}\approx-\frac{g_{m6}}{g_{m5}}\frac{\frac{1}{L_{gg}C_{gs6}}}{s^2+s\frac{1}{g_{m5}L_{gg}}+\frac{1}{L_{gg}C_{gs6}}} \quad (11)$$

$$F_{tot}=F_1+\frac{F_2-1}{A_{p1}}+\mathbf{L}+\frac{F_m-1}{A_{p1}\mathbf{L}A_{p(m-1)}} \quad (15)$$

$$A=\frac{-g_{m1}g_{m3}g_{m6}Z_{L1}Z_{L3}}{sC_{gs1}C_{gs6}L_{gg}g_{m5}(sL_1//\frac{1}{sC_2}+\frac{1}{sC_{gs1}}£)s^2£+s©\frac{1}{g_{m5}L_{gg}}+\frac{1}{L_{gg}C_{gs6}}\ddot{}\left[1+\frac{s}{1/R_s(C_{gs3}+2C_{gd3})}\right]\left[1+\frac{s}{1/\left[(1/g_{m4})(C_{gs4}+C_{gd4}/2)\right]}\right]} \quad (12)$$

$$F_{tot}\approx F_1+\frac{F_2-1}{A_{p1}}=1+2.4\frac{\gamma}{\alpha}\left(\frac{\omega}{\omega_T}\right)+\frac{\gamma}{\alpha}\frac{1}{g_{m3}R_{S3}}+\frac{\left[1+\frac{s}{1/R_s(C_{gs3}+2C_{gd3})}\right]\left[1+\frac{s}{1/\left[(1/g_{m4})(C_{gs4}+C_{gd4}/2)\right]}\right]}{g_{m3}Z_{L3}}$$
$$=1+\frac{\gamma}{\alpha}\left\{2.4\frac{\omega}{\omega_T}+\frac{\left[1+\frac{s}{1/R_s(C_{gs3}+2C_{gd3})}\right]\left[1+\frac{s}{1/\left[(1/g_{m4})(C_{gs4}+C_{gd4}/2)\right]}\right]}{g_{m3}^2R_{S3}Z_{L3}}\right\} \quad (17)$$

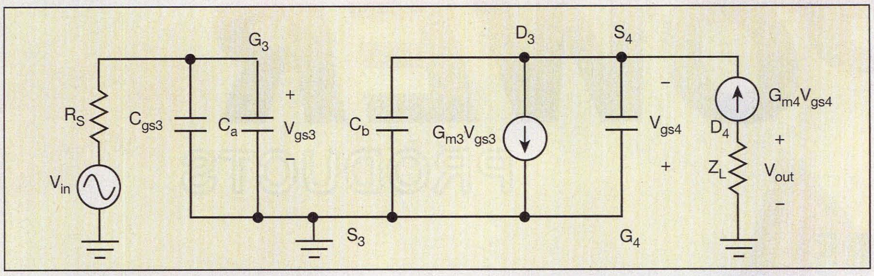

4. This small-signal model was used to simulate the LNA's cascode stage.

$$\frac{V_{out}}{V_{in}} = \frac{-g_{m1}Z_{L1}}{SC_{gs1}(SL_1 // \frac{1}{SC_2} + \frac{1}{SC_{gs1}})} \quad (2)$$

where:
g_{m1} = the transconductance of transistor M1.

The cascade second stage of the LNA includes M3, M4, L3, and its biasing circuit. The cascode stage biasing circuit is a current mirror composed of M2, R2, and R3. **Figure 4** shows a small-signal model of the proposed LNA's cascode stage.

According to the Miller Theorem, gate-source capacitance C_{gs} can be divided into capacitances C_a and C_b, as shown by Eqs. 3-5:

$$k = -g_{m3}/g_{m4} \quad (3)$$

$$C_a = G_{gd3}(1 - k) \quad (4)$$

$$C_b = G_{gd3}(1 - k) \quad (5)$$

According to the Kirchhoff Theorem, at the G1 terminal, there would be:
See eq. 6, p. 62.

$$V_{out} = -g_{m4}V_{gs4}Z_L \rightarrow V_{gs4} = \frac{-V_{out}}{g_{m4}Z_L} \quad (7)$$

and at the D1 terminal:

$$\frac{-V_{out}}{Z_L} = g_{m4}V_{gs4} = -V_{gs4} \times s(C_{gs4} + C_b) + g_{m3}V_{gs3} \quad (8)$$

See eq. 9, p. 62.

When $g_{m3} = g_{m4}$, then $k = -g_{m3}/g_{m4} = -1$; $C_a = C_{gd3}(1 - k) = 2C_{gd3}$; and $C_b = C_{gd3}/(1 - k) = C_{gd3}/2$.

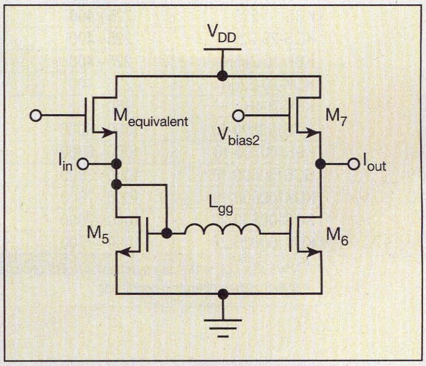

5. This NMOS current mirror with inductive series peaking was used in the current-mode LNA.

If the partial capacitances C_a and C_b are substituted into Eq. 10, then Eq. 10 appears like so.
See eq. 10, p. 62.

In this circuit, $Z_{L1} = sL_2$. By adjusting the ratio of the width to length for devices M1 and M3, it is possible to achieve high values for g_{m1} and g_{m3}, respectively, making it possible to achieve high gains for the LNA's first and second stages. Inductor L_1 has also been adjusted considering the balance between the input impedance matching and the gain.

Figure 4 shows the current mirror used in the three-stage LNA, with inductive series peaking. When the channel length modulation and the high-order effects of MOS transistors are neglected, the basic current amplifier shown in **Fig.4** with $L_{gg} = 0$ has a DC current gain of $A \approx -g_{m6}/g_{m5}$, where g_{mk} is the transconductance of transistor M_k. If a compensation inductor is placed in series with capacitance C_{gs2} (as shown in **Fig. 5**), with the assumption that $C_{gs6} >> C_{gs5}$, the transfer function of the current mirror can be given by Eq. 11.
See eq. 11, p. 62.

The series inductance was added to the NMOS current mirror to improve the amplifier's high-frequency performance. From Eq. 11, it can be seen that additional inductor L_{gg} does not affect the DC characteristics of the current mirror, but does improve the high-frequency characteristics and enhance the amplifier's wideband performance. By combining Eqs. 2 and 11, the transconductance gain of the current-mode LNA can be found from Eq. 12.
See eq. 12, p. 62.

Since an LNA is the first component block in a receiver, its noise figure will impact the overall performance of the receiver. A well-designed LNA should exhibit a noise figure of less than 3 dB.[12] For the proposed LNA, the noise performance

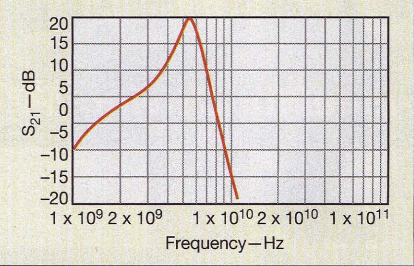

6. This is a post-layout simulation of the LNA's transconductance gain.

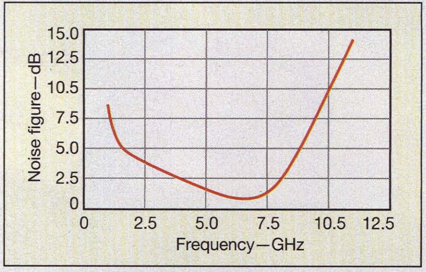

7. The simulated noise figure of the proposed LNA is plotted here.

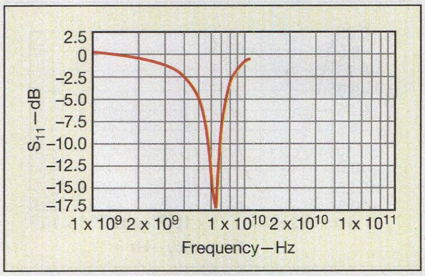

8. This plot represents the simulated S_{11} behavior of the proposed LNA.

is mainly determined by two factors: the loss of the input network and the noise of input stage M1. For the proposed LNA, the optimized noise figure of the first stage can be found from Eq. 13[13]:

$$F_{min} \approx 1 + 2.4\frac{\gamma}{\alpha}\left(\frac{\omega}{\omega_T}\right) \qquad (13)$$

while the optimized gate width of M1 is shown by Eq. 14:

$$W_{opt} = \frac{3}{2}\frac{1}{\omega_0 L_{eff} C_{ox} R_s Q_{sp}} \approx \frac{1}{3\omega L C_{ox} R_s} \qquad (14)$$

where:
α = a constant;
C_{ox} = the gate oxide capacitance per unit area;
L_{eff} = the effective gate length; and
Q_{sp} = the best quality factor, ranging from 3.5 to 5.5, as shown by Eq. 15.
See eq. 15, p. 62.

Noise in the LNA's second stage is contributed mainly by transistor M3, according to Eq. 16.

$$F_2 = 1 + \frac{\gamma}{\alpha}\frac{1}{g_{m3} R_{S3}} \qquad (16)$$

where:
g_{m3} = the transconductance of transistor M3, and
R_{s3} = the equivalent source impedance of M3.

By optimizing the gate width of M1, the noise figure of the LNA's first stage has also been optimized. Since it is a common-source stage with high gain, the value of A_{p1} is also high. By adjusting the width and the length of M3, a relatively high value of g_{m3} can be achieved, as can the low noise figure of the second stage. By combining the factors mentioned above, the circuit total noise figure can be found by Eq. 17.

See eq. 17, p. 62.

The proposed LNA was simulated with the aid of Cadence SpectreRF software from Cadence Design Systems (www.cadence.com) based on 0.18-µm RF CMOS semiconductor process parameters. A symmetrical layout was employed to minimize mismatches as much as possible. **Figure 6** shows a simulation of transconductance gain, which was 18.52 dB at 5.8 GHz. **Figure 7** shows the simulated noise figure, 0.93 dB at 5.8 GHz. **Figure 8** shows that the simulated S11 performance is –11.48 dB at 5.8 GHz, indicating good input match. **Figure 9** offers the LNA's simulated S22 performance, with return loss of 10.21 dB following optimized output matching. The power dissipation is 4.9 mW from a 0.85 V supply voltage. The layout diagram of the circuit is shown in **Fig. 10**, which takes a compact chip area of 0.9 × 0.8 mm.

The **table** compares the simulated performance levels of the proposed LNA with other published efforts. it can be seen that the proposed LNA has advantages of higher transconductance gain, lower noise figure, and lower power consumption compared to other LNAs at 5.8 GHz or at nearby frequencies.

In summary, this report has detailed the analysis and simulation of a 5.8-GHz LNA suitable for fabrication with a standard silicon CMOS process. The amplifier features a three-stage design, which includes a common-source structure without source degradation inductor, a cascode structure with shunt-peaking technique, and a current mirror with inductive series peaking. The LNA circuit promises high gain, low noise figure, and good impedance matching. MWRF

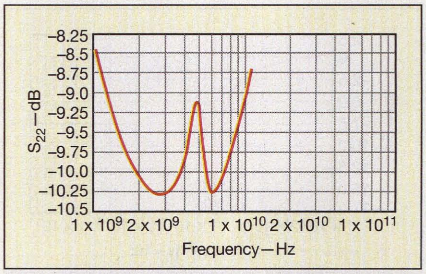

9. This plot represents the simulated S_{22} behavior of the proposed LNA.

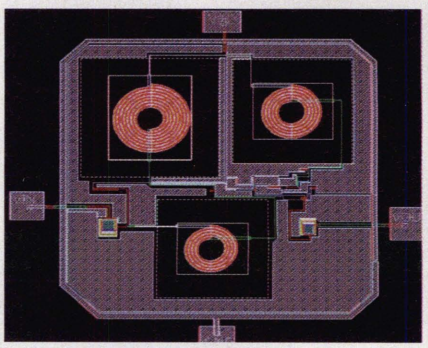

10. This layout shows the proposed current-mode LNA.

ACKNOWLEDGMENTS

The authors would like to thank the National Natural Science Foundation of China for financially supporting this research under No. 60776021, and the Open Fund Project of Key Laboratory in Hunan University No.09K011 for financially supporting this research.

REFERENCES

1. B. Kleveland, et al., "Exploiting CMOS reverse interconnects scaling in multigigahertz amplifier and oscillator design," IEEE Journal of Solid-State Circuits, Vol. 36, No. 10, October 2001, pp. 1480-1488.
2. T. Hui Teo and Yeoh Wooi Gan, "Low-power short-range radio CMOS subharmonic RF front-end using CG-CS LNA," IEEE Transactions on Circuits and Systems, 2008, pp. 658-662.

Parameters	This work	Reference 3	Reference 5	Reference 6	Reference 7
Frequency (GHz)	5.8	5.8	5.2	5.8	5.4
S_{11} (dB)	–11.48	–9	–27	–12.71	–10.1
S_{22} (dB)	–10.21	–20.7	–15	–15.52	–14
S_{21} (dB)	18.52	12.1	11.5	17.21	10.7
Noise figure (dB)	0.93	3.0	2.7	0.845	2.6
Supply (V)	0.85	1.2	2.0	N/A	0.7
Power consumed (mW)	4.9	3.8	12.0	N/A	6.3
Topology	single-ended, current-mode	single-ended, voltage-mode	single-ended, voltage-mode	single-ended, voltage-mode	single-ended, voltage-mode
Technology	CMOS 0.18 μm	SiGe BiCMOS 0.35 μm	BiCMOS 0.24 μm	FHX76LP low noise SuperHEMT FET	CMOS 0.18 μm

Comparing the LNA with previous efforts

3. M. Pourakbar, P. Langari, M. Dousti, F. Temcamani, B. Dracressoniere, and J. L. Gautier, "A 1.2-V Single-Stage SiGe BiCMOS Low-Noise Amplifier at 5.8 GHz for Wireless Applications," 3rd International Conference on Information and Communication Technologies, 2008, pp. 1-5.
4. Jyad Kebaisy, Sven Domann, and Bernd Meinerzhagen, "A 10-mW low-noise amplifier design for 5.5-GHZ wireless communication system," Information and Communications Technologies (ICTTA), 2006, pp. 2577-2582.
5. H. Chiu, Sh. Lu, and Y. Lin, "A 2.17-dB NF 5-GHz-band monolithic CMOS LNA with 10-mW DC power consumption," IEEE Transactions on Microwave Theory & Techniques, Vol. 53, 2009, pp. 813-824.
6. M.N. Husain, A.R. Othman, and M.S. Johal, "Simulation of single stage cascode low noise amplifier at 5.8GHz using t-matching network," 4th International Conference on Modeling, Simulation, and Applied Optimization (ICMSAO), 2011.
7. Baohong Liu and Junfa Mao, "A Low-Voltage 5.4 GHz monolithic cascode LNA using 0.18 μm CMOS technology," Microwave and Optical Technology Letters, 2010, pp. 386-389.
8. A. Bevilacqua and A.M. Niknejad, "An ultra-wideband CMOS LNA for 3.1 to 10.5.8-GHz wireless receivers," ISSCC Digest Technical Papers, 2006, p. 382.
9. B. Mohammadi and C.A.T. Salama, "A 5.8-GHz CMOS LNA for WLAN applications," IEEE Radio Frequency Integrated Circuits Symposium, 2004, pp.113-116.
10. Standard IEEE 802.11a-1999 (supplement to IEEE Standard 802.11-1999): "Information technology Telecommunications and information exchange between systems. Part 11: High-speed Physical Layer in the 5 GHz Band," IEEE, New York, 1999.
11. Viswanathan Subramanian, Marko Krcmar, M. Jamal Deen, and Georg Boeck, "A 6-GHz fully integrated SiGe LNA with simplified matching circuitries," Proceedings of the First European Wireless Technology Conference, 2008, pp.17-20.
12. D. Linten, et al., "A 5-GHz fully integrated ESD-protected low-noise amplifier in 90-nm RF CMOS," IEEE Journal of Solid-State Circuits, 2005.
13. Derek K. Shaeffer, Student Member, IEEE, and Thomas H. Lee, Member, IEEE, "A 1.5-V, 1.5-GHz CMOS low noise amplifier," IEEE Journal of Solid-State Circuits, Vol. 32, No. 5, May 1997.
14. Yang Lu, Kiat Seng Yeo, and Alper Cabuk, et al., "A novel CMOS low-noise amplifier design for 3.1-to-10.6-GHz ultra-wide-band wireless receivers," IEEE Transactions on Circuits and Systems, Vol. 53, No. 8, 2006, pp. 1683-1692.

CHENG ZHOU
Researcher

KE LU
Researcher

HUI-YONG ZENG
Researcher

JIAN-GANG LIANG
Researcher

GUANG-MING WANG
Researcher

Radar Engineering Department, Missile Institute of Air Force Engineering University, Shaanxi Province 713800, People's Republic of China; corresponding author: hyzeng.1023@163.com

CRLH-TLs Help Miniaturize PCBs

These innovative circuit structures can help achieve lower resonant frequencies in microstrip circuits without having to increase the length or size of the circuits, and without having to added lumped circuit elements.

MINIATURIZATION IS IMPORTANT for many high-frequency circuits, but often limited by the use of certain transmission-line technologies and circuit structures. Fortunately, compact composite right/left-handed transmission lines (CRLH-TLs) can be used to form resonant circuits without additional lumped circuit elements, helping to dramatically reduce the size of numerous printed-circuit-board (PCB) designs. In the present work, the CRLH-TLs are implemented by loading a host line with complementary split ring resonators (CSRRs) in combination with series gaps. Two designs will be presented, with the first employing equilateral triangular CSRRs and the second a novel CSRR; the latter will be realized by loading a pair of narrow slots in the split ring of the CSRR. In both approaches, the resonant frequencies are reduced by significant amounts. Equivalent circuit models will be offered for both cases.

A great deal of interest has been shown by the design community recently in metamaterials: Since they exhibit simultaneous negative values of effective permittivity and permeability, they are intriguing candidates for various high-frequency circuit structures. As far back as 1968, the existence of such materials was predicted, and the electrodynamic behavior of such materials was theorized.[1] In 2000, Smith fabricated the first left-handed structure, consisting of metallic posts and split-ring resonators (SRRs).[2] Metamaterials with negative permittivity and permeability can be implemented by SRR-based left-handed transmission lines, although another possible strategy employs a new structure based on the Babinet principle—i.e., complementary split-ring resonators (CSRRs).[3]

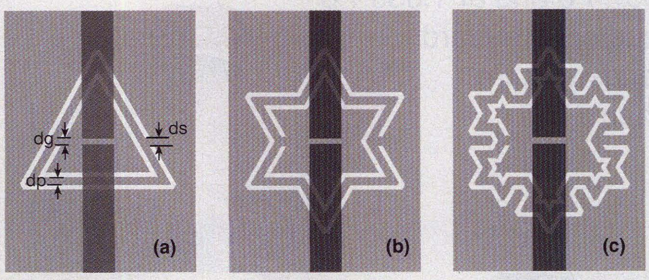

1. These diagrams show CRLH-TLs with Koch-fractal curve CSRRs of (a) zero order, (b) first order, and (c) second order.

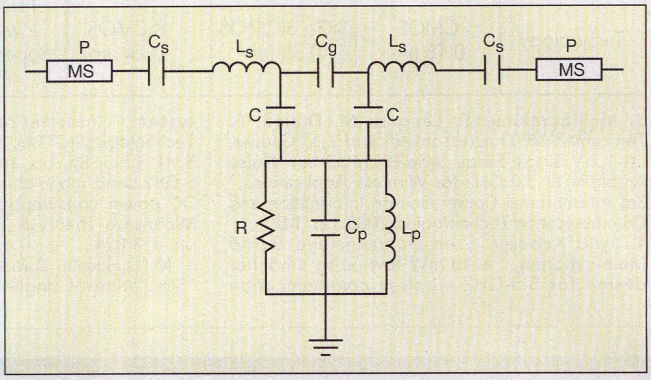

2. This is an equivalent-circuit model of the CRLH-TLs with Koch-fractal CSRRs.

These represent the negative image of SRRs, producing a sharp bandgap and negative permittivity effect around their resonant frequencies. The equivalent-circuit model of a CSRR structure behaves like a parallel inductive-capacitive (LC) resonant circuit.[4] CSRRs can be effectively excited by electric fields and are more suitable for implementation in microstrip circuits than SRRs in view of the electromagnetic (EM) field distributions of microstrip lines.[5] Composite right/left-handed transmission lines (CRLH-TL) can be synthesized in microstrip circuits, which is achieved by etching CSRRs in the ground plane and series capacitive gaps in the conductor strip.[6]

In modern communication systems, various characteristics are favored for passive circuit design. Therefore, compact CRLH-TLs are important structures for consideration in passive circuit designs.[7,8] Fractal technologies are often used to reduce the size of antennas and other components because of the unique space-filling properties of the fractal curves. These properties offers great potential for miniaturizing passive microwave circuits.[9] As an example, ref. 10 details novel CSRRs geometries that use square second- and third-order Sierpinski fractal curves.

To better understand the potential for CRLH-TLs in microstrip circuits, two compact CRLH-TLs will be examined in this report.

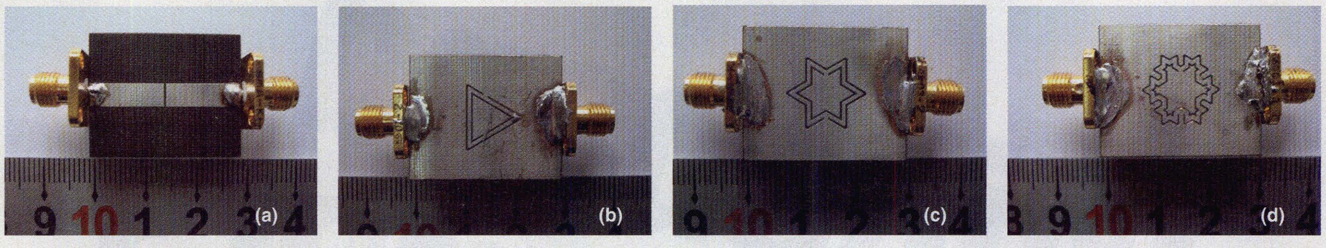

3. These photographs show top and bottom views of different CRLH-TL prototypes: (a) the top of the prototype, (b) the zero-order design, (c) the first-order design, and (d) the second-order design.

Figure 1(a) shows equilateral triangular CSRRs etched in a circuit ground plane. The dark grey area denotes the conductor strip and the light grey area is the ground plane. In **Figs. 1(b) and 1(c)**, first- and second-order Koch fractal curves are used to form equilateral triangular CSRRs (of zero order). The original curve is an equilateral triangle with side length of l. All the iterations are circumscribed inside a circumference of radius $r = (3l)^{0.5}/3$ and overall perimeter of $C_k = 3l(4/3)^k$.[11]

Figure 2 presents an equivalent-circuit model of these structures. In the model, parameter C_s represents the slot capacitance under the conductor strip, L_s is the line inductance, C_g is the gap capacitance, and C is the coupling capacitance between the line and the part surrounded by the slot. The equilateral triangular CSRRs are described by means of a tandem tank, L_p and C_p being the reactive elements and R accounting for losses. Two sections of microstrip line are used to compensate the phase response in the proposed structure.

CRLH-TL circuits were fabricated on F4B-2 woven-glass polytetrafluoroethylene (PTFE) copper-clad printed-circuit-board (PCB) material with relative dielectric constant of 2.65 and

Table 1: Comparing extracted parameters for CRLH-TLs with Koch-fractal CSRRs of different orders

Parameter	Fractal order		
	Zero	First	Second
C_g (pF)	29.63	26.59	25.01
L_s (nH)	1.51	2.03	3.40
C_s (pF)	0.88	0.68	0.47
C (pF)	4.26	2.53	1.19
C_p (pF)	8.23	3.08	0.83
L_p (nH)	0.37	1.35	4.88
R (kΩ)	0.27	5.72	16.52
p (mm)	5.18	7.41	9.82

Table 2: Comparing parameters for conventional and novel CSRRs

Parameter	Conventional CSRR	Structure 1	Structure 2	Structure 3
C (pF)	10.00	26.87	40.32	45.41
C_c (pF)	1.75	5.31	8.12	10.72
C_g (pF)	0.17	0.30	0.35	0.30
L (nH)	13.9	13.9	11.14	7.08
L_c (nH)	1.75	3.14	1.95	1.63
f_r (GHz)	2.31	1.1	1.16	1.14
f_z (GHz)	1.10	0.5	0.5	0.51

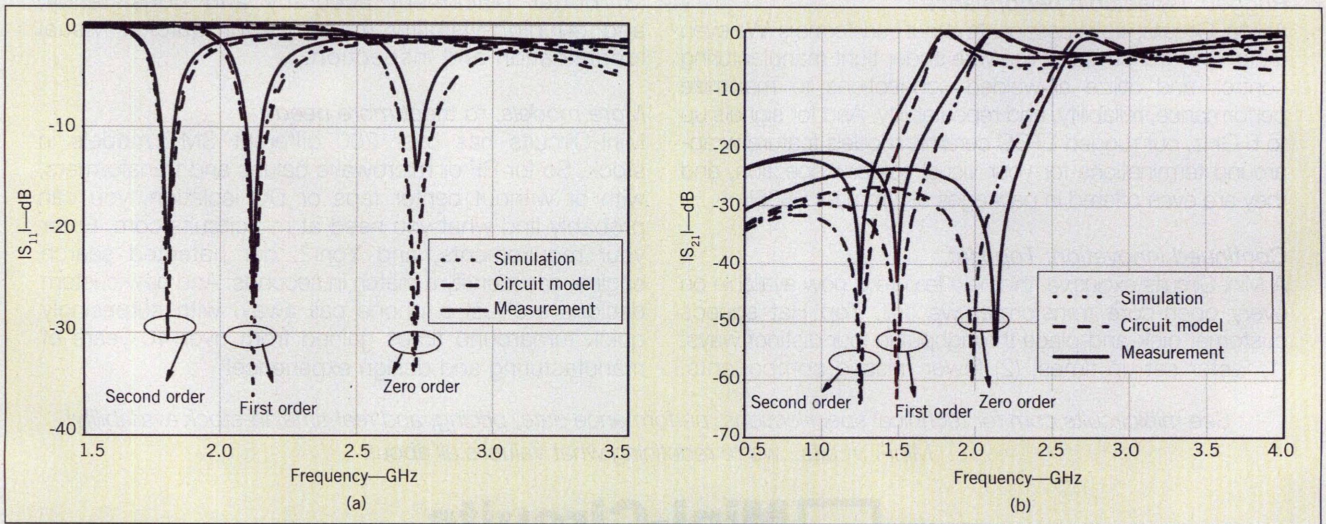

4. These curves compare simulated, circuit-model, and measured S-parameters for the CRLH-TL structures: (a) $|S_{11}|$ and (b) $|S_{21}|$.

thickness of 1.5 mm. The dimensions of the proposed structure were optimized as follows: l = 11 mm; d_p = 0.6 mm; d_s = 0.7 mm; and d_g = 0.4 mm. The width of the fractal CSRRs is 0.3 mm. The electrical parameters were extracted by means of the Ansoft Serenade circuit simulation software from ANSYS (www.ansys.com), with details shown in **Table 1**.

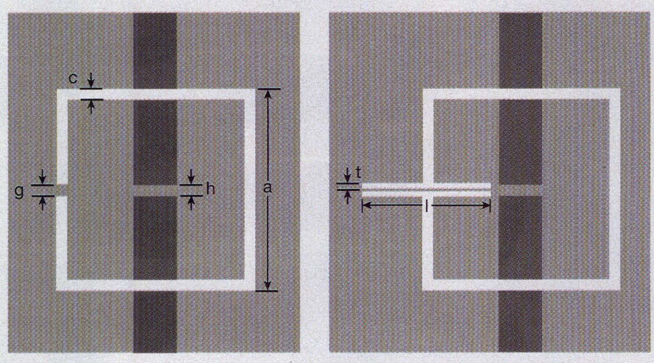

5. These diagrams compare an CRLH-TL structure with (a) a conventional CSRR and (b) the proposed CSRR.

Figure 3 shows images of the top and bottom layers of these structures, with circuit model, simulated S-parameters, and measured S-parameters shown in **Fig. 4.** The consistency of the simulated and measured results is apparent from **Fig. 4.** The resonant frequencies for the CRLH-TL structure with zero-order, first-order, and second-order Koch fractal CSRRs are 2.73, 2.12, and 1.80 GHz, respectively. As can be seen, reductions of 22% and 34% in the resonant frequencies are achieved, respectively, when first- and second-order Koch fractal CSRRs are substituted for conventional circuit structures.

Figure 5(a) shows a conventional CSRR etched into a ground plane. By loading a pair of narrow slots in the split of the ring, the second CRLH-TL approach was achieved, as shown in **Fig. 5(b)**. **Figure 6** shows simulated S-parameters for a CRLH-TL circuit

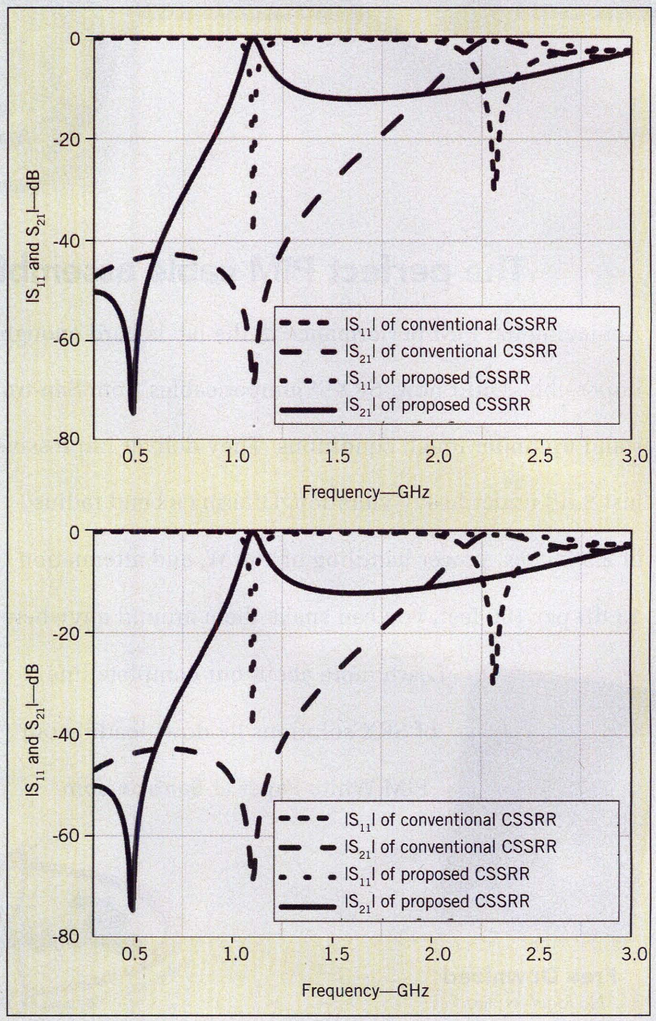

6. These curves represent simulated S-parameter data for the conventional and proposed CSRR structures.

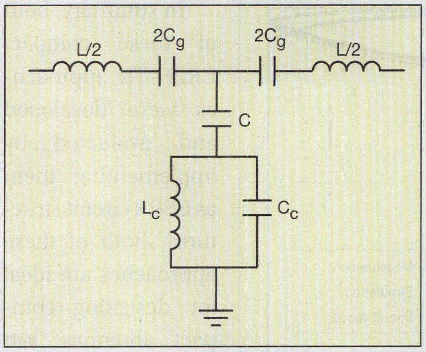

7. This is an equivalent circuit for the CRLH-TL structure with the proposed CSRR approach.

based on the conventional CSRR and one based on the loaded-slot approach. The approach with the loaded slots reveals a lower resonant frequency. This proposed CRLH-TL design can be modeled by means of the equivalent circuit of **Fig. 7**. In this model, L is the line inductance and C_g is the gap capacitance. The CSRR is modeled by the parallel resonant circuit (with inductance L_c and capacitance C_c), while its coupling to the host line is modeled by capacitance C. To reduce the size of the proposed structure, the slots are altered as the meander-shaped lines shown in **Fig. 8.** The total length of the slots is fixed.

This second CRLH-TL circuit was fabricated on a TP-2 circuit substrate with relative dielectric constant of 6.0 and thickness of 1 mm. The dimensions of the proposed structure were: a = 8.8 mm; c = 0.4 mm; g = 0.25 mm; h = 0.4 mm; l = 14 mm; and t = 0.25 mm. In order to demonstrate the correctness of the equivalent circuit model and analyze the reason why the resonant frequency is lower than the conventional cell, the electrical parameters are extracted as follows in **Table 2**.

Two specific frequencies are used in the process: the resonant frequency, f_r, and the transmission zero frequency, f_z, where $f_z = 1/2\pi[L_c(C + C_c)]^{0.5}$ at which the impedance of the shunt branch is equal to zero. The shunt branch presents inductive impedance between $1/[L_c(C + C_c)]^{0.5}$ and $1/(L_cC_c)^{0.5}$, which denotes equivalent negative permittivity. The series branch presents capacitive impedance when the frequency is less than $1/(LC_g)^{0.5}$, which denotes equivalent negative permeability.

Therefore, the left-handed band (including f_r) will appear if the frequency of the equivalent negative permittivity and negative permeability overlap. By comparing the results presented in **Table 2**, the frequencies f_r and f_z of the proposed structures can be lowered with respect to the resonant frequencies of a conventional CSRR,while proposed structures 1, 2, and 3 remain physically almost the same. Capacitances C and C_c are increased largely due to the significant increase of the coupling between the CSRR and the host line, essentially explaining why the resonant frequencies are lower in these modified approaches compared to conventional

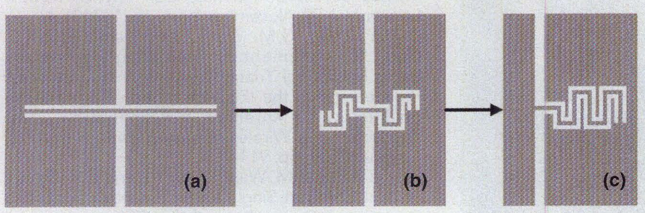

8. In these structures, the slots are shaped differently but the lengths are the same: (a) structure 1, (b) structure 2, and (c) structure 3.

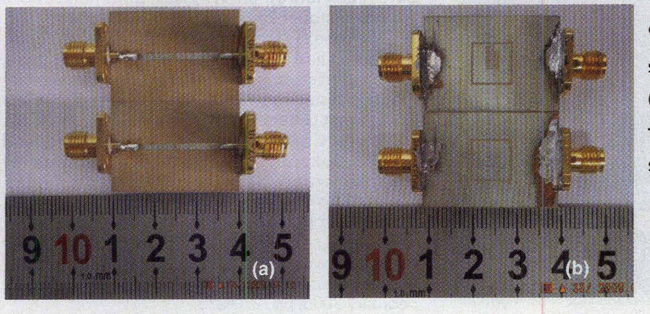

9. These photographs show the (a) top and (b) bottom sides of the fabricated CRLH-TL structures.

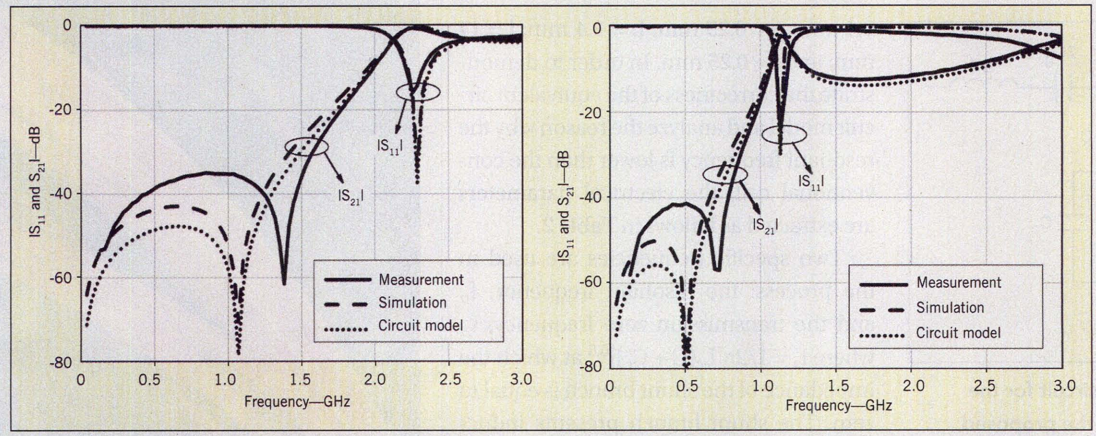

10. These curves compare simulated, circuit-model, and measured S-parameters for CRLH-TL circuits with (a) a conventional CSRR and (b) with one based on proposed structure 3.

CSRR circuits.

The resonant and transmission-zero frequencies, f_r and f_z, of CSRR structures 1, 2, and 3 using the second CRLH-TL approach are almost the same. Only one of the structures, structure 3, was fabricated **(Fig. 9)** and then simulated to compare its modeled and measured behavior **(Fig. 10)**. The simulated and measured results were consistent, revealing that the resonant frequency in this second CRLH-TL approach can be reduced by 52% when the CSRR structure 3 is substituted for a conventional CSRR.

In summary, both of these compact CRLH-TL approaches were developed and evaluated by implementing them as CSRR circuit structures. Both of these approaches are ideal for designing compact antennas. MWRF

ACKNOWLEDGMENT

This research has been supported by National Natural Science Foundation of China under Grant 60971118.

REFERENCES

1. V.G. Veselago, "The electrodynamics of substances with simultaneously negative values of ε and μ," Soviet Physics Uspeaki, Vol. 10, 1968, pp. 509-514.
2. D.R. Smith, W.J. Padilla, D.C. Vier, S.C. Nemat-Nasser, and S. Schultz, "Composite medium with simultaneous negative permeability and permittivity," Physical Review Letters, Vol. 84, May 2000, pp. 4184-4187.
3. F. Falcone, T. Lopetegi, J. D. Baena, R. Marqués, F. Martín, and M. Sorolla, "Effective negative-ε stopband microstrip lines based on complementary split ring resonators," IEEE Microwave and Wireless Component Letters, Vol. 14, June 2004, pp. 280-282.
4. J.D. Baena, J. Bonache, F. Martín, R. Marqués, F. Falcone, T. Lopetegi, M.A.G. Laso, J. García, I Gil, and M. Sorolla, "Equivalent circuit models for split ring resonators and complementary split rings resonators coupled to planar transmission lines," IEEE Transactions on Microwave Theory & Techniques, Vol. 53, April 2005, pp. 1451-1461.
5. Sheng Zhang, Jian-kang Xiao, and Ying Li, "Novel microstrip band-stop filters based on complementary split rings resonator (CSRRs)," Microwave Journal, Vol. 49, November 2006, pp. 100-112.
6. F. Falcone, T. Lopetegi, M. A.G. Laso, J.D. Baena, J. Bonache, R. Marqués, F. Martín, and M. Sorolla, "Babinet principle applied to the design of metasurfaces and metamaterials," Physical Review Letters, Vol. 93, November 2004, pp. 197401-4.
7. H.Y. Zeng, G.M. Wang, J.G. Liang, and X.J. Gao, "Complementary Split Ring Resonators Using Equilateral Triangular Koch Fractal Curves," Proceedings of the IEEE International Symposium on Microwave Antennas & Propagation, EMC Technology on Wireless Communications (MAPE), October 2009, pp. 911-913.
8. H.Y. Zeng, G.M. Wang, Z.W. Yu, and C.X. Zhang, "Novel Compact Single Complementary Split Ring Resonator," Proceedings of the IEEE International Symposium on Microwave Antennas & Propagation, EMC Technology on Wireless Communications (MAPE), October 2009, pp. 914-916.
9. F. Falcone, T. Lopetegi, J.D. Baena, R. Marqués, F. Martín, and M. Sorolla, "Effective negative-ε stopband microstrip lines based on complementary split ring resonators," IEEE Microwave and Wireless Component Letters, Vol. 14, June 2004, pp. 280-282.
10. Vesna Crnojevic-Bengin, Vasa Radonic, and Branka Jokanovic, "Fractal Geometries of Complementary Split-Ring Resonators," IEEE Transactions on Microwave Theory & Techniques, Vol. 56, October 2008, pp. 2312-2321.
11. V. Crnojevic-Bengin, "Novel compact microstrip resonators with multiple 2D Hilbert fractal curves," Microwave and Optical Technology Letters, Vol. 48, February 2006, pp. 270-273.

MILAD MIRZAEE
Engineer
Department of Electrical and Electronics Engineering, Eslamabad-E-Gharb Branch, Islamic Azad University, Eslamabad-E-Gharb, Kermanshah, Iran; e-mail: milad.mirzaee@gmail.com

SIR Cells Support UWB Lowpass Filter

This microstrip lowpass filter uses compact folded resonator cells to achieve an extremely broadband response with sharp rolloff characteristics in a small circuit size.

MICROSTRIP FILTERS provide vital frequency control functions in a wide range of RF/microwave systems. To be effective, they must be compact, with low passband insertion loss and high stopband rejection. In particular, lowpass filters can help limit spurious and harmonic signal content in higher-frequency systems, including at millimeter-wave frequencies, by passing desired frequency bands with minimal loss while attenuating unwanted higher frequencies. Among different emerging techniques for improving high-frequency circuit performance, the use of defected ground structures (DGSs) has shown great promise in the synthesis of microwave filters. A DGS is fabricated by etching a geometric shape from the ground plane of a printed circuit board (PCB); this results in an increase in the effective inductance and capacitance of a microstrip transmission line, supporting the design of ultrawideband (UWB) filters in relatively small circuit sizes. The use of UWB frequencies from 3.1 through 10.6 GHz in the United States, for example, is expected to increase rapidly in the next few years for short-range, high-data-rate communications.

DGS circuit elements offer great promise for the design and

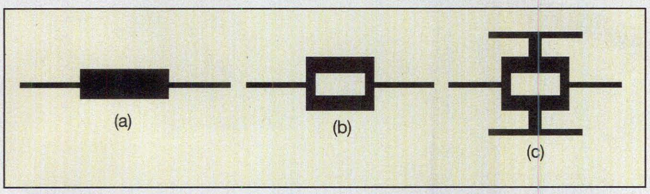

1. These approaches show the evolution of the TSSL-FSIR from its (a) basic format, to (b) a folded configuration, to (c) a T-shaped stub loaded, folded SIR.

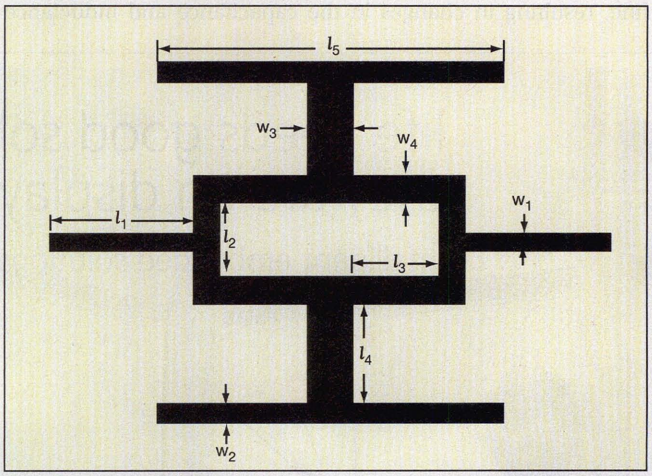

2. This diagram shows the key parameters of the TSSL-FSIR.

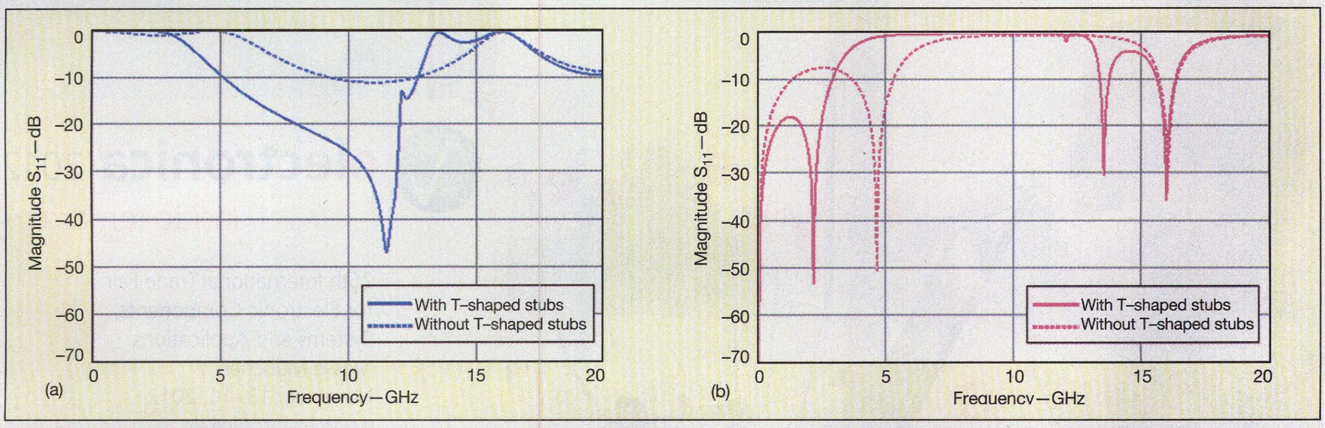

3. These plots show simulated S-parameters for the proposed TSSL-FSIR with and without T-shaped stubs: (a) S_{21} of the proposed lowpass filter with and without the T-shaped stubs and (b) S_{11} of the proposed lowpass filter with and without the T-shaped stubs.

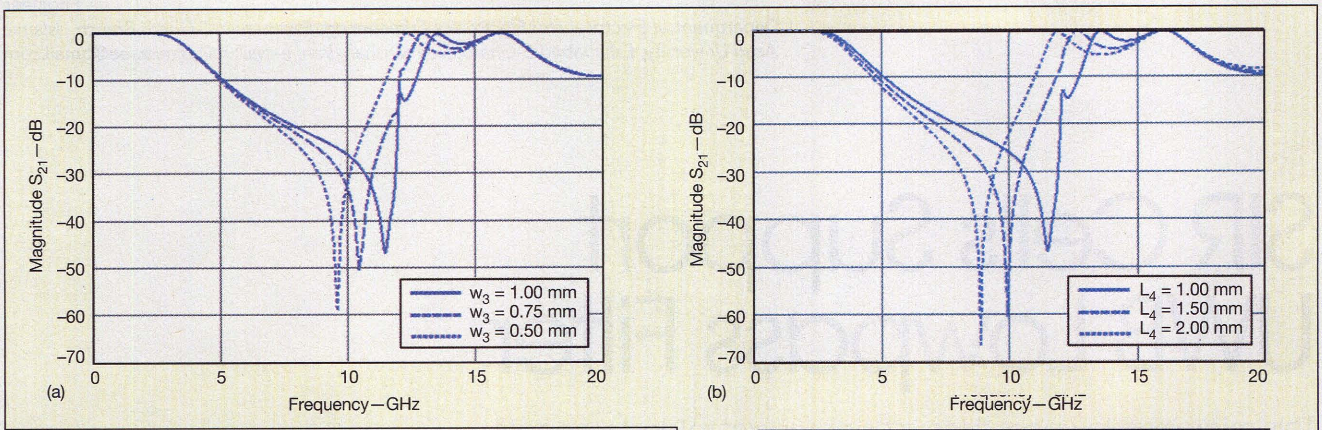

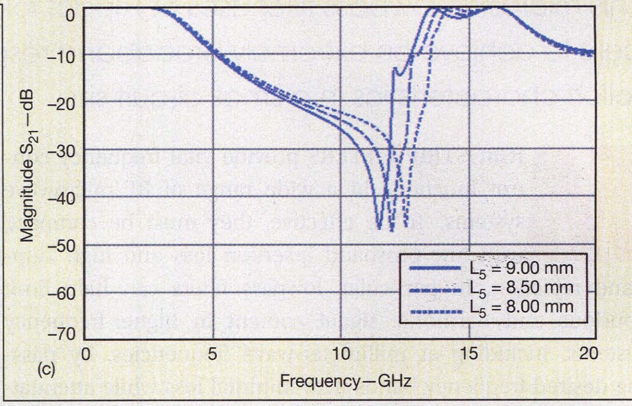

4. These simulated responses show the effects of different W3, L4, and L5 values: (a) S_{21} of the TSSL-FSIR with different values of W3, (b) S_{21} with different values of L4, and (c) S_{21} with different values of L5.

fabrication of not only filters and other passive planar circuits, but also in active circuits, such as amplifiers and oscillators. Essentially, a DGS is an intended defect etched into the ground plane of a planar transmission line, such as a microstrip or coplanar-waveguide (CPW) transmission line. The defect in the ground plane affects the current distribution of the transmission line, resulting in changes in the capacitance and inductance

characteristics. In fact, any defect that is etched into the ground plane of a microstrip circuit can increase the effective capacitance and inductance of the transmission line in proximity to the defect or DGS circuit element.

A DGS can be formed in a periodic or nonperiodic cascaded configuration, with the resulting circuit becoming much smaller than a conventional circuit without DGS elements. The key to successful implementation of DGS-based planar circuits is the use of DGS circuit elements that are relatively simple to design and fabricate, and which have also been well characterized. Although there is still much to know about the effective use of DGS circuit elements, many researchers have reported on different DGS configurations for which S-parameters have been measured and equivalent circuits extracted, for the purpose of analyzing DGS-based circuits with commercial computer-aided-engineer (CAE) software tools.

A number of circuit approaches have been employed to achieve good out-of-band performance and sharp rolloff in UWB lowpass filters, including cross-shaped DGS forms,[1] dumbbell and spiral-shaped slots,[2] semicircular DGS forms,[3] and quasi-π slots in the ground plane.[4] However, the radiating fields from the defected structures can also cause problems in the measurement and integration of other components to the circuit. The use of tapered compact microstrip resonator cells (TCMRCs) has been proposed for creating lowpass filters with wide stopbands.[5] Even though the performance of such a filter is good, the periodic arrangement of the CMRCs can result in a large physical size. Lowpass filters recently developed with slit-loaded tapered CMRC (SLTCMRC) structures have achieved sharp cutoff frequency. But they yield inadequate stopband rejection at typically 20 dB and can also suffer poor impedance matching in the passband that makes the design unsuitable for UWB use.[6]

One study revealed that open complementary split ring resonators (OCSRRs) can contribute to lowpass filters with very narrow transition bands.[7] Unfortunately, the design is still unreasonably large. In attempts to improve filter performance and reduce size, some of these filter configurations employ symmetrically loaded triangular or radial patches and a meandered main transmission line.[8,9] These filter designs do not appear suitable for applications requiring an extended passband, however. Different filter topologies using folded stepped impedance resonators (FSIRs) with parallel high-impedance segments have been proposed by this author for a compact notched UWB band-

pass filter[10] and an UWB lowpass filter offering a wide stopband.[11]

The use of a T-shaped stub loaded (TSSL) folded-stepped-impedance-resonator (TSSL-FSIR) approach, using a folded compact microstrip resonator cell, has shown great promise for designing compact, UWB lowpass filters with sharp rolloff response. This approach yields a deeper and broader rejection bandwidth than previously reported for such UWB lowpass filters. It achieves smaller size than lowpass filters that have been realized with other cascaded microstrip structures, including tapered compact microstrip resonator cells (TCMRCs), slit-loaded tapered compact microstrip resonator cells (SLTCMRCs), and OCSRRs.

Figure 1 depicts the evolution of the proposed TSSL-FSIR lowpass filter from a basic SIR circuit element. In the beginning, the SIR of **Fig. 1(a)** is converted into two parallel segments to create the loop shown in **Fig. 1(b)**. Then, the folded SIR is symmetrically loaded by T-shaped open stubs in the middle of parallel low-impedance segments at the top and bottom sections of the loop as shown in **Fig. 1(c)**. The use of T-shaped open stubs (compared to other structures) yields a steeper descent from the passband to the stopband, with a lower cutoff frequency and higher return loss in the passband. **Figure 2** shows the parameters for the proposed TSSL-FSIR lowpass filter.

To study the frequency response of the TSSL-FSIR circuit, its behavior was simulated by means of a commercial computer-aided-engineering (CAE) software tool, the Advanced Design System (ADS) suite of simulators from Agilent Technologies (www.agilent.com). Assumptions for the simulation included a printed-circuit-board (PCB) material with relative dielectric constant (ε_r) of 2.2 and a thickness of 20 mil and loss tangent equal to 0.0009. The parameters for the folded SIR are L_1 = 4 mm, L_2 = 1.5 mm, L_3 = 1.8 mm, L_4 = 1 mm, L_5 = 9 mm, W_1 = 0.2 mm, W_2 = 0.5 mm , W_3 = 1 mm, and W_4 = 0.5 mm. To better understand the impact of the T-shaped open stubs, the proposed resonator structure was simulated with and without the T-shaped open stubs, as shown in **Figs. 3(a) and 3(b)**, respectively. As these responses indicate, the T-shaped open stubs support a sharpness in transition from the filter passband to the stopband, while also improving the return loss and lowering the cutoff frequency compared to the resonator structure without the T-shaped stubs.

To better understand the influence of different T-shape open stub parameters on the frequency response of the resonator, simulated S-parameters were calculated for different dimensions of L_4, L_5, and W_3, as shown in **Figs. 4(a), 4(b), and 4(c),** respectively. One transmission zero is located at about 11.23 GHz, but its location can be adjusted by changing the values of W3, L4, and L5. As can be seen from **Fig. 4(a),** when W_3 increases from 0.5 to 1 mm in 0.25-mm steps, while the other parameters remain fixed, the transmission zero at 11.23 GHz will move higher in frequency. As shown in **Figs. 4(b) and 4(c),** however, by increasing L_4 from 1 to 2 mm and L_5 from 8 to 9 mm in 0.5-mm steps, the transmission zero at 11.23 GHz will approach the lower frequency.

Although the simulation results indicate impressive lowpass filter response, the filter design falls short of some requirements, notably in the transition region. By utilizing three TSSL-FSIRs, it was possible

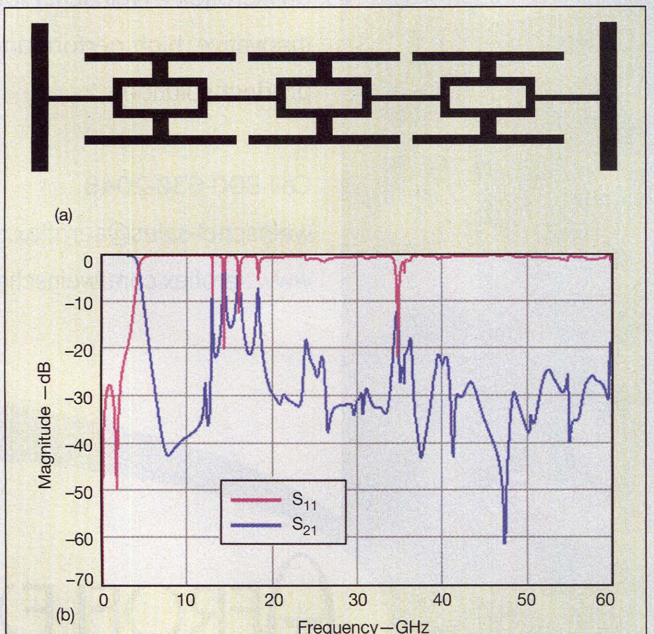

5. This schematic diagram (a) shows the proposed lowpass filter with cascaded TSSL-FSIRs along with (b) simulated S-parameter responses.

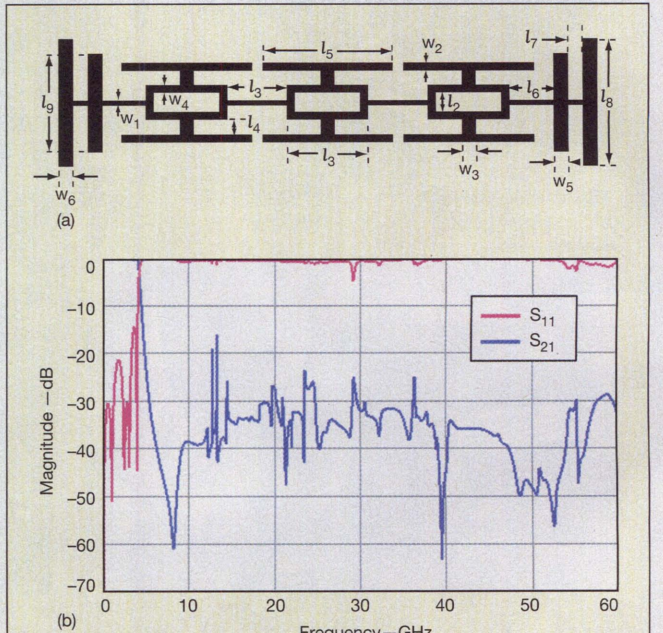

6. This schematic diagram (a) shows the final configuration of the novel lowpass filter (a) along with (b) its simulated S-parameter responses.

to develop a lowpass filter with wide stopband, as shown in **Fig. 5(a)**. It is constructed by using three cascaded TSSL-FSIRs with same physical dimensions and microstrip open stubs at the input and output ports in order to obtain low stopband radiation loss. The simulated response of this lowpass filter is shown in **Fig. 5(b)**. To eliminate unwanted harmonics that are not completely suppressed by the other circuit structures, so as to achieve a wide stopband, multiple open stubs are used in combination with the TSSL-FSIRs to form the final filter structure.

A schematic diagram of this final filter configuration is shown in **Fig. 6(a)**, along with its simulated S-parameter responses in **Fig. 6(b)**. The parameters of the filter were obtained and optimized as followed: L_1 = 4 mm; L_2 = 1.5 mm; L_3 = 5.6 mm; L_4 = 1 mm; L_5 = 9 mm; L_6 = 3 mm; L_7 = 1.2 mm; L_8 = 8.9 mm; L_9 = 4.1 mm; W_1 = 0.2 mm; W_2 = 0.5 mm; W_3 = 1.0 mm; W_4 = 0.5 mm; W_5 = 1 mm; and W_6 = 1 mm. The results show that the proposed filter has a 3-dB cutoff frequency of 4.17 GHz and insertion loss of less than 0.1 dB from DC to 3.23 GHz, or around 77% of the bandwidth. The return loss is better than 20 dB in this region.

The stopband return loss indicates that this filter structure exhibits low radiation loss. A transmission zero can be observed near the passband edge at 8.17 GHz, with an attenuation level of 62.92 dB. The transition band is a relatively narrow 13% of the bandwidth from 4.17 to 4.72 GHz, with attenuation levels of 3 and 20 dB, respectively, at those two frequency points. The filter design promises a stopband extending from 5.3 to 60 GHz with better than 30-dB stopband suppression and approximately 168% relative stopband bandwidth. The design has demonstrated a 123% increase in passband and 40% increase in relative stopband with –20 dB rejection, while achieving a 55% reduction in size compared with its classical counterpart in ref. 6 using the same PCB substrate.

In summary, a novel T-shaped stub loaded, folded SIR cell (TSSL-FSIRC) has been proposed as an effective design element for a lowpass filter with deep and wide stopband. A proposed filter consists of three TSSL-CMRCs connected in series. To cancel the spurious response resulting from the expanded rejection bandwidth, multiple open-circuited stubs were used in combination with the FC-MRCs in the filter structure. The simulation results confirm that at a 3-dB cutoff frequency of 4.17 GHz the lowpass filter exhibits less than 0.1 dB passband insertion loss, better than 20-dB passband return loss, sharp skirt performance, wide stopband with high suppression to 60 GHz, and compact physical size. This filter offers great potential for UWB communication systems where wide stopband, compact size, and easy integration with other microwave circuits are essential requirements. MWRF

REFERENCES

1. H.J. Chen, T.H. Huang, C.S. Chang, L.S. Chen, N.F. Wang, Y.H. Wang, and M.P. Houng, "A novel cross-shaped DGS applied to design ultra-wide stopband low-pass filters," IEEE Microwave and Wireless Components Letters, Vol. 16, No. 5, 2006, pp. 252-254.
2. J. Yang and W. Wu, "Compact elliptic-function low-pass filter using defected ground structure," IEEE Microwave and Wireless Components Letters, Vol. 18, No. 9, 2008, pp. 578-280.
3. F. Wei, L. Chen, X.-W. Shi, Q.-L. Huang, and X.-H. Wang, "Compact lowpass filter with wide stopband using coupled-line hairpin unit," Electronic Letters, Vol. 46, No. 1, 2010, pp. 88-90.
4. C.-J. Wang and C.-H. Lin, "Compact lowpass filter with sharp transition knee by utilizing a quasi-π-slot resonator and open stubs," IET Microwave Antennas and Propagation, Vol. 4, No. 4, 2010, pp. 512-517.
5. L. Li, Z.-F. Li, and W.-F. Wei, "Compact and selective lowpass filter with very wide stopband using tapered compact microstrip resonant cells," Electronic Letters, Vol. 45, No. 5, 2009, pp. 267-268.
6. M. Hayati and A. Lotfi, "Elliptic-function lowpass filter with sharp cutoff frequency using slit-loaded tapered compact microstrip resonator cell," Electronic Letters, Vol. 46, No. 2, 2010, pp. 143-144.
7. F. Aznar, A. Velez, J. Bonache, J. Menes, and F. Martin,"Compact lowpass filters with very sharp transition bands based on open complementary split ring resonators," Electronic Letters, Vol. 45, No. 6, 2010, pp. 316-317.
8. L. Ge, J.P. Wang, and Y.-X. Guo, "Compact quasi-elliptic microstrip lowpass filter with wide stopband," Electronic Letters, Vol. 46, No. 20, 2010, pp. 689-691.
9. J. Wang, J.L.-J. Xu, S. Zhao, Y.-X. Guo, and W. Wu,"Compact quasi-elliptic microstrip lowpass filter with wide stopband," Electronic Letters, Vol. 46, No. 20, 2010, pp. 1384-1385.
10. M. Mirzaee, "A novel small ultra-wideband bandpass filter including narrow notched band utilizing folded-T-shaped stepped impedance resonator," Progress in Electromagnetics Research C, Vol. 22, 2011, pp. 85-96.
11. M. Mirzaee, "UWB Lowpass Filter Features Wide Stopband," Microwaves & RF, Vol. 51, No. 3, March 2012, pp. 74-78.

ZHANG ZHAO-XIA
Lecturer

TONG HAI-LI
Postgraduate Student

ZHANG JIAN-ZHONG
Lecturer

XIAO BAO-JIN
Professor

SS Method Employs Novel Encryption

This spread-spectrum communications approach is based on true random sequence encryption for improved data-transfer efficiency and enhanced security compared to traditional systems.

SPREAD-SPECTRUM (SS) methods have long been used in communications systems to achieve certain levels of transmission efficiency and security. Unfortunately, traditional spread-spectrum approaches have typically employed pseudorandom sequences of codes characterized by an inherent periodicity which can be detected over time. As a solution, true random sequences generated by chaotic lasers can help achieve increased SS gain at a lower bit error rate (BER) than traditional SS systems based on pseudorandom bit sequences, while also improving the communications security.

In traditional SS systems, high-speed random codes are substituted for a 1-b source stream, making these transmissions more robust in the presence of interference. Typical techniques for spread spectrum communications are direct-sequence spread spectrum (DSSS), frequency-hopping spread spectrum (FHSS), time-hopping spread spectrum (THSS), and chirp modulation. Among them, pseudorandom sequences generated by an n-level m-sequence shift register with longest period of $2^n - 1$ are commonly adopted as SS codes. But theoretical studies have shown that this kind of SS spread spectrum communications systems based on pseudorandom sequences are prone to deciphering. Essentially, the m sequence can be determined when 2n b of m sequence transmission is received and decoded.[1]

In traditional DSSS communications systems, the SS sequence cannot be changed during the process of communications, allowing hackers to use the inherent periodicity to acquire the SS codes.[2] To enhance the anti-interference capabilities and the safety of SS systems, the codes should be varied. In 2005, Xingang Wang, et al.[3] proposed a scheme to generate chaotic binary codes by using a chain of coupled chaotic maps. Those researchers demonstrated that the codes can be applied to baseband SS communications systems. Although the period of such chaotic codes is, in theory, infinitely long, the period is practically limited by the word length of the system's microprocessor and can still be deciphered.[4] For true SS communications security, true random sequences are needed. Compared with the pseudorandom numbers as spreading codes, true random sequences have the characteristics of aperiodicity, unpredictability, and nonreplicability, and can only be deciphered with great difficulty.

There are many methods available for generating true random numbers. Traditional random-number generators are based on the thermal noise of circuits or resistances,[5] the oscillation frequency of an oscillation circuit,[6] the randomness of a quantum mechanics fundamental quantity,[7,8] circuit chaos,[9] or biological random characteristics.[10] But the rates of these ap-

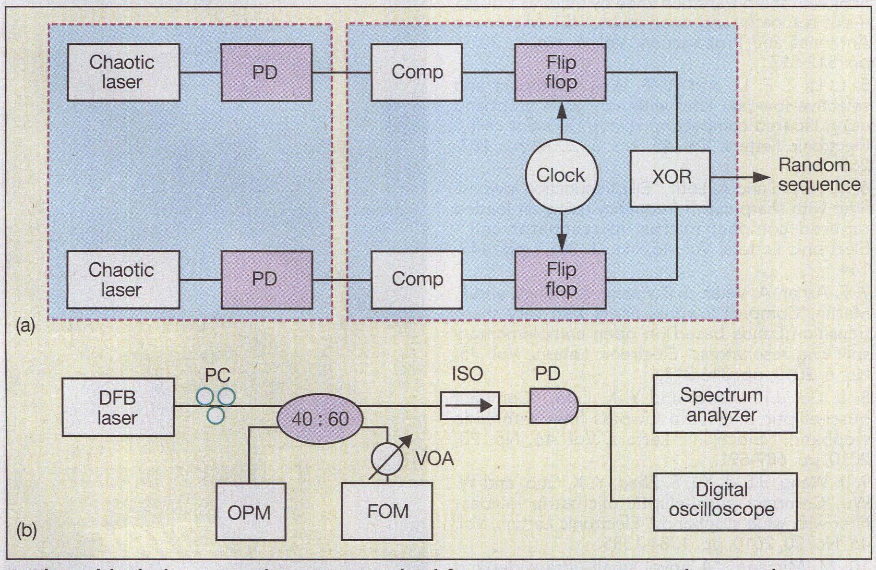

1. These block diagrams show (a) a method for generating true random-number sequences using chaotic lasers and (b) an experimental setup based on DFB lasers, where PD is a photodetector, OPM is an optical power meter, XOR is an exclusive OR gate, ISO is an optical isolator, FOM is a fiber-optic mirror, and VOA is a variable optical attenuator.

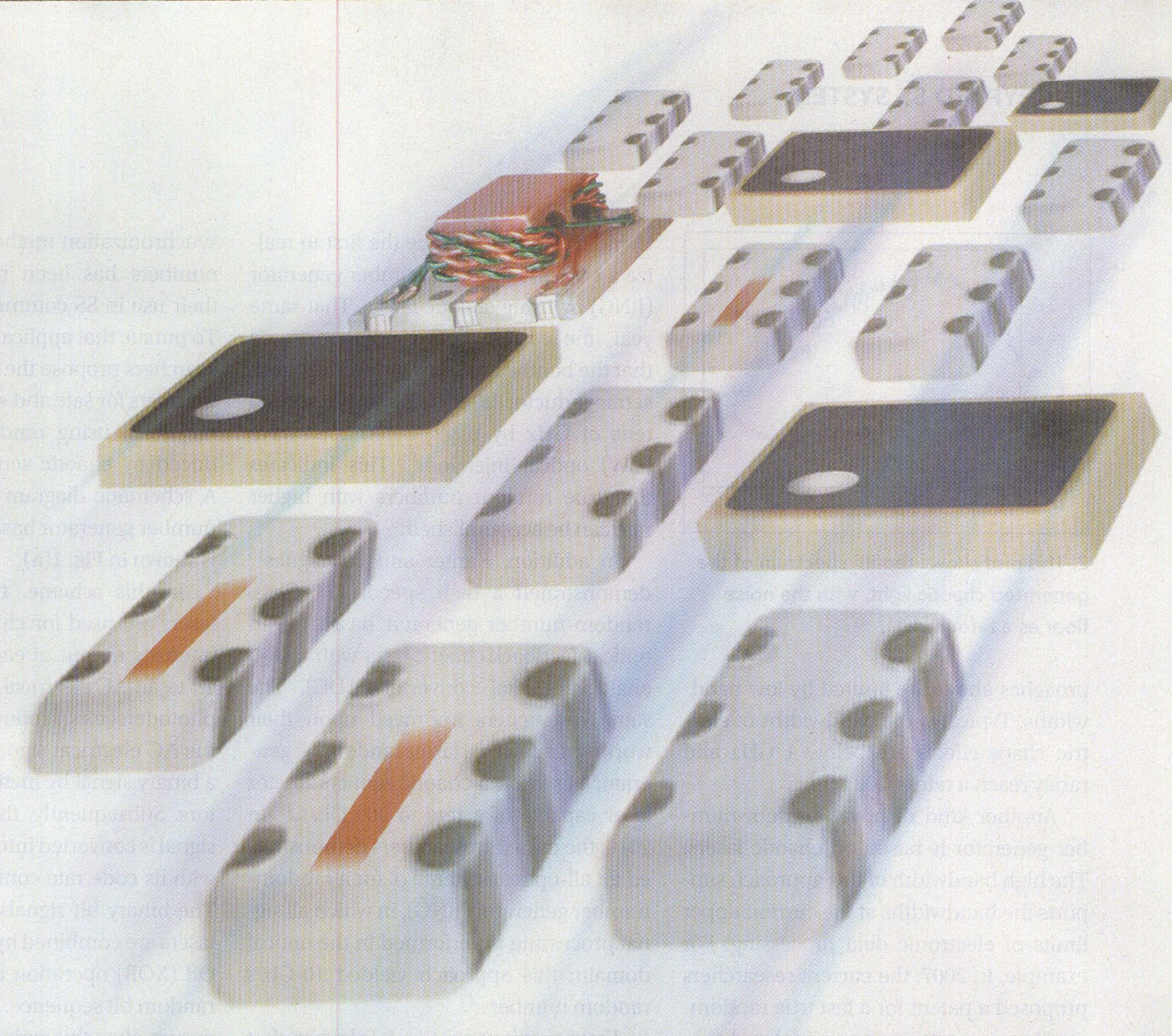

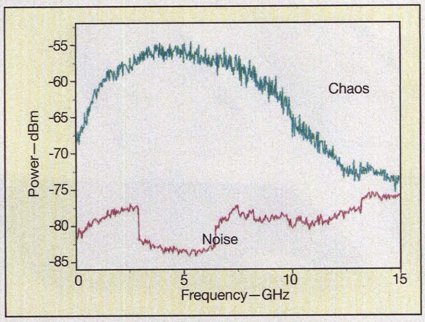

2. This plot shows the RF spectrum of the generated chaotic light, with the noise floor as a reference.

proaches above are limited by low bandwidths. Typically, the bandwidths of electric chaos effects are below 1 GHz and rarely reach a rate of 200 Mb/s.[9]

Another kind of novel random-number generator is based on chaotic lasers. The high bandwidth of this approach supports the bandwidths at the current upper limits of electronic data processing. For example, in 2007, the current researchers proposed a patent for a fast true random-number generator using a wideband chaotic light source, realized by an optical-feedback semiconductor laser.[11] In 2008, Uchida, et al.[12,13] became the first to realize a 1.7-Gb/s random-number generator (RNG) by using chaotic lasers. That same year, the current authors demonstrated that the bandwidth of an optical-feedback semiconductor laser can achieve several tens of GHz by using continuous-wave (CW) optical injection.[14] This indicates that true random numbers with higher rate can be accomplished.

In addition, Kanter and colleagues[15] demonstrated a high speed, 12.5-Gb/s, random-number generator based on an optical-feedback chaotic laser with an 8-b analog-to-digital converter (ADC). The same researchers improved upon their work by achieving a faster random bit generator based on a chaotic semiconductor laser capable of a rate to 300 Gb/s.[16] In 2010, the current researchers demonstrated an all-optical scheme of for a random-number generator (RNG), in which all signal processing is performed in the optical domain; this approach yielded 10-Gb/s random numbers.[17]

From previous studies, it is known that true random-number generators have reached Gb/s rates. It is also known that a synchronization method for true random numbers has been realized,[18] allowing their use in SS communications systems. To pursue that application, the current researchers propose the use of true random numbers for safe and efficient SS communications, using random numbers produced by chaotic semiconductor lasers. A schematic diagram of a true random-number generator based on chaotic lasers is shown in **Fig. 1(a)**.

In this scheme, two semiconductor lasers are used for chaotic intensity. The intensity output of each laser is converted to an AC electrical signal by means of photodetectors. Following amplification, the AC electrical signals are converted to a binary signal by means of two comparators. Subsequently, the generated binary signal is converted into a random number, with its code rate controlled by the clock. The binary bit signals obtained from the lasers are combined by a logical exclusive-OR (XOR) operation to generate a single random bit sequence. Any processing that occurs after this point can be applied to improve the randomness of the sequence.

Figure 1(b) shows the authors' experimental setup for a chaotic laser using distributed-feedback (DFB) semiconductor lasers. A circuit for chaotic signals based on semiconductor lasers can be seen in ref. 14. In experiments, the feedback light from semiconductor laser, a model LMD5S752 from Wuhan Telecommunications Devices Co. (WTD; www.wtd.com.cn), with center wavelength stabilized at 1550 nm and threshold current, I_{th}, set at 22.5 mA, is injected into the resonant oscillation cavity via a fiber reflection mirror. The intensity and polarization state of the optical feedback signals can be adjusted by a variable attenuator and a polarization controller, respectively. The intensity of the feedback light is monitored by an optical power meter. If the operating current of the laser is biased at 1.6 times more than I_{th}, at 22.5 mA, and the feedback intensity is 10%, the signal power of the chaotic laser from the DFB laser is 0.5 mW through a 40/60 optical fiber coupler. When the amplitude of optical signals is about 45 mV, the optical signals are converted to electrical signals

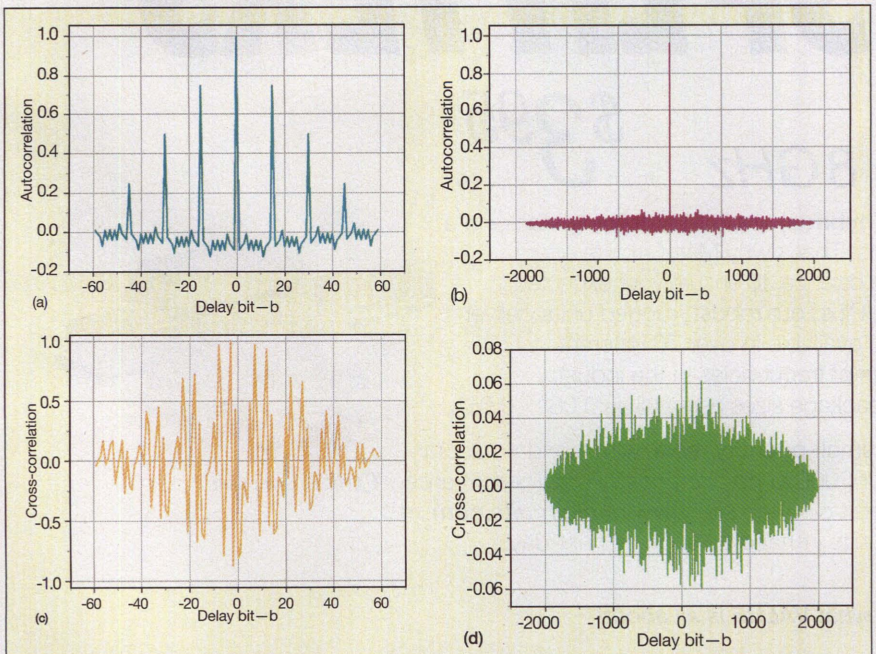

3. These plots show autocorrelation and cross-correlation functions: (a) an autocorrelation of m sequences with a period of 15, (b) an autocorrelation of a generated random sequence, (c) a cross-correlation of an m sequence with period of 15, and (d) a cross-correlation of a generated random sequence.

through a photoelectric detector.

Figure 2 shows the RF spectrum of the generated chaotic light and the noise floor. As can be seen, the bandwidth of the chaotic laser is about 6 GHz—considerably greater than a traditional entropy source, such as circuit chaos. The signal is sampled and stored by a real-time oscilloscope, a model TDS3052 from Tektronix (www.tek.com), which has a bandwidth of 500 MHz and sampling rate of 5 GSamples/s. For improved randomness of the generated random sequence, a post-processing method was adopted, such as the use of a two-way exclusive-OR (XOR) for post-processing. This yields true random-number sequences at 1 Gb/s, which pass all standard tests for randomness according to the United States National Institute for Standards and Technology (NIST) and their Special Publication 800-22.[19]

The "randomness" of the random sequence can be investigated by analyzing the self-similarity of the generated sequence. The similarity between two random sequences can be expressed by using the autocorrelation function, $R_{ac}(m)$, and the cross-correlation function, $R_{cc}(m)$. The expressions for these two functions are shown in Eqs. 1 and 2, respectively:

$$R_{ac}(m) = \lim_{N\to\infty} \frac{1}{N} \sum_{i=0}^{N-1} (x_i - \bar{x})(x_{i+m} - \bar{x}) \quad (1)$$

$$R_{cc}(m) = \lim_{N\to\infty} \frac{1}{N} \sum_{i=0}^{N-1} (x_{1i} - \bar{x})(x_{2(i+m)} - \bar{x}) \quad (2)$$

where:

x_i = the i-th bit value of the random sequence;

x_{i+m} = the i + m bit value of the random sequence;

$\bar{x}$ = the mean value of the random sequence;

x_{1i} = the i-th bit value of the first random sequence; and

$x_{2(i+m)}$ = the (i + m) bit value of the second random sequence.

The autocorrelation coefficient and the cross-correlation coefficient are the normalization of the autocorrelation function and the cross-correlation function. Ideally, the value of the autocorrelation function and the value of the cross-correlation function for the true random-number sequence should be values of some δ function and 0, respectively.

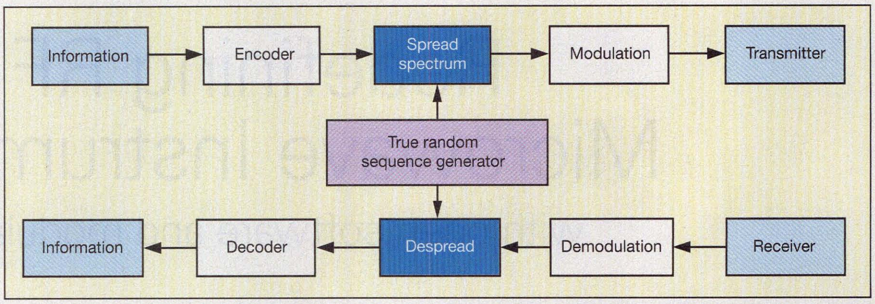

4. This schematic diagram shows a SS communications system using a true random-number sequence generator.

Figure 3(a) shows the autocorrelation function of a traditional m-sequence function. It reveals that the m-sequence function exhibits a strong periodicity. In comparison, the autocorrelation function of the random sequences generated by the chaotic lasers is shown in **Fig. 3(b)**. From it, we can see that its shape is similar with an δ function, indicating an improvement for these true random-numbers sequences compared to m sequences.

Figures 3(c) and 3(d) show cross-correlation functions of m sequences and true random numbers, respectively. They reveal a sharp pulse spiking in the cross-correlation function of m sequences, while the true random numbers present a relatively better cross-correlation function (and thus, their suitability as SS codes).

What is the impact of using random-number sequences on the capacities of different communications systems? In a traditional direct-sequence, code-division-multiple-access (DS-CDMA) communications system, the capacity of the system is determined by the available SS numbers. For example, if the spreading factor N is 1023, the available number of m sequences is only 60, which limits the capacity of the system. In contrast, if true random-number sequences are as SS codes, it can greatly enhance the capacity of the system. The true random-number sequence generated by chaotic semiconductor lasers is a kind of sequence with codes that are truly random and independent each other. The higher-order complexity of these codes enhances the anti-decryption and anti-interference characteristics of a SS system.

Figure 4 depicts a schematic diagram of a SS communication system. The transmitter converts an analog signal into a digital signal through an information source encoder. Following the SS operation, the signal is frequency modulated (FM) and transmitted via antennas. In this system, true random sequences are used for SS codes. In the receiver, the original signals can be recovered by following a reverse set of procedures.

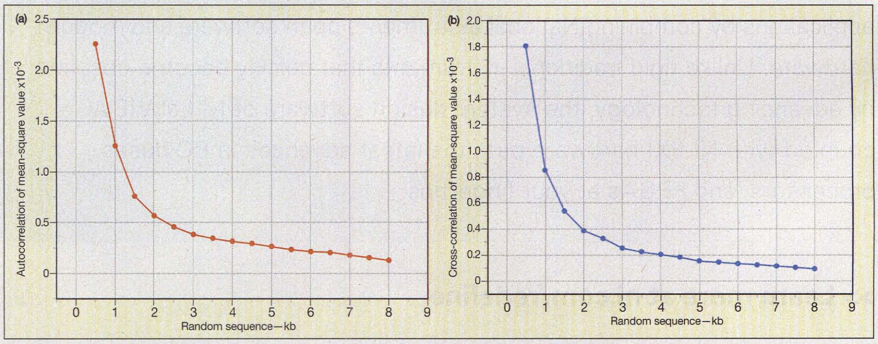

5. These plots show (a) autocorrelation and (b) cross-correlation mean-square values for the generated random sequence.

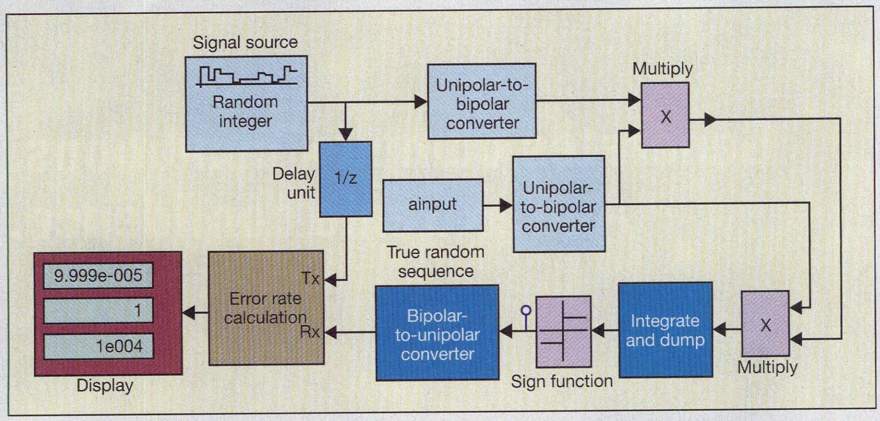

6. This model of a DSSS communications system was used in a MATLAB Simulink simulation.

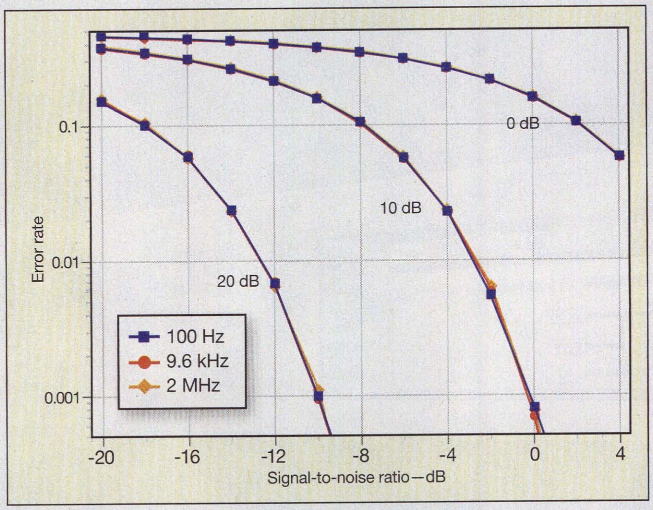

7. This plot shows the relationship of the bit-error ratio to SS gain and system SNR.

The use of a true random-number sequence in a SS communications system greatly increases the anti-interference capability of the system. Such a system faces two main forms of interference: multipath and multiple-user. Multipath interference is associated with the autocorrelation of SS codes, while multiple-user interference is mainly relative to the cross-correlation of SS codes. It is possible to choose SS codes with good orthogonality to minimize relevance between codes. In addition, the authors' experiments have found that the autocorrelation and cross-correlation of a true random-number sequence will decrease with an increase in the length of the random-number sequence. With an appropriate SS code length, SS system interference can be reduced.

The performance levels versus multipath interference and multiple-user interference can be characterized respectively via the mean-square value of the autocorrelation sidelobe and the mean-square value of the cross-correlation sidelobe.[4] The mean-square value of the autocorrelation sidelobe, $\delta^2_{ac}(m)$, and the cross-correlation sidelobe, $\delta^2_{cc}(m)$, can be written as Eqs. 3 and 4, respectively:

$$\delta^2_{ac}(m) = \frac{1}{M}\sum_{m=1}^{M}(R_{ac}(m))^2 \qquad (3)$$

$$\delta^2_{cc}(m) = \frac{1}{2M+1}\sum_{m=-M}^{M}(R_{cc}(m))^2 \qquad (4)$$

where:

$R_{ac}(m)$ = the value of the autocorrelation of the m-th bit of the generated sequence and

$R_{cc}(m)$ = the value of the cross-correlation of the m-th bit of the generated sequence.

Figure 5 shows a curve of the mean-square value of the generated random-number sequence. It can be seen that the mean-square value of the autocorrelation and cross-correlation sidelobes decrease with an increase in the length of the random-number sequence. When the random-number sequence length increases to 2000, the mean-square value of the autocorrelation and cross-correlation sidelobes will be less than 0.6×10^{-3}.

To analyze this further, a simulation was performed using MATLAB Simulink simulation software from The MathWorks (www.mathworks.com), choosing 2000 to 5000 b random sequences as SS codes. Simulink was used to build a simulation model of a DSSS communications system, as shown in **Fig. 6**. The binary random signal source is multiplied by the input true random-number sequences following polarity-reversal, to realize a SS communications system. Subsequently, the signal passes through an additive-white-Gaussian-noise (AWGN) channel. In the receiver, the signal multiplies the true random sequences to complete the dispreading process. Following that point, the signal will become binary random sequences though polarity reversal. During the simulation, an error bit analyzer is used to compare the transmitted binary random codes with the despreaded random codes in order to calculate the bit-error ratio.

Figure 7 shows the relationship among the information rate, spread spectrum gain, and bit-error ratio. When the information rate is constant, the SS gain increases with a decrease in the bit-error ratio. When signal noise ratio (SNR) is –20 dB, increasing the SS gain can effectively reduce the system bit-error ratio. It can be seen from **Fig. 7** that the SS gain is 0 in this system, while the bit-error ratio is 0.4623 when the information bandwidth is 2 MHz. If the information rate is also 2 MHz and the SS gain is 10 dB, the system bit-error ratio will be 0.3765. When the SS gain is 20 dB, the system bit-error ratio will be 0.1567. In essence, the influence of the information rate on the bit-error ratio is minimal. The channel bandwidth is enhanced when the information rate increases. Therefore, it is possible to reduce the bit-error ratio by increasing the SS gain in a practical SS communications system. In this system with true random-number sequences, a section of the sequence is used to represent digital "1" values, while a different section is used to represent digi-


i2S®
INTELLIGENT INTERACTIVE
SYNTHESIZERS
UP TO
18 GHZ
RF OUT
Product Features
> Exceptional Phase Noise Performance
> Ultra Low RMS Jitter, As Low As 3.7 Femtosecond
> Fast Switching
> Selectable Or Standard Programming Interface
> Single Or Dual Supply Options
> Surface Mount Or Connectorized
PATENTED TECNOLOGY
RoHS
REL-PRO®
For additional information, contact Synergy's sales and application team.
Phone: (973) 881-8800 | Fax: (973) 881-8361
E-mail: sales@synergymwave.com
Web: WWW.SYNERGYMWAVE.COM
SYNERGY®
MICROWAVE CORPORATION

tal "0" values. This processing method can double the noise margin of a SS communications system compared to one using orthogonal code.

In summary, the inherent periodicity of the pseudorandom sequences used in traditional SS communications systems limits the capacities of those systems. In the proposed SS scheme, improved capacity and security can be achieved. MWRF

ZHANG ZHAO-XIA, Lecturer, College of Physics and Optoelectronics, Taiyuan University of Technology, Taiyuan 030024, People's Republic of China, and State Key Laboratory of Millimeter Waves, Southeast University, Nanjing 210096, People's Republic of China; (+86) 13803436295.

TONG HAI-LI, Postgraduate Student, College of Information Engineering, Taiyuan University of Technology, Taiyuan 030024, People's Republic of China.

ZHANG JIAN-ZHONG, Lecturer, College of Physics and Optoelectronics, Taiyuan University of Technology, Taiyuan 030024, People's Republic of China.

XIAO BAO-JIN, Professor, College of Information Engineering, Taiyuan University of Technology, Taiyuan 030024, People's Republic of China.

ACKNOWLEDGMENTS

This project was supported by the Special Funds of the National Natural Science Foundation of China (Grant No. 60927007) and the National Natural Science Foundation of China (Grant No. 60872019), and was an open subject of the State Key Laboratory of Millimeter Waves (Grant No: K201108).

REFERENCES

1. K. Kurosawa, F. Sato, T. Sakata, and W. Kishimoto, IEEE Transactions on Information Theory, Vol. 46, 2000, p. 694.
2. Z. Zhong, X.T. Zhao, and G.H. Ren, Information Technology Journal, Vol. 8, 2009, p. 1076.
3. X.G. Wang, M. Zhan; X.F. Gong, C.H. Lai, and Y.C. Lai, Physics Letters A, Vol. 334, 2005, p. 30.
4. Z.B. Yu and Y.C. Feng, Acta Physics Sinica, Vol. 57, 2008, p. 1409.
5. C.S. Petrie and J.A. Connelly, IEEE Transactions on Circuits & Systems I, Vol. 47, 2000, p. 615.
6. M. Bucci, L. Germani, R. Luzzi, A. Trifiletti, and M. Varanonuovo, IEEE Transactions on Computers, Vol. 52, 2003, p. 403.
7. J. Liao, C. Liang, Y.J. Wei, L.A. Wu, and S.H. Pan, Acta Physics Sinica, Vol. 50, 2001, p. 467 (in Chinese).
8. M.M. Feng, X.L. Qin, C.Y. Zhou, L. Xiong, and L.E. Ding, Acta Physics Sinica, Vol. 52, 2003, p. 72 (in Chinese).
9. Z. Huang, T. Zhou, G.Q. Bai, and H.Y. Chen, Chinese Journal of Semiconductors, Vol. 25, 2004, p. 333 (in Chinese).
10. Q. Zhou, Y. Hu, and X.F. Liao, Acta Physics Sinica, Vol. 57, 2008, p. 5413 (in Chinese).
11. Y.C. Wang, J.H. Tang, and M J. Zhang, Chinese patent No. ZL200710062140.1, 2007 (in Chinese).
12. A. Uchida, K. Amano, M. Inoue, K. Hirano, S. Naito, H. Someya, I. Oowada, T. Kurashige, M. Shiki, Yoshimori S, Yoshimura K, Davis P, Nature Photonics, Vol. 2, 2008, p. 728.
13. K. Hirano, K. Amano, A. Uchida, S. Naito, M. Inoue, S. Yoshimori, K. Yoshimura, and P. Davis, IEEE Journal of Quantum Electronics, Vol. 45, 2009, p. 1367.
14. Anbang Wang, Yuncai Wang, and Hucheng He, IEEE Photonics Technology Letters, Vol. 20, 2008, p. 1633.
15. I. Reidler, Y. Aviad, M. Rosenbluh, and I. Kanter, Physical Review Letters, Vol. 103, 2009, p. 024102
16. I. Kanter, Y. Aviad, I. Reidler, E. Cohen, and M. Rosenbluh, Nature Photonics, Vol. 4, 2010, p. 58.
17. Li Pu, Yun-Cai Wang, and Jian-Zhong Zhang, Optics Express, Vol. 18, 2010, p.20360.
18. I. Kanter, M. Butkovski, Y. Peleg, M. Zigzag, Y. Aviad, I. Reidler, M. Rosenbluh, and W. Kinzel, Optics Express, Vol. 18, 2010, p. 17.
19. NIST Special Publication 800 - 22, 2001, http://csrc.nist.gov/groups/ST/toolkit/rng/documentation_software.html.

KNOW THE INS AND OUTS OF TESTING IEEE 802.11AC

CURRENTLY, wireless-local-area-networking (WLAN) standards are evolving to satisfy an increasing number of usage models. These efforts have spawned two IEEE project groups. Working Group TGac wants to specify IEEE 802.11ac as an extension of 802.11n. Running in the 5-GHz band, this standard will provide a minimum of 500 Mb/s single link and 1 Gb/s overall throughput. In partnership with the Wireless Gigabit Alliance (WiGig), Working Group TGad has proposed IEEE 802.11ad. It provides short-range throughput ranging to 7 Gb/s using about 2 GHz of spectrum at 60 GHz. In an 11-page application note titled, "Testing New-Generation Wireless LAN," Agilent Technologies (www.agilent.com) looks at the testing needs of IEEE 802.11ac in particular.

As an extension of the IEEE 802.11n standard, the IEEE 802.11ac PHY is already backward compatible with 802.11n. The theoretical maximum data rate for IEEE 802.11ac is 6.93 Gb/s using 160-MHz bandwidth, eight spatial streams, MCS9 with 256QAM, and a short guard interval. In contrast, the theoretical maximum data rate for IEEE 802.11n is 600 Mb/s using 40-MHz bandwidth with four spatial streams.

Some of IEEE 802.11ac's new features add complexity to both design and test. 256QAM demands better error-vector-magnitude (EVM) or constellation-error performance in the transmitter and receiver. EVM issues may be derived from imperfections in the in-phase/quadrature (I/Q) modulator, phase noise or error in the local oscillator (LO), or amplifier nonlinearity. To measure and identify causes of poor EVM, vector signal analysis may be used.

When it comes to 80-MHz-bandwidth signals, a lot of RF signal generators do not have a sufficiently high sampling rate to support the typical, minimum 2X oversampling ratio. The result may be images in the signal due to aliasing. With proper filtering and oversampling of the waveform file, however, 80-MHz signals can be generated with good spectral characteristics and EVM.

To generate 160-MHz-bandwidth signals, a wideband arbitrary waveform generator (AWG) can be used to create the analog I/Q signals. Those signals, in turn, can be applied to the external I/Q inputs in a vector signal generator for upconversion to RF frequencies. Alternatively, a 160-MHz-bandwidth signal can be created using 80+80-MHz models to create two 80-MHz segments in separate signal generators. The RF signals would then be combined.

By going from an overview of the standard to test needs and how they can be satisfied, this application note succeeds in providing essential information about IEEE 802.11ac. The note underscores the need for system simulation tools and the generation and analysis of 80- and 160-MHz-bandwidth signals and 256QAM for 802.11ac. With IEEE 802.11ac slated to be finalized at the end of 2013, such information is much in demand.

Agilent Technologies, Inc., 5301 Stevens Creek Blvd., Santa Clara, CA 95051; (408) 345-8886, FAX: (408) 345-8474, www.agilent.com.

CUT PIM IN CABLES AND CONNECTORS

PASSIVE INTERMODULATION (PIM) is evidence of nonlinear behavior in a communications system and some of its components. PIM is caused by the mixing of multiple tones, which results in unwanted signals. If the levels of these signals are high enough, the operation of a cellular base transceiver station (BTS) will be impacted. The result will be dropped calls for cellular customers and lost capacity for cellular network operators. In a five-page white paper, Fred Hull, Director of Engineering at San-tron (www.santron.com), explains how various mechanical structures can contribute to high PIM levels. Current flow through certain materials also can produce PIM signal energy.

The paper, titled "Minimizing PIM Generation from RF Cables and Connectors," begins with an explanation of PIM. When two signals (f1 and f2) mix, they can produce third-order, fifth-order, seventh-order, and higher-order harmonic-signal products. The third-order products, which are at the highest power levels, pose the greatest threat in terms of potential interference. These third-order PIM products can be produced by a combination of 2f2 - f1 or 2f1 - f2.

The nonlinear characteristics that cause PIM stem from the effects of corona generation, the use of paramagnetic materials, and the effects of current saturation. To avoid corona generation, one should develop RF geometries that support an application's expected power levels. Simply put, paramagnetic materials should not be used in any components that are intended for low-PIM communications applications. To deal with current saturation, additional mating force can be used at junctions between conductors. Micro-mountain tops can then be flattened to increase the contact surface area and reduce current saturation within the junction or connection.

San-tron, Inc., 4 Turnpike Rd., Ipswich, MA 01938; (978) 356-1585, FAX: (978) 356-1573, www.santron.com.

The bulk of the paper is devoted to a discussion of coaxial cable assemblies with braids, as they can present challenges when trying to achieve low PIM performance in a communications system. When the cables undergo flexure, for example, the braids rub over each other and are constantly repositioning themselves. Ground currents are continuously re-routed through the fine braids, which invites current saturation and non-transverse-electromagnetic (non-TEM) conditions or eddy currents within the cable braid structure. The paper emphasizes that braid structure is critical to the development of low-PIM system integration. Armed with an understanding of the mechanical tolerances, coaxial design details, and connector materials used in cable assemblies, designers can produce communications equipment with the lowest possible PIM levels.

JACK BROWNE | Technical Contributor

SIGNAL GENERATORS STRIVE FOR PRECISION

These 6-GHz analog and vector signal generators provide the types of signals that closely simulate those used in modern commercial and military electronic systems.

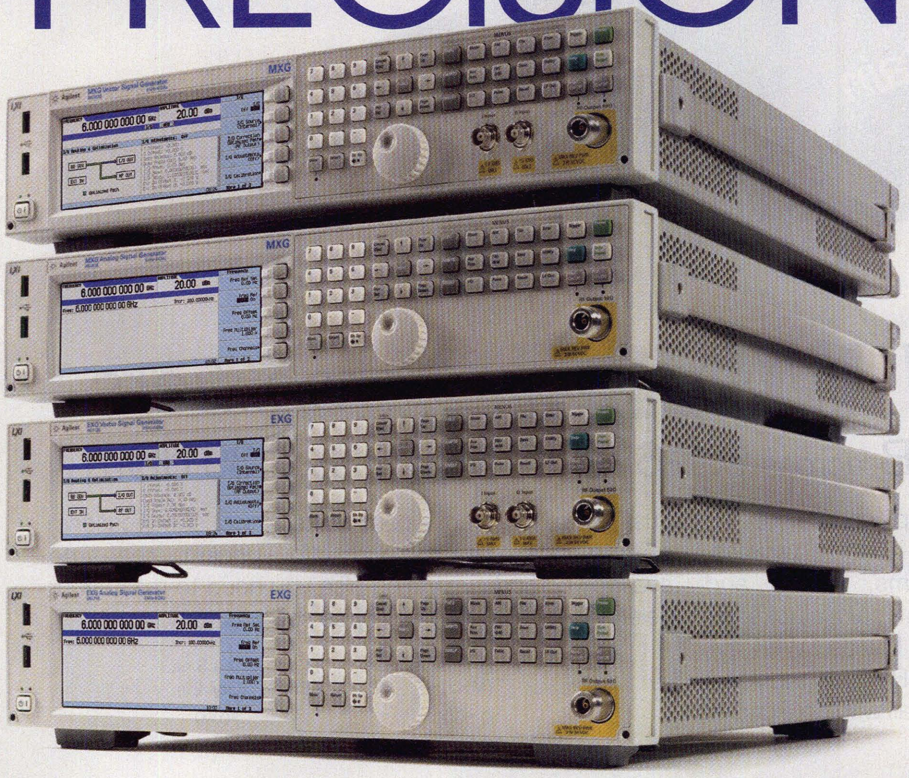

1. The X-Series signal generators include models with analog and digital (I/Q) modulation capable of covering a frequency range of 9 kHz to 6 GHz in a single instrument.

TEST SIGNAL GENERATORS were once much simpler, reflective of a time when engineers simply wanted to send a signal through a circuit to check a design's functionality. But as high-frequency circuit designs have grown in complexity, test signal generators have been forced to follow, so as to accurately emulate the signals that will be found under actual operating conditions. The new MXG and EXG X-Series signal generators from Agilent Technologies (www.agilent.com) reflect this obsession with accuracy, delivering new standards for signal purity for analog and vector test signals through 6 GHz.

The X-Series **(Fig. 1)** features four 6-GHz signal generators, two of which offer traditional analog output signals (models N5171B and N5181B) and two capable of providing vector in-phase/quadrature (I/Q) output signals (models N5172B and N5182B). The EXG models N5171B and N5172B deliver output levels to +21 dBm, while the higher-power MXG models N5181B and N5182B reach output levels to +24 dBm. Among other performance enhancements, the MXG models boast improved spectral purity over their EXG counterparts, with considerably better phase noise at all offsets and carrier frequencies **(see table)**.

However, even the "economy" models in this signal-generator family offer noteworthy performance over a bandwidth that is a match for many commercial communications applications—as well as a good number of military and industrial test applications through 6 GHz. The "low-end" model EXG N5171B **(Fig. 2)**, for example, is actually available per three different options (501, 503, and 506) in frequency ranges of 9 kHz to 1 GHz, 9 kHz to 3 GHz, and 9 kHz to 6 GHz, each with 0.01-Hz frequency resolution. The frequency synthesis architecture of the N5171B and the other signal generators enables a great deal of flexibility in terms of performance options, allowing users to select the limits that best suit their applications.

The N5171B signal generator features analog modulation (amplitude, frequency, phase, and narrowband pulse), while the model N5172B provides as much as 120-MHz internal I/Q digital modulation bandwidth (200 MHz with external inputs. Either can switch frequencies quickly in list/step sweep mode or under Standard Commands for Programmable Instruments (SCPI) program control. For standard models, the switching speed is typically less than 5 ms. Option UNZ can reduce the SCPI switching speed to less than 1.15 ms and the list/step sweep-mode switching speed to under 900 μs. Typical switching speed is better than 800 μs for both modes with this option. Switching is slightly slower in the model N5172B when digital modulation is switched on. For both models, the amplitude switching speed is similar: about 5 ms for standard units and under 1 ms for signal generators with fast-switching options, using list/step sweep mode or SCPI control.

The two EXG signal generators are stabilized by an internal 10-MHz crystal reference oscillator with nominal aging rate of better than ±5 ppm/10 years and temperature stability of ±1 ppm from 0 to +55°C. The generators also provide access to the internal reference via a coaxial connector, at a nominal level of +4 dBm into a 50-Ω load. The EXG signal generators can also be used with an external frequency reference source, operating at 10 MHz (and –3 to +20 dBm), with another option allowing the use of external frequency reference sources from 1 to 50 MHz.

Signal output levels for the N5171B and N5172B signal generators can be adjusted from –144 to +30 dBm with 0.01-dB resolution. Amplitude adjustments are made with the aid of an internal electronic step attenuator with an attenuation range of 0 to 130 dB, adjustable in 5-dB steps. The two EXG signal generators achieve maximum output-power

The X-Series Signal Generators At A Glance

Parameter	N5171B	N5172B	N5181B	N5182B
Frequency range	9 kHz-6 GHz	9 kHz-6 GHz	9 kHz-6 GHz	9 kHz-6 GHz
Generator type	analog	vector	analog	vector
Output power range (dBm)	-144 to +13	-144 to +13	-144 to +18	-144 to +18 dBm
Harmonics (dBc)	-35 dBc	-35 dBc	-35 dBc	-35 dBc
Spurious (dBc)	-60 dBc	-60 dBc	-65 dBc	-65 dBc
Phase noise (20 kHz offset from 1 GHz) (dBc/Hz)	-122	-122	-131	-131
Frequency switching speed (in list mode) (μs)	800	800	800	800

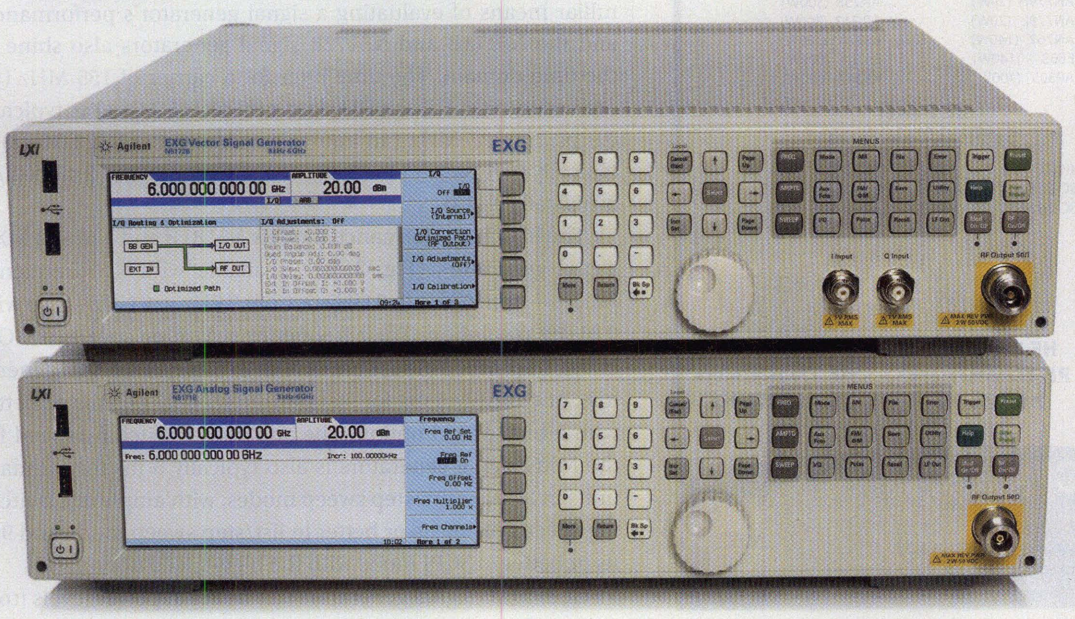

2. The EXG signal generators include the model N5172B instrument (top) with digital modulation and the model N5171B (bottom) with analog modulation.

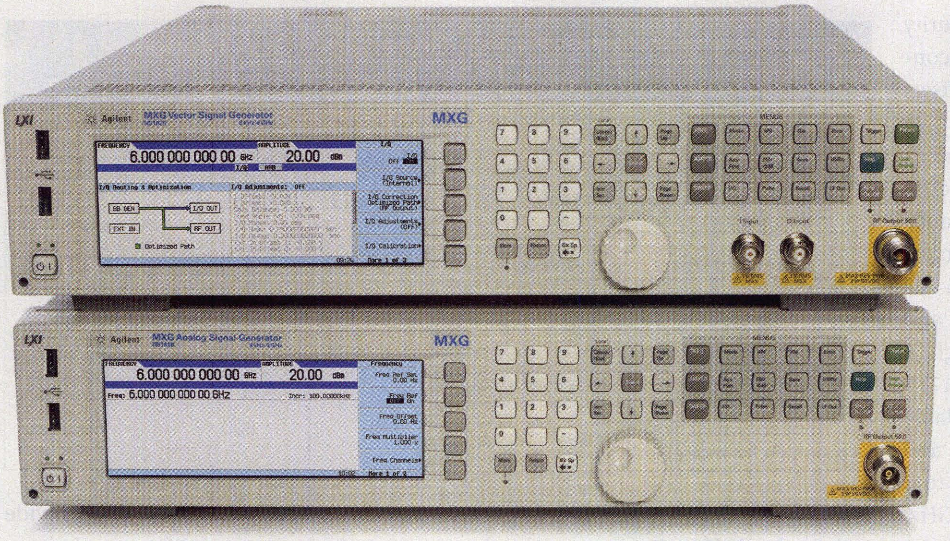

3. The MXG signal generators include the model N5182B synthesizer (top) with digital modulation and the model N5181B (bottom) with analog modulation.

levels in standard units of +13 dBm through 10 MHz, better than +18 dBm from 10 MHz to 3 GHz, and better than +16 dBm from 3 to 6 GHz. An option provides for increased output levels of +17 dBm through 10 MHz, +21 dBm from 10 MHz to 3 GHz, and +18 dBm from 3 to 6 GHz in both EXG signal generators. The absolute level accuracy for these generators in continuous-wave (CW) output mode and with the automatic level control (ALC) on is ±0.6 dB or better for output levels from –127 to –110 dBm from 5 MHz to 6 GHz, ±0.9 dB or better for output levels from –110 to –60 dBm from 9 kHz to 3 GHz, ±1.1 dB for those same output levels from 3 to 6 GHz, and ±0.8 dB or better for all frequencies at output levels from –60 to +21 dBm. For the N5172B, the absolute level accuracy in digital I/Q mode adds ±0.25 dB to the level accuracy numbers across the full frequency range.

The N5171B and N5172B EXG signal generators offer outstanding spectral purity, with standard units showing harmonic levels of typically –35 dBc from 9 kHz to 4 GHz and –53 dBc from 4 to 6 GHz when measured at an output signal level of +4 dBm. Nonharmonic spurious levels for standard units are typically –65 dBc from 9 kHz to 5 MHz, –75 dBc from 5 to 750 MHz, –72 dBc from 750 to 1500 MHz, –66 dBc from 1.5 to 3.0 GHz, and –60 dBc from 3.0 to 6.0 GHz. The absolute phase noise measured at a 20-kHz offset is typically –133 dBc/Hz at a carrier of 250.1 MHz, –122 dBc/Hz at 1 GHz, –110 dBc/Hz at 3 GHz, and –103 dBc/Hz at 6 GHz.

Of course, phase noise is a frequency-domain measure of a signal generator's stability. For high-speed data communications systems, the time-domain parameter jitter is a more familiar means of evaluating a signal generator's performance, and the N5171B and N5172B signal generators also shine in the time domain. The time jitter for a carrier of 155 MHz (an equivalent SONET or SDH data rate of 155 Mb/s) is typically 0.9 ps; for 622 MHz (an equivalent data rate of 622 Mb/s) is typically 0.11 ps; and for 2.488 GHz (a data rate of 2.488 Gb/s) is typically 0.11 ps.

The higher-performance models N5181B and N5182B MXG signal generators **(Fig. 3)** are available with two frequency ranges—from 9 kHz to 3 GHz or from 9 kHz to 6 GHz—also with 0.01-Hz resolution. Their frequency switching speeds in SCPI or list/step sweep modes are similar to those of the EXG generators, at typically 5 ms for standard units and 1.05 ms or better with a high-speed option. The amplitude switching speed for the MXG signal generators is also typically 5 ms for standard units in SCPI or list/step sweep modes, with amplitude switching speeds of 400 μs or better in list/step sweep mode and 950 μs or better in SCPI mode with the high-speed option.

Both MXG signal generators can be set at power levels from

Even the "economy" models in this signal-generator family **offer noteworthy performance.**

–144 to +30 dBm with 0.01-dB resolution. As with the EXG signal generators, the MXG instruments leverage the control of an internal electronic step attenuator with attenuation range of 0 to 130 dB, adjustable in 5-dB steps. The maximum output-power levels for standard MXG models is +13 dBm from 9 kHz to 10 MHz, +18 dBm from 10 MHz to 3 GHz, and +16 dBm from 3 to 6 GHz. With a high-power option (Option 1EA), the following maximum levels are available: +17 dBm from 9 kHz to 10 MHz, +24 dBm from 10 MHz to 3 GHz, +19 dBm from 3 to 5 GHz, and +18 dBm from 5 to 6 GHz.

The absolute level accuracy for the MXG signal generators in CW mode and with the ALC on is ±0.6 dB from 9 to 100 kHz at power levels from –60 to +24 dBm; it is ±0.9 dB across the same frequency range at power levels from –110 to –60 dBm. The absolute level accuracy is ±0.8 dB from 100 kHz to 5 MHz at power levels from –60 to +24 dBm; it is ±0.9 dB across the same frequency range at power levels from –110 to –60 dBm. The level accuracy is ±0.6 dB from 5 MHz to 3 GHz at power levels from –60 to +24 dBm; it is ±0.8 dB across the same frequency range at power levels from –110 to –60 dBm, and ±0.6 dB from 3 to 6 GHz at power levels from –60 to +24 dBm. Also, it is ±1.1 dB across the same frequency range at power levels from –110 to –60 dBm. For the model N5182B, the absolute level accuracy in digital I/Q mode adds ±0.25 dB to the level accuracy numbers across the full frequency range.

The MXG models N5181B and N5182B signal generators derive their outstanding spectral purity from a new triple loop synthesizer architecture and an internal frequency reference with ±1 x 10^{-7}/year nominal aging rate. After 30 days, this reference source exhibits a nominal aging rate of ±5 x 10^{-10}/day. The signal generators can also operate with an external 10-MHz reference oscillator (in standard units) or external reference oscillators operating from 1 to 50 MHz with square or sine-wave outputs (in signal generators with the proper option, Option 1ER).

Their spectral-purity performance levels include harmonics of typically –35 dBc measured at an output setting of +4 dBm from 9 kHz to 4 GHz and typically –53 dBc from 4 to 6 GHz. Non-harmonic spurious levels for signal generators with low phase noise options are –65 dBc from 9 kHz to 5 MHz, –75 dBc from 5 to 250 MHz, –96 dBc from 250 to 750 MHz,–92 dBc from 750 to 1.5 GHz, –86 dBc from 1.5 to 3.0 GHz, and –80 dBc from 3.0 to 6.0 GHz.

The absolute phase noise, which is noticeably lower than that of the EXG signal generators, measured at a 10-kHz offset with low noise option (UNY) is –144 dBc/Hz at a carrier of 250.1 MHz, –141 dBc/Hz at 1 GHz, –132 dBc/Hz at 3 GHz, and –126 dBc/Hz at 6 GHz. With an option (UNX), the phase noise can be diminished even further—as much a 10 dB or more at some carriers. The time-domain jitter for low phase noise optioned (UNX/UNY) MXG models for a carrier of 155 MHz (an equivalent SONET or SDH data rate of 155 Mb/s) is typically 0.25 ps; for 622 MHz (an equivalent data rate of 622 Mb/s) is typically 33 fs; and for 2.488 GHz (a data rate of 2.488 Gb/s) is typically 29 fs.

Both the N5172B and N5182B signal generators with wideband digital (I/Q) modulation can operate with either an internal or external I/Q modulation source. As much as 160 MHz I/Q bandwidth is available with the internal source and as much as 200 MHz I/Q modulation bandwidth is available with an external source. The two signal

4G 4 U

Dual RF Mixer Needs Only 600mW

Actual Size

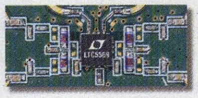

LTC5569 Total Solution Size: <220mm^2 Including External Components

300MHz to 4GHz, 26.8dBm IIP3 Dual Active Mixer

The LTC®5569 is the lowest power dual mixer with the highest performance and widest bandwidth. Its small form factor is optimized so you can pack more diversity or MIMO receiver channels in compact Remote Radio Heads. The mixer's wide frequency range allows you to build a wide range of multiband radios cost effectively. With integrated RF and LO balun transformers, the LTC5569 saves cost and precious board space. Each channel can be independently shut down, providing maximum flexibility to efficiently manage energy use.

▼ Dual Mixer Family

Part Number	Frequency Range	IIP3 (dBm)	Conv. Gain (dB)	NF/5dBm Blocking (dB)	Power (mW)	Package
LTC5569	0.3GHz to 4GHz	26.8	2	11.7/17.0	600	4mm x 4mm QFN
LTC5590	0.9GHz to 1.7GHz	26.0	8.7	9.7/15.5	1250	5mm x 5mm QFN
LTC5591	1.3GHz to 2.3GHz	26.2	8.5	9.9/15.5	1260	5mm x 5mm QFN
LTC5592	1.7GHz to 2.7GHz	26.3	8.3	9.8/16.4	1340	5mm x 5mm QFN
LTC5593	2.3GHz to 4.5GHz	26.0	8.5	9.5/15.9	1310	5mm x 5mm QFN

▼ Info & Free Samples

www.linear.com/product/LTC5569

1-800-4-LINEAR

Free Wireless Solutions Brochure

www.linear.com/wireless

LINEAR TECHNOLOGY

generators provide great flexibility in modulation formats, with capabilities for phase-shift-keying (PSK), quadrature-amplitude-modulation (QAM), frequency-shift-keying (FSK), minimum-shift-keying (MSK), and amplitude-shift-keying (ASK) formats.

In addition, these digitally modulated signal generators can be equipped with an optional (Option 403) internal additive white Gaussian noise (AWGN) generator with bandwidth of 1 to 60 MHz or 1 to 160 MHz, depending upon other options. Capable of a carrier-to-noise ratio (CNR) of better than 100 dB, the AWGN source is ideal for carrier-to-noise (C/N) measurements and evaluation of a device under test (DUT) under impaired performance conditions.

The MXG achieve their outstanding phase-noise performance **(Fig. 4)** thanks to a new triple-loop frequency synthesizer architecture and frequency plan that works with that synthesis approach. The result is improved phase noise close to the carrier and at wide offsets from the carrier. The combination of carefully selected reference frequency and frequency conversion, through mixers and multipliers, provides adequate spacing to allow filtering of signal artifacts (such as spurious signal products). The MXG vector signal generators even incorporate a real-time application-specific integrated circuit (ASIC) for some control over phase-noise levels in both CW and modulated signals.

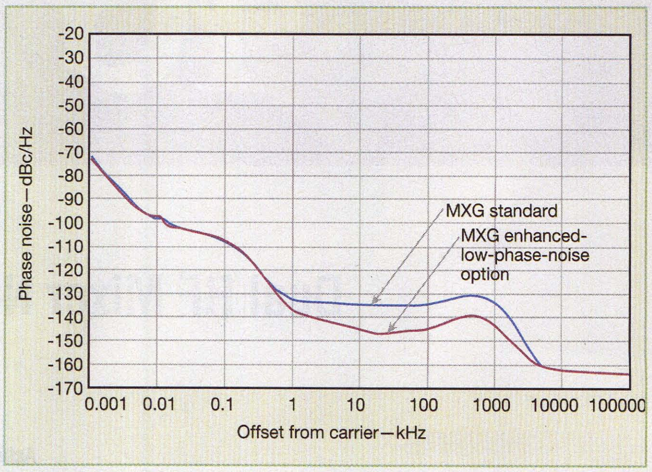

4. The MXG signal generators employ a triple-loop synthesis approach and unique frequency plan to achieve outstanding spectral purity to 6 GHz.

Given the many features and capabilities of these signal generators, operating them may seem intimidating. To help gain the greatest benefits from these test sources, each instrument is supplied with a trial version of Agilent's powerful Signal Studio control software for creating a wide range of test waveforms and controlling the signal generators.

For example, the software can greatly simplify the creation of digitally modulated waveforms as well as standardized test signals for wireless communications, such as for wireless local area networks (WLANs), Bluetooth, Global Positioning System (GPS) & GLONASS navigation systems, and cellular GSM, EDGE, and Long-Term-Evolution (LTE) testing. In fact, those not yet committed to the purchase of an EXG or MXG signal generator can try a free 14-day trial license of Signal Studio at www.agilent.com/find/SignalStudio_trial. P&A: from $6,900 (N5171B, from $16,970 N(5172B), from $15,500 (N5181B), and from $19,320 (N5182B); 30 days. MWRF

AGILENT TECHNOLOGIES, INC., 5301 Stevens Creek Blvd., Santa Clara, CA 95051; (877) 424-4536, (408) 345-8886, FAX: (408) 345-8475, e-mail: us@agilent.com, *www.agilent.com.*


TRM
MICROWAVE
COMPLETING YOUR IDEAS®
Custom component ZONE
military · space · commercial
Integrated Beamformer
Custom SQ Power Divider
Quadrature Hybrid
16 Way Broadband Power Divider
TRM is a recognized leader in the design and manufacture of custom RF and microwave components, integrated assemblies and subsystems solutions for defense, space and commercial applications.
• Unique mechanical packaging
• Excellent electrical performance
• HF through Ku band
• ISO 9001: 2008 certified
• High-mix / low volume
Over its 42 year history, TRM Microwave has built its solid reputation by engineering innovative solutions for mission critical applications. Our catalog of standard power dividers, couplers and hybrids provides a cost-effective path for upgrading to hi-rel space-qualified components. To learn more about TRM's custom capabilities email info@trmmicrowave.com or call us today at 603.627.6000.
F35
F22
F15
E18
Global Hawk
trmmicrowave.com
Custom Solutions
trmmicrowave.com
603.627.6000 | info@trmmicrowave.com

Analyzing Recent Advances in Antennas

Antenna technology is moving forward as a result of improved printed circuits and mechanical designs, and even through the use of arrays backed by advanced signal processing.

ANTENNAS ARE the most visible components of communications systems. They come in many forms, including large parabolic dishes pointing towards space and rectangular sector antennas on cell towers. But in some cases, they also must be designed not to be seen, such as for use inside cell phones and other wireless products.

In terms of antenna advances, few commercial companies can match the recent efforts of the US Army's Communications-Electronics Research, Development, and Engineering Center (CERDEC) at Fort Monmouth, NJ, including body-wearable antennas (BWAs) and distributed antenna arrays (DAAs). BWAs include plate structures built into a soldier's protective armor as well as antennas fabricated as part of a helmet. Both approaches have been demonstrated with wideband radios capable of operating through 1 GHz.

One of the challenges in designing such antennas is making them small enough to operate at military wavelengths within very-high-frequency (VHF) and ultra-high-frequency (UHF) bands, since wavelengths grow larger at those lower frequencies, and an antenna's physical size is a function of the operating frequency wavelength. Another issue in having antennas that are part of a soldier's uniform is the effects of electromagnetic (EM) radiation on the human body.

CERDEC is also studying DAAs, with an eye toward using them to jam improvised explosive devices (IEDs) in the field. In one study, directional DAAs were mounted on both sides of a military vehicle, with the vehicle given a clear zone between the two antennas for its own communications. By transmitting broadband signals with circular polarization, remote communications to the UEDs are prevented. Since most IEDs are assembled with whip antennas, which may use vertical or horizontal polarization, the circular polarization helps enhance the jamming effectiveness of the DAA-based jamming transmitter.

Growing needs for small, broadband antennas for surveillance and monitoring purposes have driven the development of some extremely wideband antennas, such as the model 3164-05 open boundary quad-ridged horn from ETS-Lindgren (www.ets-lindgren.com), which is capable of operating from 2 to 18 GHz. The unique appearance of the antenna is due to the absence of side plates and a configuration that is similar to having a pair of Vivaldi printed-circuit-board (PCB) antennas positioned orthogonally. The antenna's orthogonal input feeds allow it to generate both linear and circularly polarized patterns across the full frequency range. Since it is physically small, its phase center changes very little across the broad frequency range.

1. A small cross section and cylindrical radome design helps dramatically reduce the wind loading on these broadcast antennas. [Photo courtesy of Radio Frequency Systems (RFS; www.rfsworld.com).]

In addition to its novel antennas, the company also offers the model AMS-8050 antenna measurement system, a portable anechoic chamber that provides over-the-air (OTA) performance measurements of small wireless devices and mobile handsets. It is built on a movable cart for convenience and features a fully anechoic test chamber measuring 30 x 30 in. (76.2 x 76.2 cm), complete with RF shielded door. The shielded chamber has a dual-polarized antenna installed in the enclosure ceiling, with frequency range of 700 MHz to 10 GHz. It provides connections to outside test equipment, including vector network analyzers (VNAs) and spectrum analyzers. The measurement chamber can be used to analyze two-dimensional (2D) and three-dimensional (3D) antenna patterns, total radiated power (TRP), and effective isotropic radiated power (EIRP). It is shipped with the company's model EMQ-100 Antenna Pattern Measurement Software to simplify measurements.

Some antennas are as simple as radiating cables, especially for certain applications that require coverage within long, narrow confines, such as within aircraft and mines. Notable in this category are the GORE® cable-based antennas for aircraft and mining

applications from W.L. Gore & Associates (www.gore.com). These lightweight radiating cables can be fit within small-radius bends and over long distances, supporting antenna lengths of 65 m or longer and frequency ranges of 400 MHz to 6 GHz.

For the most part, microwave antennas are designed for clearly defined operating bands, and often for extremely narrow frequency bands. PCTEL (www.antenna.com), for example, offers a variety of antenna types for military and government-service applications, including the model 2225NW Global Positioning System (GPS)/aviation antenna. It is a wide area augmentation system (WAAS) antenna that can withstand winds to 100 mph. It employs right-hand circular polarization and is available for use in L1 band at 1575.42 MHz, L2 band at 1227.60 MHz, and L3 band at 1176.45 MHz, with –3 dBic gain at 90-deg elevation in each of the three bands.

For broadcast applications, Radio Frequency Systems (RFS; www.rfsworld.com) has achieved significant antenna advances by paying close attention to mechanical design. The company recently unveiled "R variants" of its PCP, PHP, and PVP broadband panel array antennas, using a cylindrical radome to cut wind load by one-half compared to conventional panel antennas **(Fig. 1)**. With their small cross sections and low wind loads, these antennas can reduce structural requirements for broadcast towers and also withstand ice and snow buildup.

The PCP panel antennas support digital television (DTV), analog television, and multiple-input, multiple-output (MIMO) system configurations. They are available from 500 to 700 MHz with horizontal, vertical, circular, and elliptical polarization. The PVP panel antennas are designed for DTV applications from 470 to 860 MHz using vertical polarization. The PHP panel antennas also operate from 470 to 860 MHz, but with horizontal polarization.

The firm also recently announced that its RADIAFLEX radiating cables, which support indoor applications from 698 to 2700 MHz, would be used for in-tunnel wireless service in China's Hangzhou Metro Line 1 transportation system. The in-tunnel radiating cables will be used to support the GSM, CDMA, DCS, UMTS, and LTE standards.

Broadband operation has long been a challenge for antenna designers, whether for communications or other applications [such as surveillance and electronic warfare (EW)]. Many of these broadband applications work with directional antennas. For emerging applications in ultrawideband (UWB) communications systems, antennas must not only cover a broad range of frequencies, but they must do so with consistent, omnidirectional radiation patterns. The frequency range for UWB communications in the United States as approved by the Federal Communications Commission (FCC) is 3.1 to 10.6 GHz.

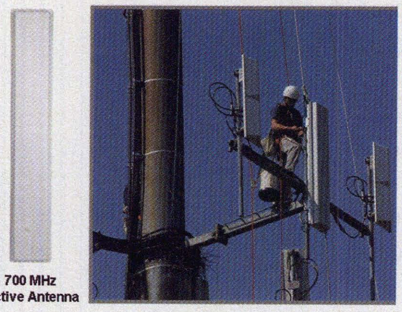

2. Advanced signal processing and arrays of antenna elements are used in "smart" or active antennas to provide performance that can change with operating conditions. [Photo courtesy of Andrew-Commscope (www.commscope.com).]

An example of an antenna with this type of performance is the model QOM0.8-40KL from Q-par Angus Ltd. (www.q-par.com), which spans 0.8 to 40.0 GHz with vertical polarization. It is 108 mm long by 100 mm in diameter and weighs 720 g, so it is small enough for monitoring and surveillance applications, yet also suitable for airborne and harsh environments. Bandwidth-wise, it more than meets the needs of UWB systems, with –2.2 to +6.9 dBi gain from 1 to 40 GHz, 3.50:1 maximum VSWR, and 2.50:1 typical VSWR across the full frequency range. It uses a male K coaxial connector and can handle as much as 40 W transmit power. The low-profile antenna is constructed from aluminum and engineered plastic materials and achieves typically less than ±1 dB azimuth ripple when measured on the horizon. Another supplier of antennas for UWB use is SkyCross (www.skycross.com), which offers antenna meeting the 7-GHz bandwidth requirements in a footprint as small as 15 x 15 mm.

Another area of growth for antenna developers lies in the millimeter-wave frequency range. Millitech (www.millitech.com), a company name synonymous with millimeter-wave frequencies, offers a wide range of antennas—including planar antennas and arrays, monopulse antennas, reflector antennas, and multiband antennas. The firm's ODA series of omnidirectional antennas includes models from 18 to 140 GHz with as much as 5% bandwidths. As an example, model ODA-15 has a center frequency at 60 GHz, while model ODA-10 operates at a center frequency of 94 GHz (both with vertical polarization and nominal gain of 2 dBi).

These antennas support high-data-rate transfers from cellular base stations, as well as automotive distance-measuring and collision-avoidance systems. Several years ago, Radio Waves, Inc. (www.radiowavesinc.com) launched its models HPCPE-42 and HP2-42 antennas for use from 40.5 to 43.5 GHz for short-haul European communications applications. The trend is increasing in the use of millimeter-wave signals, with a growing need for compact antennas capable of supporting these applications.

Andrew-Commscope (www.commscope.com) has been an innovator in a variety of different antenna technologies. The company even offers a free white paper on its unique active antenna technology for cellular communications, notably in Long-Term-Evolution (LTE) systems. Essentially, an active antenna system (AAS) is actually an array of antenna elements and supporting electronic components. By using electronic tuning and extensive digital signal processing (DSP), these active or "smart" antennas **(Fig. 2)** can respond to changing conditions, providing extended cellular communications coverage with fewer antennas and cell sites.—*JB*

Quiet Synthesizers Span 2 To 20 GHz

These YIG-based frequency synthesizers provide wide tuning bandwidths and generous output levels across frequency and temperature, with minimum frequency tuning steps of 1 kHz.

BROADBAND FREQUENCY synthesizers serve a multitude of systems, finding application in the commercial, industrial, military electronics, and medical electronics markets. The latest lines of frequency synthesizers from Micro Lambda Wireless (www.microlambdawireless.com), the MLSP-Series, build on the company's proven YIG-oscillator technology to deliver stable and reliable broadband sources in frequency bands as wide as 2 to 18 GHz and 2 to 20 GHz. The frequency synthesizers, which are designed to provide consistent performance over a wide operating temperature range, are small and lightweight. They can serve as local oscillators (LOs) in test equipment, terrestrial receivers, and satellite communications (satcom) systems.

The MLSP-Series of frequency synthesizers includes models MLSP-2018, with a frequency range from 2 to 18 GHz, and MLSP02020, which runs from 2 to 20 GHz **(see figure)**. Both provide minimum output power of +10 dBm across their frequency ranges, although they can deliver as much as +13 dBm output power. Both synthesizers maintain output-power variations within a 6-dB window across their full frequency ranges and across standard operating temperatures from 0 to +60°C (versions with extended operating temperature ranges of –20 to +75°C are also available as special orders).

Both MLSP-Series frequency synthesizers can switch frequencies in minimum step size of 1 kHz, using five-wire SPI or standard Universal-Serial-Bus (USB) interface for control. Although YIG-based frequency synthesizers are better known for their excellent spectral purity rather than their tuning speeds, the MLSP-Series synthesizers can accomplish a 100-MHz change in frequency in only 1 ms. The switching time for a larger 1-GHz change in frequency is typically 3 ms, and typically 7 ms for a full-band change.

The broadband frequency synthesizers exhibit typical harmonic levels of –12 dBc and typical nonharmonic spurious levels of –60 dBc. The single-sideband (SSB) phase noise is a function of carrier frequency and offset from the carrier. For example, with carriers from 2 to 8 GHz, the phase noise is typically –76 dBc/Hz offset 100 Hz from the carrier, –93 dBc/Hz offset 10 kHz from the carrier, –114 dBc/Hz offset 100 kHz from the carrier, and –142 dBc/Hz offset 1 MHz from the carrier.

For carriers from 8 to 16 GHz, the phase noise is typically –72 dBc/Hz offset 100 Hz from the carrier, –85 dBc/Hz offset 10 kHz from the carrier, –107 dBc/Hz offset 100 kHz from the carrier, and –135 dBc/Hz offset 1 MHz from the carrier. And for the highest-frequency carriers from 16 to 20 GHz, the phase noise is typically –72 dBc/Hz offset 100 Hz from the carrier, –72 dBc/Hz offset 10 kHz from the carrier, –95 dBc/Hz offset 100 kHz from the carrier, and –125 dBc/Hz offset 1 MHz from the carrier.

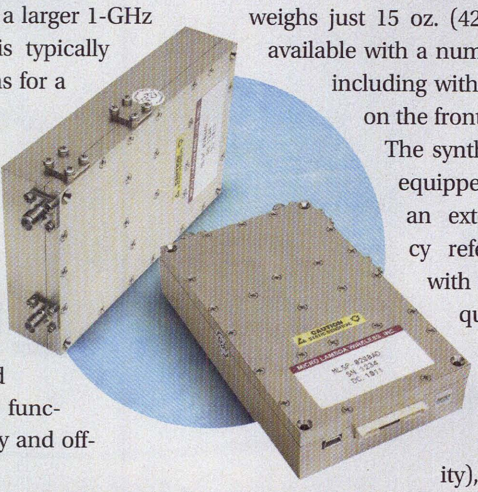

The MLSP-Series of frequency synthesizers include models for use from 2 to 18 GHz and 2 to 20 GHz, in compact coaxial housings measuring just 5 x 3 x 1 in.

The YIG-based frequency synthesizers measure just 5 x 3 x 1 in. and can fit into a two-slot PXI chassis; each synthesizer weighs just 15 oz. (426 g). They are available with a number of options, including with RF connectors on the front or on the side. The synthesizers can be equipped for use with an external frequency reference source, with an internal frequency reference (a 100-MHz crystal oscillator with ±1 ppm stability), or with both. Options are available for use with external reference sources of either 1 to 100 MHz or 1 to 200 MHz. Model MLSP-2018 draws 1975 mA from a +15 VDC supply and 350 mA from a +5 VDC supply for power consumption of 31 W. MLSP-2020 draws 2075 mA from a +15 VDC supply and 350 mA from a +5 VDC supply, for 33-W power consumption. In addition to the options, special frequency ranges are available upon special order. P&A: 8 wks. ARO.—*JB*

MICRO LAMBDA WIRELESS, INC., 46515 Landing Pkwy., Fremont, CA 94538; (510) 770-9221, FAX: (510) 770-9213; *www.microlambdawireless.com.*

Europe's Premier Microwave, RF, Wireless and Radar Event

EUROPEAN MICROWAVE WEEK
EuMW 2012
RAI Amsterdam
28 October – 2 November 2012
www.eumweek.com

Space for Microwaves

EuMW2012 returns to this city for what promises to be an important and unforgettable event. Bringing industry, academia and commerce together, European Microwave Week 2012 is a SIX day event, including THREE cutting edge conferences and ONE exciting trade and technology exhibition featuring leading players from across the globe.

THE EXHIBITION (29th - 31st October 2012)

- 7500 sqm of gross exhibition space
- 5000 key visitors from around the globe
- 1700 - 2000 conference delegates
- In excess of 250 exhibitors

THE CONFERENCES

Spanning the length of the week, choose from three separate but complementary conferences:

- European Microwave Integrated Circuits Conference (EuMIC) 29th - 30th October 2012
- European Microwave Conference (EuMC) 29th October - 1st November 2012
- European Radar Conference (EuRAD) 31st October - 2nd November 2012
- Plus, Workshops and Short Courses (From 28th October 2012)

In addition, for the third year, the free, full-day Defence and Security Executive Forum.

EuMA European Microwave Association

Official Publication: Microwave Journal

Organised by: horizon house

Supported by: IET The Institution of Engineering and Technology

Co-sponsored by: MTT-S

Co-sponsored by: IEEE

EuRAD 2012 The 9th European Radar Conference

42nd European Microwave Conference 2012 The 42nd European Microwave Conference

EuMIC 2012 The 7th European Microwave Integrated Circuits Conference

Co-sponsored by: Electron Devices Society

GAAS

Interested in exhibiting?

Call +44(0) 20 7596 8742 or visit www.eumweek.com

Cable Assemblies Are Rock Steady

These precision cables provide repeatable and reliable performance with flexure at frequencies through 40 GHz, and they are also built to last a lifetime.

CABLE ASSEMBLIES have long been known as "the weak link" (forgive the pun) in any precision microwave test system. Experienced engineers have even resorted to creating fixtures for their broadband test cables, keeping them from moving in a given test setup and changing the phase and amplitude values of a measurement. Such histrionics are no longer necessary with the Stability™ RF/microwave cable assemblies from Maury Microwave (www.maurymw.com), which provide amplitude- and phase-stable measurements through 40 GHz even with flexure. The Stability cable assemblies include the Series SC-35 cables (for use from DC to 26.5 GHz) and the SC-292 models (for applications from DC to 40 GHz).

These Stability cable assemblies **(Fig. 1)** are suitable not only for use with microwave/millimeter-wave vector network analyzers (VNAs), but also for any kind of high-frequency prototype or production testing where measurement accuracy is a concern. The amplitude stability with flexure numbers for these cable assemblies are eye-popping, at ±0.02 dB through 26.5 GHz for the SC-35 cables and ±0.05 dB through 40 GHz for the SC-292 cables. Considering the upper-end frequencies of these cable assemblies, the typical phase stability with flexure characteristics are as impressive, at ±3.5 deg. through 26.5 GHz for the SC-35 cables and ±5.0 deg. through 40 GHz for the SC-292 cables. And these are not cable assemblies that have to be treated gently: They are designed for long operating lifetimes with minimal performance degradation.

1. Stability RF/microwave cable assemblies can be ordered in standard lengths of 24, 36, 48, and 60 in. for use to 26.5 GHz and to 40 GHz.

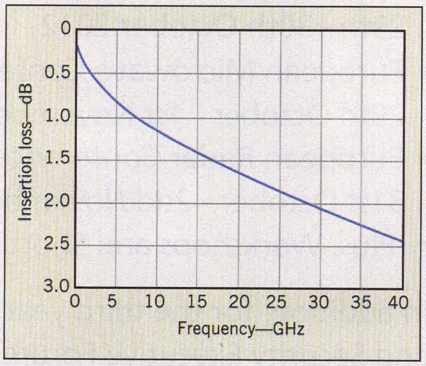

2. The low insertion loss of the Stability RF/microwave cable assemblies follows an extremely linear slope with frequency.

The 50-Ω cable assemblies, which feature a silver-plated, copper-clad steel center conductor, have a minimum bend radius of 1 in. In addition to the center and outer conductors, the cables contain an inner braid layer, an inner jacket, a crush protection layer, a braided strength member, and a braided outer jacket. The combination adds to a crush resistance of greater than 260 lbs/in. of cable. The RoHs-compliant cable assemblies weigh 1.61 oz. per foot of cable and are available in standard lengths of 24, 36, 48, and 60 in. SC-35 cable assemblies are fitted with 3.5-mm male coaxial connectors while SC-292 cable assemblies are terminated with 2.92-mm male connectors.

The mechanically durable cables offer excellent overall electrical performance, with low insertion loss and low VSWR across their full frequency ranges. The typical insertion loss for the cables is 0.84 dB/ft. for the SC-292 assemblies and 0.67 dB/ft. for the SC-35 cable assemblies **(Fig. 2)**. The typical VSWR for either cable assembly type is 1.25:1, with a maximum value of 1.40:1 through 40 GHz for the SC292 cables and maximum VSWR of 1.35:1 through 26.5 GHz for the SC-35 cables. In addition to their phase stability with flexure, the cable assemblies are also phase-stable with temperature, at better than 4°/m/GHz from −55 to +125°C.

Series SC-292 and SC-35 Stability cable assemblies are also characterized by shielding effectiveness (SE) better than 90 dB from DC to 18 GHz. They exhibit nominal time delay of 1.3 ns/in. (4.4 ns/m) with nominal velocity of propagation of 76%. With their excellent electrical performance and outstanding durability, they will help lower the total cost of test for any prototype or production test setup.—*JB*

MAURY MICROWAVE, INC., 2900 Inland Empire Blvd., Ontario, CA 91764-4804; (909) 987-4715, FAX: (909) 987-1112, www.maurymw.com.

Two-Way Divider Channels 2 To 18 GHz

This broadband coaxial power divider minimizes insertion loss while delivering high isolation between ports, with balanced output amplitude and phase characteristics.

POWER DIVIDERS provide a simple but important function in RF/microwave systems: distributing signals as evenly as possible across a required operating frequency range. When designed effectively, a power divider can produce two or more outputs from an input signal with negligible loss or distortion to the signals, other than the expected dividing loss. For example: When dividing by two, each of the divided signal paths have one-half as much power (or 3-dB less) than the original signal.

Of course, real-world circuits yield losses and other imperfections, meaning some amplitude and phase deviations will occur when signals are split through a power divider. But the passive power dividers from MECA Electronics (www.e-meca.com)—among them, the two-way, 2-to-18-GHz model 802-2-10.000—aim for optimum performance over broad bandwidths. They do so by utilizing straightforward design approaches and quality manufacturing methods.

Model 802-2-10.000 is a two-way coaxial power divider designed for applications from 2 to 18 GHz.

Model 802-2-10.000 **(see figure)** is a broadband example of the firm's power-divider lines. These also include configurations with as many as 16 output ports as well as power combiners. In an application note (www.e-meca.com/tech_papers/why_dividers.php), the company points out that not all power dividers are truly reciprocal devices and can be used equally well in reverse, as power combiners. In the case of the model 802-2-10.000, it is designed for use as a power divider, with a single input port and two output ports, as well as 20-W input power-handling capability.

Under ideal conditions, such a power divider would accept input signals to 20 W and provide a pair of output signals to 10 W each. But in practical designs, loss will occur due to such things as connectors to printed-circuit-board (PCB) junctions and passive circuit elements—even from dissipative losses from the PCB dielectric material.

In the model 802-2-10.000, these losses amount to typically 0.5 dB from 2 to 18 GHz, which will cause a slight drop in output power from the ideal maximum 10 W. The model 802-2-10.000 two-way power divider achieves high isolation between its two output ports, with minimum isolation of 17 dB and typical isolation between output ports of 19 dB. The typical VSWR at its input and output ports is 1.50:1.

In comparing the quality of different power dividers, how well the output arms are balanced in terms of amplitude and phase characteristics provide some insight into the precision of the circuit design, as well as the quality of the manufacturing process. In the model 802-2-10.000, the amplitude unbalance between output ports is minimized to a mere ±0.3 dB, while the phase unbalance is held to a worst-case value of ±5 deg. across the full 2-to-18-GHz frequency range.

Model 802-2-10.000 is designed for use across an operating temperature range of –55 to +85°C. It is supplied in an aluminum housing equipped with stainless-steel SMA connectors. For those needing less bandwidth, the company also offers model 802-2-11.500-M01, which keeps the maximum 20-W input rating across a bandwidth of 4 to 18 GHz. It exhibits maximum insertion loss of 0.5 dB across the full frequency range, with typical insertion loss of only 0.4 dB. The isolation between ports is 18 dB or better, and typically 20 dB. The power divider shows amplitude unbalance of ±0.3 dB with phase unbalance of ±6 deg. across the frequency range.

The maximum input VSWR is 1.40:1, with typical value of 1.30:1, while the maximum output VSWR is 1.35:1, with a typical output VSWR of 1.25:1. The model 802-2-10.000 is supplied in an aluminum housing with stainless-steel SMA connectors.

The two power dividers are just two examples of the company's many lines of power dividers and power combiners, from 2-way through 16-way units. The firm also offers a wide range of other passive components, including power combiners, attenuators (including high-power Type N units rated for 150 W), bias tees, circulators/isolators, directional couplers, and terminations.—*JB*

MECA ELECTRONICS, INC., 459 East Main St., Denville, NJ 07834; (866) 444-6322, (973) 625-0661, FAX: (973) 625-9277, *www.e-meca.com.*

Infocenter

Advertiser	Website, E-Mail Address	Page
A		
Advanced Switch Technology	www.astswitch.com, email: info@astswitch.com	120
Aeroflex Weinschel	www.aeroflex.com/weinschel	81
Aethercomm	www.aethercomm.com, email: sales@aethercomm.com	43
Agilent Technologies	www.testequity.com/agilent	17
Agilent Technologies	www.agilent.com/find/n6700power	53
Agilent Technologies	www.agilent.com/find/mxgwireless	89
Anritsu	www.anritsu.com	IFC
Ansys Inc.	www.ansys.com	49
Applied Interconnect	www.onlinecables.com , email: sales@onlinecables.com	120
ARRA INC.	www.arra.com, email: sales@arra.com	IBC
Avtech Electrosystems Inc	www.avtechpulse.com, email: info@avtechpulse.com	120
AWR	www.awrcorp.com	4
B		
Berex	www.berex.com	68
BL Microwave Ltd	www.blmicrowave.com, email: commercial@elhyte.f	100
C		
CIAO Wireless, Inc	www.ciaowireless.com, email: sales@ciaowireless.com	8
Coilcraft	www.coilcraft.com, email: info@coilcraft.com	10
Communication Concepts, Inc.	www.communication-concepts.com, email: cci.dayton@pobox.com	98
CST of America	www.cst.com	113
CTT	www.ctt.com, email: sales@cttinc.com	40
D		
dBm, LLC	www.dbmcorp.com	22
Delta Electronics Manufacturing	www.deltarf.com, email: sales@deltarf.com	38
Dow Key Microwave	www.dowkey.com, email:dkm@dowkey.com	45
E		
Eclipse Microwave	www.eclipsemicrowave.com, email: sales@eclipsemicrowave.com	16
European Microwave Conference	www.eumweek.com	109
Exelis Inc.	www.exelisinc.com/microwavesystems.com	7
G		
Gigoptix, Inc.		74, 75
H		
Herotek Inc	www.herotek.com, email: sales@herotek.com	13
Hittite Microwave Corporation	www.hittite.com	65
Huber + Suhner	www.hubersuhner.com, email: info@hubersuhner.com	44
I		
IMS 2012	http://ims2012.mtt.org	115
International Manufacturing Services	www.ims-resistors.com	76
IXYS Colorado	www.ixysrf.com	19
K		
Krytar, Inc	www.krytar.com, email: sales@krytar.com	80
L		
Lark Engineering Company	www.larkengineering.com, email: sales@larkengineering.com	56
Linear Technology Corporation	www.linear.com	101
LPKF CAD/CAM	www.lpkfusa.com/pcb	42
M		
Maury Microwave, Inc	www.maurymw.com, email: maury@maurymw.com	111
Meese Munich		78
Megaphase	www.megaphase.com, email: fastquote@megaphase.com	64
Mini Circuits/Sci Components	www.minicircuits.com	12
Mini Circuits/Sci Components	www.minicircuits.com	14
Mini Circuits/Sci Components	www.minicircuits.com	15
Mini Circuits/Sci Components	www.minicircuits.com	23
Mini Circuits/Sci Components	www.minicircuits.com	29
Mini Circuits/Sci Components	www.minicircuits.com	35
Mini Circuits/Sci Components	www.minicircuits.com	41
Mini Circuits/Sci Components	www.minicircuits.com	47
Mini Circuits/Sci Components	www.minicircuits.com	57
Mini Circuits/Sci Components	www.minicircuits.com	61
Mini Circuits/Sci Components	www.minicircuits.com	71
Mini Circuits/Sci Components	www.minicircuits.com	79
Mini Circuits/Sci Components	www.minicircuits.com	85
Mini Circuits/Sci Components	www.minicircuits.com	95
Mini Circuits/Sci Components	www.minicircuits.com	99
Mini Circuits/Sci Components	www.minicircuits.com	117
Mini Circuits/Sci Components	www.minicircuits.com	30-31
MITEQ	www.miteq.com	1
MITEQ	www.miteq.com	11
N		
Narda An L-3 Communications	www.nardamicrowave.com	3
Narda An L-3 Communications	www.nardamicrowave.com	66
National Instruments	www.ni.com/redefine	87
Networks International	www.nickc.com	27
Noisecom	www.noisecom.com	BC
P		
Phase Matrix	www.phasematrix.com, email: sales@phasematrix.com	24
Phonon Corporation	www.phonon.com	102
Planar Monolithics Industries	www.pmi-rf.com, email: sales@pmi-rf.com	37
Polyfet RF Devices	www.polyfet.com	120
Pro-Comm, Inc.	www.procomm222.com, email: sales@procomm222.com	120
Pulsar Microwave Corp.	www.pulsarmicrowave.com, email: sales@pulsarmicrowave.com	92
R		
RF Depot	www.rfdepot.com	59
RFMW Ltd.	www.rfmw.com	6
Richardson RFPD	www.richardsonrfpd.com	18
RLC Electronics	www.rlcelectronics.com, email: sales@rlcelectronics.com	25
Rohde & Schwarz	www.rohde-schwarz.com	105
Rohde & Schwarz	www.rohde-schwarz.com	107
S		
San-tron	www.santron.com	73
Sector Microwaves Inc Inc	www.sectormicrowave.com	120
Skyworks Solutions, Inc.	www.skyworksinc.com	2
Synergy Microwave	www.synergymwave.com, email: sales@synergymwave.com	51
Synergy Microwave	www.synergymwave.com, email: sales@synergymwave.com	63
Synergy Microwave	www.synergymwave.com, email: sales@synergymwave.com	91
T		
Tecdia	www.tecdia.com	83
Teledyne Microwave Solutions	www.teledyne-cougar.com, email:cougar@teledyne.com	67
TRM Microwave	www.trmmicrowave.com, email: info@trmmicrowave.com	103
TTE Incorporated	www.tte.com	69
V		
Vectron International	www.vectron.com/products/saw.html	93
W		
Wenteq Microwave Corporation	www.wenteq.com, email: sales@wenteq.com	120

**Domestic Edition only* ***International Edition only* *This index is provided as an additional service by the publisher, who assumes no responsibility for errors or omissions.*

MARKETING & ADVERTISING STAFF

VICE PRESIDENT & MARKET LEADER
Bill Baumann
T: (201) 845-2403
F: (201)845-2484
E: bill.baumann@penton.com

GROUP SALES MANAGER
Paul Milnamow
T: (312)-840-8462
F: (312)-514-3957
E: paul.milnamow@penton.com

NORTHEAST
David Madonia
T: (212)-204-4331
E: dave.madonia@penton.com

NORTHERN CALIFORNIA, NEVADA, NORTHWEST
Jamie Allen
T: (415) 608-1959
F: (913) 514-3667
E: jamie.allen@penton.com

SOUTH
Bill Yarborough
T: (713) 636-3809
T: (713) 523-8384
E: bill.yarborough@penton.com

CENTRAL, SOUTHERN CALIFORNIA, ARIZONA
Tracy Smith
T: (913) 967.1324
F: (913) 514.6881
E: tracy.smith@penton.com

DIRECT CONNECTION ADS CLASSIFIED ADVERTISING
Phyllis L. Schroder
E: phyllis.schroder@penton.com
Kevin Dern
E: kevin.dern@penton.com

Penton
Design Engineering & Sourcing Group

EUROPEAN SALES REP
Mark Durham
T: +44 (0)7958 564137
E:mark.durham@penton.com

TAIWAN, R.O.C.
Charles C.Y. Liu
T: (886)-2-2727-7799
F: (886)-2-2728-3686

JAPAN
Hiro Morita
T: 81-3-3261-4591
F: 81-3-3261-6126

KOREA
Jo Young Sang
T: 011-82-2-739-7840
F: 011-82-732-3662

CUSTOMER SERVICE - SUBSCRIPTIONS
New/Renew/Cancel/Change Address/Missing and Back Issues
T: 866-505-7173 F: 847-763-9673
E: microwaves&rf@halldata.com

Subscription Assistance and Information: Microwaves & RF (ISSN 0745-2993) is published monthly, except semi-monthly in December. **Microwaves & RF** is sent free to individuals actively engaged in high-frequency electronics engineering. In addition, paid subscriptions are available. Subscription rates for U.S. are $95 for 1 year ($120 in Canada, $150 for International). Published by Penton Media, Inc., 9800 Metcalfe Ave., Overland Park, KS 66212-2216. Periodicals Postage Paid at Shawnee Mission, KS and at additional mailing offices.

POSTMASTER: Send change of address to Microwaves & RF, Penton Media Inc., P.O. Box 2095, Skokie, IL 60076-7995. For paid subscription requests, please contact: Penton Media Inc., P.O. Box 2100, Skokie, IL 60076-7800. Canadian Post Publications Mail agreement No. 40612608. Canadian GST# R126431964. Canada return address: Bleuchip International, P.O Box 25542,London, ON N6C6B2.

Coupler Directs 1 To 18 GHz

Model 180120 is a stripline directional coupler with frequency range of 1 to 18 GHz. Ideal for military electronic-warfare (EW) systems, commercial wireless system applications, and broadband testing, the 20-dB coupler features coupling flatness within ±1 dB with frequency sensitivity within ±0.3 dB from 1 to 12.4 GHz, and ±0.4 dB from 1 to 18 GHz. Directivity is better than 16 dB across the full frequency range. The maximum VSWR at any port is 1.35:1, while the insertion loss is less than 0.95 dB (including coupled power) across the full frequency range. The model 180120 directional coupler measures 3.5 x 0.53 x 0.73 in. and is rated for 20 W maximum average input power and 3 kW peak input power. It is designed for operating temperatures from –54 to +85°C. It can be supplied with a variety of different coaxial connectors, including SMA female, SMA male, and Type N female connectors.

KRYTAR, INC., 1288 Anvilwood Ave., Sunnyvale, CA 94089; (408) 734-5999, FAX: (408) 734-3017, e-mail: ***sales@krytar.com, www.krytar.com.***

VCXOs Offer Low Jitter

The V8F/V8M family of voltage-controlled crystal oscillators (VCXOs) are available at frequencies suitable for Gigabit Ethernet, backhaul communications, and test and measurement applications (including 122.88 MHz, 153.6 MHz, 155.52 MHz, 245.76 MHz, and 320.00 MHz). Based on LVPECL technology, these VCXOs employ high-quality crystals to generate fundamental tones from 50 to 250 MHz, and analog frequency multiplication to reach higher frequencies through 800 MHz. Through 250 MHz, typical jitter is about 0.4 ps. Through 800 MHz, jitter is controlled to typically 0.6 ps with stability of about ±150 ppm. The oscillators are supplied in RoHS-compliant FR4 housings measuring 9 x 14 mm. They operate on supplies of +3.3 VDC over operating temperatures from –40 to +85°C.

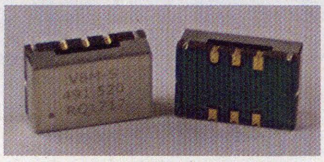

RUBYQUARTZ TECHNOLOGY LLC, 18205 Biscayne Blvd., Ste. 2217, Aventura, FL 33160; (305) 406-0211, FAX: (305) 647-2169, e-mail: ***sales@rubyquartz.com, www.rubyquartz.com.***

Amplifier Drives 400 W To 500 MHz

Model SSPA 01-05-400 is a high-power amplifier system that delivers 400 W output power from 100 to 500 MHz. Suitable for linear military communications systems, the amplifier is designed for harsh environments and operating conditions. It requires just 10 W input power to achieve its rated output power, and can work with continuous-wave (CW) or pulsed signals. The amplifier system, which operates from a +28-VDC supply, is equipped with DC and RF switching circuitry that enables and disables critical components in 20 μs or less. It exhibits maximum input/output VSWR of 2.0:1 with typical system efficiency of 40%. Standard features include reverse polarity protection, output short and open circuit protection, and over/under voltage protection. The typical noise figure is 10 dB across the operating band. The amplifier can handle operation at base-plate temperatures from –40 to +65°C. It measures approximately 11.5 x 25.0 x 50 in. with Type N connectors.

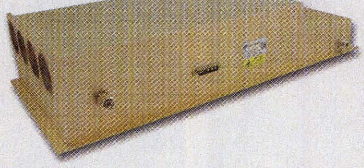

AETHERCOMM, INC., 3205 Lionshead Ave., Carlsbad, CA 92010; (760) 208.6002, FAX: (760) 208.6059, e-mail: ***sales@aethercomm.com, www.aethercomm.com.***

Relay Switches Signals To 9 GHz

A new microstrip/coplanar-waveguide-mount relay from Rel-Comm Technologies offers outstanding performance from DC to 9 GHz. Designed for high packaging density and a great deal of circuit layout flexibility, the rugged relay measures just 0.880 x 0.575 in. It provides a double-pole, double-throw (DPDT) transfer configuration with better than 50-dB isolation and 0.4-dB maximum insertion loss to 9 GHz. Ideal as a building-block component in switch matrices, the compact relay exhibits maximum VSWR of 1.40:1 and is designed for operation from +12 and +28 VDC supplies. The relay is available with failsafe or latching operation with optional configured "circuit insertion" whereby one internal bridging contact is removed to provide a non-shorting circuit path. The RoHS-compliant relay is silver plated for enhanced passive-intermodulation (PIM) performance.

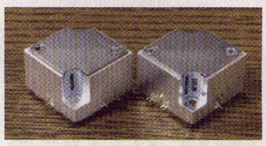

RELCOMM TECHNOLOGIES, INC., 610 Beam St., Salisbury, MD 21801; (410) 749-4488, FAX: (410) 860-2327, e-mail: ***sales@relcommtech.com, www.relcommtech.com.***

Variable Attenuator Spans 7.2 to 8.4 GHz

Model 5-6813-30A is a continuously variable attenuator with a total attenuation range of 30 dB from 7.9 to 8.4 GHz. The attenuation remains within ±1 dB across the full 500-MHz operating bandwidth, with maximum insertion loss of 0.5 dB and maximum VSWR of 1.50:1. The attenuator is designed to handle 5 W average power and 3 kW peak power. The unit is specified for operating temperatures of –55 to +85°C. Standard units are supplied with SMA female connectors although versions are available with Type N connectors. Versions are also available in panel-mount configurations, as well as with a turns-counting dial or digital counter.

ARRA, INC., 15 Harold Ct., Bay Shore, NY 11706; (631) 231-8400, FAX: (631) 434-1116, ***E-mail: sales@arra.com, www.arra.com.***

Modulator Runs 50 To 1000 MHz

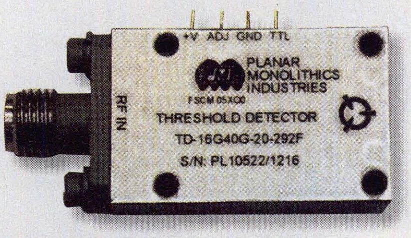

Model PSM-50M1G-CD-1 is a single sideband (SSB) modulator designed for use from 50 MHz to 1 GHz. It has an intermediate-frequency (IF) range of DC to 10 MHz and IF modulation power range of +7 to +13 dBm into 50 Ω. The SB modulator features an input 1-dB compression point of typically +5 dBm. It has maximum conversion loss of 10 dB. The modulator achieves typically carrier suppression of –20 dBc, with worst-case quadrature phase accuracy of ±10 deg. and worst-case quadrature amplitude accuracy of ±2.0 dB. The wideband SSB modulator is supplied in a coaxial package measuring 6.0 x 3.5 x 1.0 in. with SMA female connectors. It is designed for operating temperatures from –40 to +85°C.

PLANAR MONOLITHICS INDUSTRIES, INC. (PMI), 7311-F Grove Road, Frederick, MD 21710; (301) 662-5019, FAX: (301) 662-1731, e-mail: *sales@pmi-rf.com, www.pmi-rf.com.*

GaN Amplifier Boosts 6 To 18 GHz

Model AML618P4015 is a gallium-nitride (GaN) power amplifier designed to provide 20 W output power from 6 to 18 GHz. The high-power-density amplifier achieves power-added efficiency (PAE) of typically 12% in a package measuring just 2.45 x 2.09 x 0.41 in. It achieves 40-dB minimum small-signal gain across its full operating bandwidth and operates

from a +32-VDC supply. The rugged amplifier is supplied in a hermetic aluminum housing with field-removavble female SMA connectors. It features a transistor-transistor-logic (TTL) controlled muting function capable of 200-ns on/off speed. The amplifier has an operating temperature range of –40 to +85°C.

MICROSEMI CORP., RF INTEGRATED SOLUTIONS, 3295 Scott Blvd., Ste. 150, Santa Clara, CA 95054; (408) 986-8031, FAX: (408) 988-8659, e-mail: *sales.support@microsemi.com, www.microsemi.com/rfis.*

Mixers, Amplifiers Reach 46.5 GHz

Several components have been developed for microwave/millimeter-wave radios and other high-frequency applications from 24.0 to 46.5 GHz. The components include two amplifiers and three mixers. Model HMC1040LP3CE is a low-noise amplifier (LNA) with 2.2-dB noise figure and 23-dB gain from 24.0 to 43.5 GHz. It consumes only 70 mA from a +2.5-VDC supply but achieves a third-order intercept to +22 dBm. It is housed

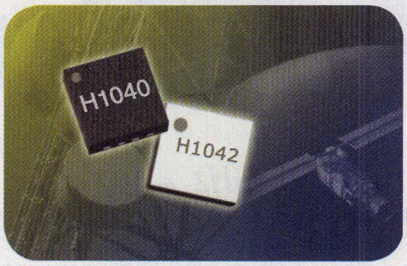

in a 3 x 3 mm QFN package. Model HMC1016 is a medium-power amplifier in die form with 22-dB gain from 34.0 to 46.5 GHz. It also offers +26-dBm saturated output power and 17% power-added efficiency (PAE) from a +6-VDC supply.

Models HMC1041LC4 and HMC1042LC4 are in-phase/quadrature (I/Q) mixers for bands of 17 to 27 GHz and 15.0 to 33.5 GHz, respectively. They feature conversion loss as low as 9 dB and are supplied in 4 x 4 mm QFN packages. Finally, model HMC1043LC3 is a triple-balanced mixer with RF port range of 26 to 32 GHz and intermediate-frequency (IF) range of 16 to 22 GHz. It works with LO drive as low as +9 dBm from 7 to 11 GHz and is ideal for upconversion and downconversion in satellite transponder applications. It is supplied in a 3 x 3 mm QFN package and requires no external matching components.

HITTITE MICROWAVE CORP., 2 Elizabeth Dr., Chelmsford, MA 01824; (978) 250-3343, FAX: (978) 250-2273, e-mail: *sales@hittite.com, www.hittite.com.*

Driver Amp Serves 30 To 4000 MHz

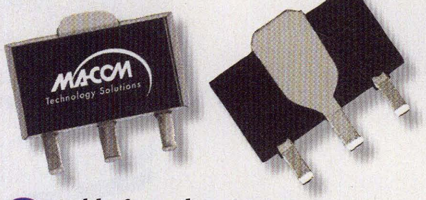

Suitable for military communications and commercial communications infrastructure applications, model MAAM-010617 is an RF driver amplifier with a frequency range of 30 to 4000 MHz. It offers 13-dB gain over that span, with 4.5-dB noise figure. The driver amplifier, which is supplied in an SOT-89 package, exhibits 18-dB input and output return loss. Designed for a single +5-VDC supply, it draws 420 mA quiescent current. The amplifier achieves +31 dBm output power at 1-dB compression with a +42.5-dBm third-order intercept point.

M/A-COM TECHNOLOGY SOLUTIONS, INC., 100 Chelmsford St., Lowell, MA 01851; (978) 656-2507, FAX: (978) 656-2644, *www.macomtech.com.*

Tiny Amp Offers Flat Gain To 6 GHz

Based on heterojunction-bipolar-transistor (HBT) technology, model CMA-62+ is an extremely broadband amplifier, with flat gain of 15 dB (typically 15.4 dB at 2 GHz) across a frequency range of 10 MHz to 6 GHz. The gain remains flat within ±0.7 dB from 50 to 4000 MHz. The RoHS-compliant monolithic-microwave-integrated-circuit (MMIC) amplifier is bonded to a multilayer

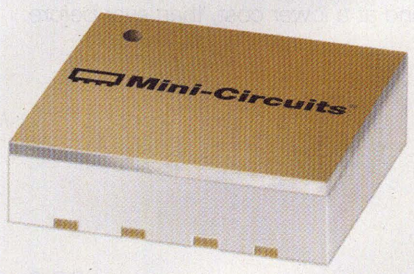

integrated low-temperature-cofired-ceramic (LTCC) substrate for outstanding thermal stability, then hermetically sealed in a miniature surface-mount package. The rugged amplifier delivers +19.8 dBm typical output power at 1-dB compression at 2 GHz, and provides excellent linearity, with a typical third-order intercept point of +37.8 dBm at 50 MHz and +33.6 dBm at 2 GHz. It is Class 1C rated in terms of electrostatic-discharge (ESD) protection per the human body model (HBM). Ideal for cellular base stations, cable television (CATV), and portable wireless applications, the amplifier has a noise figure of typically 5.2 dB at 1 GHz and 5.5 dB at 6 GHz. It typically draws 82 mA from a +5-VDC supply and does not require any external matching components.

MINI-CIRCUITS, P.O. Box 350166, Brooklyn, NY 11235-0003; (718) 934-4500, FAX: (718) 332-4661, ***www.minicircuits.com.***

OCXO Cuts Noise To 40 MHz

Model OX-501 is a surface-mount oven-controlled crystal oscillator (OCXO) that is ideal for cellular base stations and military communications equipment, as well as in test equipment. It is supplied in a 6-pin surface-mount package and available in frequencies from 10 to 40 MHz, with standard frequencies of 10, 12.8, 19.2, 20, and 38.88 MHz. Model OX-501 can be furnished with stabilities of ±20 PPB or ±100 PPM from –20 to +70°C or from –40 to +85°C. The initial frequency tolerance is ±0.5 PPM, with variations of ±20 PPB with changes in supply voltage (within ±5%), and ±30 PPB with changes in load (within ±5%). After 30 days of operation, the aging rate is ±5 PPM per day. The typical warmup time is 3 minutes. The OCXO consumes 0.5 W typical power at +3.3 VDC under steady-state operation. The phase noise for a supply of +1.4 VDC is –60 dBc/Hz offset 1 Hz from the carrier, –100 dBc/Hz offset 10 Hz from the carrier, –128 dBc/Hz offset 100 Hz from the carrier, –140 dBc/Hz offset 1 kHz from the carrier, and –148 dBc/Hz offset 10 kHz from the carrier.

VECTRON INTERNATIONAL, 267 Lowell Rd., Hudson, NH 03051; 1-88-VECTRON-1; ***www.vectron.com.***

High-Power Coupler Collects 2 To 8 GHz

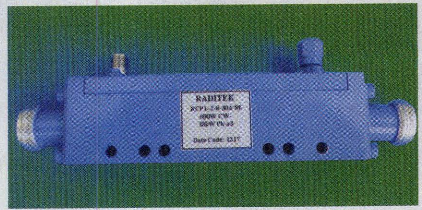

Model RCPL-2-8-30d-Nf-600W is a high-power coaxial directional coupler designed for use from 2 to 8 GHz. It can handle continuous power inputs to 600 W and peak input power levels to 10 kW. The component provides 3-dB coupling with Type N female connectors on the input port and SMA female connectors on the coupled port. The RoHS-compliant coupler measures just 3.0 x 1.1 x 0.80 in. It exhibits insertion loss of typically 0.2 dB with frequency sensitivity of typically ±0.60 dB. The minimum directivity is 16 dB while the typical VSWR is 1.30:1. The high-power coupler is capable of handling operating temperatures of –35 to +55°C with minimal impact on performance.

RADITEK, 1702L Meridian Ave., Ste. 127, San Jose, CA 95125; (408) 266-7404, FAX: (408) 266-4483, e-mail: ***sales@raditek, www.raditek.com.***

Simulator Handles Multiple Disciplines

Version 4.3 of the COMSOL Multiphysics modeling and simulation software is now available, with a number of improvements and increased functionality. COMSOL Multiphysics 4.3 includes three new discipline-specific add-on modules, fast and powerful meshing, a "Double Dogleg" solver for mechanical contact and highly nonlinear simulations, and a number of user-inspired enhancements. With this latest release, users can run multiple-parameter sweeps with easy specification of one or more parameters, performing sweeps for

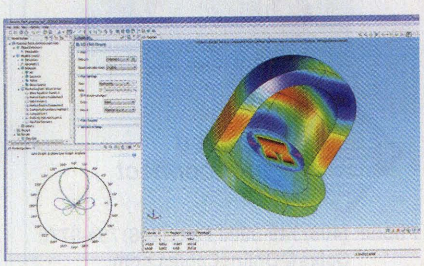

all of the parameters or for a subset of them. User interfaces for cluster and batch sweeps facilitate defining massively parallel and independent parametric sweeps. Visualizations of results from these parameter sweeps can be easily selected to include combinations of the swept parameters in a single presentation. The modules for electrical, mechanical, fluid-flow, and chemical simulations have all been updated with exciting new features and capabilities. In addition, this latest version of the software features a user interface within the AC/DC module for modeling three-dimensional (3D) rotating mechanical designs—such as rotary joints—as well as for generators, brushless motors, and equipment with brushed DC motors.

COMSOL, INC., 1 New England Executive Park, Ste. 350, Burlington, MA 01803; (781) 273-3322, FAX: (781) 293-6603, e-mail: ***info@comsol.com, www.comsol.com.***

OMTs Operate Over K- and Ka-Bands

Models SAT-KB-39642-T1 and SAT-KA-25028-T1 are full-band K-band (18.0 to 26.5 GHz) and Ka-band (26.5 to 40.0 GHz) orthomode transducers (OMT), respectively. These components separate orthogonally polarized signals within the same band, allowing two channels to be used within the band simultaneously. Combined with a polarizer, right-hand circular polarization (RHCP) and left-hand circular polarization (LHCP) can be realized in one assembly. The OMTs exhibit 0.4-dB insertion loss, with 45-dB channel isolation and 35-dB cross polarization across the full waveguide bands. OMTs for use in other frequency bands, from WR-22 through WR-10, are also available.

SAGE MILLIMETER, INC., 3043 Kashiwa St. Torrance, CA 90505; (424) 757-0168, FAX: (424) 757-0188, ***www.sagemillimeter.com.***

DAVE MADONIA (e) dave.madonia@penton.com, 212-204-4331 • **TRACY SMITH** (e) tracy.smith@penton.com, 913-967-1324

Bigger where it counts...

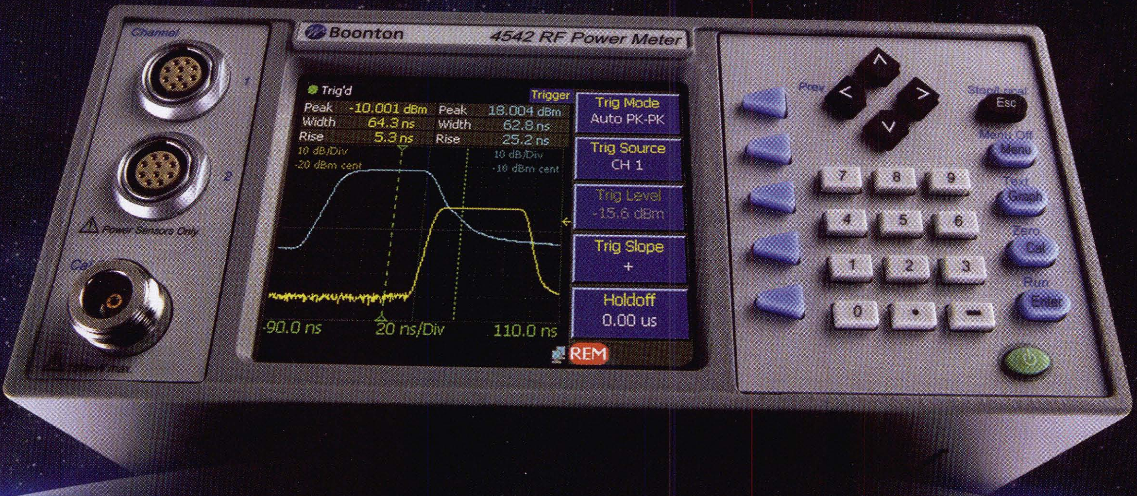

in the Performance.

Boonton's 4540 Peak Power Meter delivers the outstanding performance needed for today's demanding radar and communication applications. By incorporating advanced technology from our flagship 4500B peak power analyzer, the smaller, economically priced 4540 outperforms higher priced competitors in many areas. It's fast update rate enables tuning high power amplifiers and processing large amounts of statistical data for CCDF measurements. Advanced trigger technology provides a rock solid view of fast rise time signals and the wide dynamic range allows measuring low duty cycle pulses. The 4540 power meter provides automatic settings for a large number of technologies including WCDMA, WiMAX, WLAN, Wi-Fi, LTE, and Radar.

- Frequency range: 9.9kHz to 40 GHz
- Time resolution: 200 ps
- Video bandwidth: 70MHz
- Rise time: <7ns
- Effective sampling rate (RSS): 5GSamples/second
- Statistical analysis including CCDF
- GPIB, USB (device) and LAN standard

For more information visit us at boonton.com or call +1 973-386-9696.

Boonton: Redefining How You Use Power Meters.

4530 RF Power Meter Series

4500B RF Peak Power Analyzer

4240 RF Power Meter

Scan QR Code

Wireless Telecom Group

Boonton Microlab Noisecom

Boonton